ANALYSIS OF TRANSIENTS AND CONTROL OF ADVANCED HIGH TEMPERATURE REACTOR-
COUPLED HEAT EXCHANGERS SYSTEM

A Thesis

Presented in Partial Fulfillment of the Requirements for the

Degree of Master of Science

with a

Major in Chemical Engineering

in the

College of Graduate Studies

University of Idaho

by

Isaac J. Skavdahl

Major Professor: Vivek Utgikar, Ph.D., P.E.

Committee Members: Soumya Srivastava, Ph.D.; Richard Christensen, Ph.D.

Department Chair: D. Eric Aston, Ph.D.

July 2016

AUTHORIZATION TO SUBMIT THESIS

This thesis of Isaac J. Skavdahl, submitted for the degree of Master of Science with a Major in Chemical Engineering and titled, "ANALYSIS OF TRANSIENTS AND CONTROL OF ADVANCED HIGH TEMPERATURE REACTOR-COUPLED HEAT EXCHANGERS SYSTEM," has been reviewed in final form. Permission, as indicated by the signatures and dates given below, is now granted to submit final copies to the College of Graduate Studies for approval.

Major Professor: _____ Date: _____
                     Vivek Utgikar, Ph.D.

Committee Members: _____ Date: _____
                     Soumya Srivastava, Ph.D.

                     _____ Date: _____
                     Richard Christensen, Ph.D.

Department
Administrator: _____ Date: _____
                     Eric Aston, Ph.D.

ABSTRACT

Control of advanced reactor system consisting of a nuclear reactor, an intermediate heat exchanger (IHX), and a secondary heat exchanger (SHX) is investigated in this research. Initial transient analysis of the system was conducted using commercially available process simulation softwares PRO-II and DYNSIM. System parameters of significance – controlled and manipulated variables – were identified, and a control strategy was developed to maintain the controlled variables at their set points. The system response was simulated for various load disturbances, initially for the coupled heat exchangers system, followed by incorporation of the reactor dynamics in the system. Alternate strategies to control the temperature entering the process or power conversion unit (PCU) by either manipulating the secondary loop flow rate, controlling reactor power, or a combination of the two methods were investigated. Combining both methods of control showed great utility in controlling the temperature entering the process and may be an ideal method for control.

ACKNOWLEDGEMENTS

TABLE OF CONTENTS

LIST OF FIGURES

LIST OF TABLES

NOMENCLATURE

Variable	Definition	Units
A	heat transfer area	m^2
C_p	heat capacity	$J/kg.^oC$
c	precursor concentration	n/cm^3
F	flow rate	kg/s
G	transfer function	-
h	individual heat transfer coefficient	$kW/m^2.^oC$
K	gain value	$^oC.s/kg$
M	FC_p	$J/s.^oC$
m	mass of coolant or metal	kg
n	average neutron density	n/cm^3
P	Power	kW
Q	thermal duty	kW
T	temperature	^oC
T	time constant	s
t	time	s
U	overall heat transfer coefficient	$kW/m^2.^oC$

Greek	Definition	Units
α	reactivity coefficient	$^oC^{-1}$
β	delay neutron fraction	-
Λ	prompt neutron lifetime	s
λ	decay constant	s^{-1}
μ	mC_p	$J/^oC$
ρ	reactivity	-
τ	time delay	s
Ω	Ah	$kW/^oC$

Subscripts	Definition
0	initial value
1	SHX parameter
2	IHX parameter
3	reactor parameter
c	cold
c	controller
c	coolant
D	derivative
e	exit
f	fuel
h	hot
I	IHX
I	integral
i	in
i	subspecies *i*
o	out
P	proportional
rod	control rod movement
S	SHX
v	valve
w	wall

Superscripts	Definition
*	set point value

CHAPTER 1: INTRODUCTION AND BACKGROUND

1.1 NUCLEAR REACTORS

1.1.1 Nuclear Fission

For over half a century nuclear reactors have been utilized to produce electricity in the U.S. and around the world. Currently nuclear reactors constitute the second largest source of electricity in the U.S. behind coal, generating 19.5% of the nation's electricity (Nuclear Energy Institute, 2016). Nuclear power is a safe, and clean way of producing energy and though not renewable, has practically unlimited capacity for supplying the energy needs well into the foreseeable future. Nuclear reactors, no matter the design, use the fission process which releases energy that can be utilized. Most nuclear reactors today use uranium-235 (U-235) as the fuel, with a possible fission process for U-235 shown in Figure 1a. The nucleus is bombarded with neutrons, causing the uranium atom to split into two smaller atoms while releasing additional neutrons and energy. The overall number of nucleons (neutrons and protons) is conserved in a fission reaction. For example in the process shown in Figure 1a the mass number of uranium (235) plus a neutron (1) is equal to the mass number of krypton (91), the mass number of barium (142) and the 3 released neutrons (3). However, the total mass of the products is less than U-235 because some of the mass is converted to energy that is released. The binding energy of the U-235 nucleus is greater than the sum of binding energies of both the fission products. Thus, as fission takes place the excess binding energy, which is initially seen as mass, is released to the environment. The overall number of neutrons released in the fission reaction depends on the fission products. The emitted neutrons then either split additional uranium atoms producing energy, are absorbed, or escape from the system. Other products may be formed as well in the process including but not limited to iodine, zirconium, and xenon. The fission yield curve in Figure 1b shows the distribution of the mass numbers of fission products and the percentage of the isotope that occurs. The mass number of the smaller fission product is usually around 85-105 and the larger fission product mass number is around 130-150. However, the addition of the fission products atomic numbers and number of neutrons released always equals 236. The mass ratio of the two atoms that split from the U-235 atom is always around 3:2 (Averill and Eldredge, 2012). For example, the ratio of Ba-142 to Kr-91 is 3.12:2. Depending on the products different amounts of energy will be released per fission. However, on average 194 MeV is the amount released per U-235 fission which is equivalent to ~3.11×10^{-11} J (Kessler et al., 2014). This may appear to be rather negligible but in reality is an incredibly large amount of energy. The energy obtained from the fission

of 1 gram of uranium is equivalent to that obtained from 2 million grams of crude oil or 3 million grams of coal (European Nuclear Society, 2016).
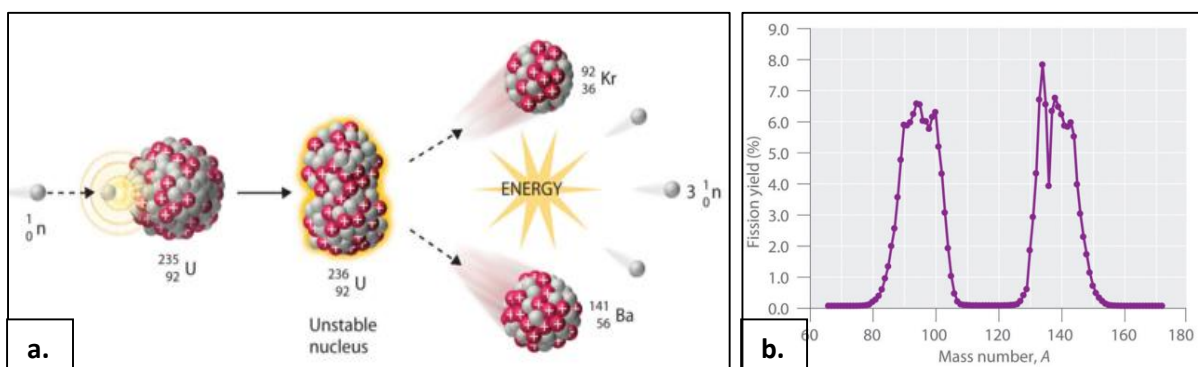
Figure 1. a: Possible fission process for U-235. b: mass number distribution for fission products of U-235 (Averill and Eldredge, 2012).

1.1.2 Historical Advances of Nuclear Reactors

Initially, the nuclear fission process was suggested for use in creating bombs. It was found that 12 kg of uranium would cause an explosion roughly equivalent to 1,800 tons of TNT. After the end of World War II, focus shifted to using nuclear energy for electricity production. The first test reactor made for producing electricity started operating in 1951 in Idaho. Civilian use of nuclear power increased significantly over the next two decades with many of the reactors built between 1960 and 1970 (World Nuclear Association, 2014).

Around 100 nuclear reactors are operating today in the U.S., all of them light water reactors (LWRs) which use water as the coolant. Two main designs for LWRs are the pressurized water reactor (PWR) and boiling water reactor (BWR). The main difference between the two is that the BWR is a single loop design while the PWR is a double loop design: in a BWR, water enters the reactor and as it travels through is heated up until exiting as steam. The steam then travels through a turbine and the generator producing electricity. The coolant circulation loop is completed by feeding the water produced by the condensing steam back into the reactor, as shown in Figure 2. The PWR design is shown in Figure 3. In the PWR, the coolant water travels through the reactor and is heated up, however, maintained under high pressure to prevent boiling. This primary coolant provides heat to a secondary loop consisting of a steam generator in which water in the secondary loop is converted into steam and utilized for electricity production similar to the BWR.
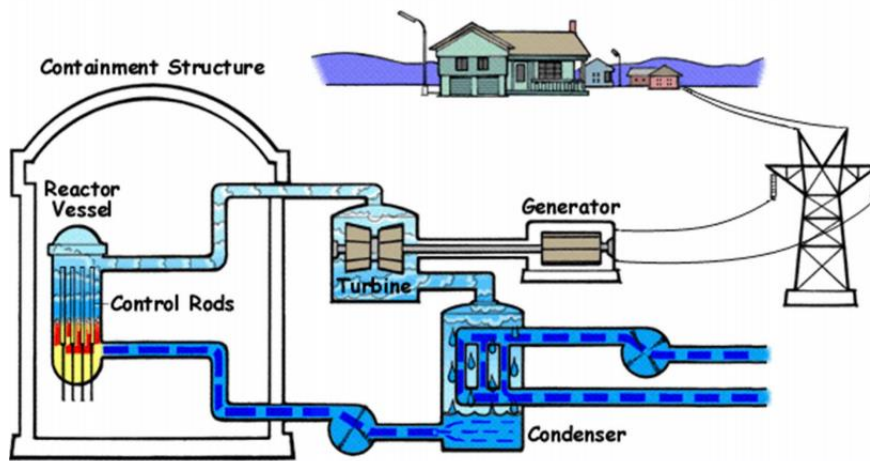
Figure 2. BWR schematic (NRC, 2015).
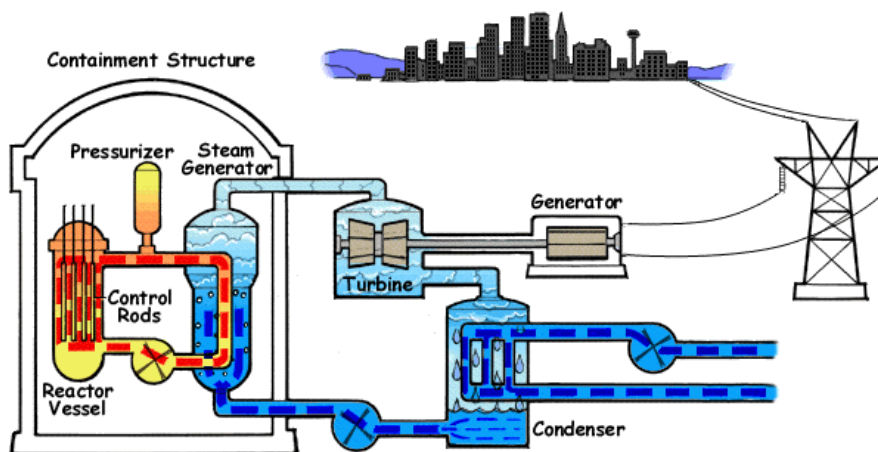
Figure 3. PWR schematic (NRC, 2015).

Naturally occurring uranium has ~0.7% U-235, which is the fissile isotope of uranium. The LWRs must use enriched uranium that has ~3.2% U-235. However, natural uranium can be directly used as the fuel in heavy water reactors (HWRs). In these reactors rather than light water (H_2O) as the coolant and moderator, heavy water (D_2O) is used. Though both H_2O and D_2O can absorb a neutron in a similar matter, D_2O already has an extra neutron that H_2O would normally absorb in LWRs. The extra neutrons not absorbed by D_2O may be used to promote further fission of uranium atoms. For this reason natural uranium may be used if D_2O is used as the coolant and moderator. One such reactor is the Canadian Deuterium Uranium (CANDU) reactor operating in Canada. It is a pressurized reactor that uses D_2O and natural, unenriched uranium to produce electricity.

Between 1970 and 2002 the development and interest of reactors decreased significantly. Several reactor accidents occurred between those years. 2 of these accidents were at the Three Mile

Island and Chernobyl nuclear power plants. In 1979 incident at the Three Mile Island plant in the US involved a cooling malfunction causing part of the core to melt in one of the reactors. However, there were no injuries or adverse health effects from this accident (World Nuclear Association, 2012). In Chernobyl, Ukraine, a reactor that was poorly designed had a steam explosion that released 5% of the radioactive core into the environment. 2 people died initially and many more died later due to radiation poisoning (World Nuclear Association, 2016). Interest in nuclear energy decreased until around 2002. Issues such as global warming, environmental concern and fossil fuel limitations have created a renewed interest in the use of nuclear energy. Nuclear energy is clean and has the ability to produce much more energy than renewable energy sources such as solar or wind energy. Much research has been put into making new designs that are superior to reactors currently in operation.

1.1.3 Advanced Nuclear Reactors

These new designs are called advanced nuclear reactors or Gen-IV reactors. Gen-IV nuclear reactors are presumably superior to the current nuclear reactors, particularly with respect to their sustainability, economics, safety and reliability, and proliferation resistance/physical protection characteristics (Galvez, 2011). Figure 4 shows preliminary designs for 6 alternative proposed next generation nuclear reactors. They all use different methods and different coolants for the transfer of heat. They all have the same purpose and that is to produce electricity or directly use the thermal energy for other industrial applications. One of the designs is the very-high-temperature reactor (VHTR) also called the high-temperature gas reactor (HTGR) shown as the top left design in Figure 4. This design uses a graphite-moderated nuclear reactor that can theoretically have an outlet temperature up to 1000 $^{\circ}$C as compared to ~300 $^{\circ}$C that is seen in a typical LWR. However, material limitations may decrease the actual outlet temperature that can be achieved.
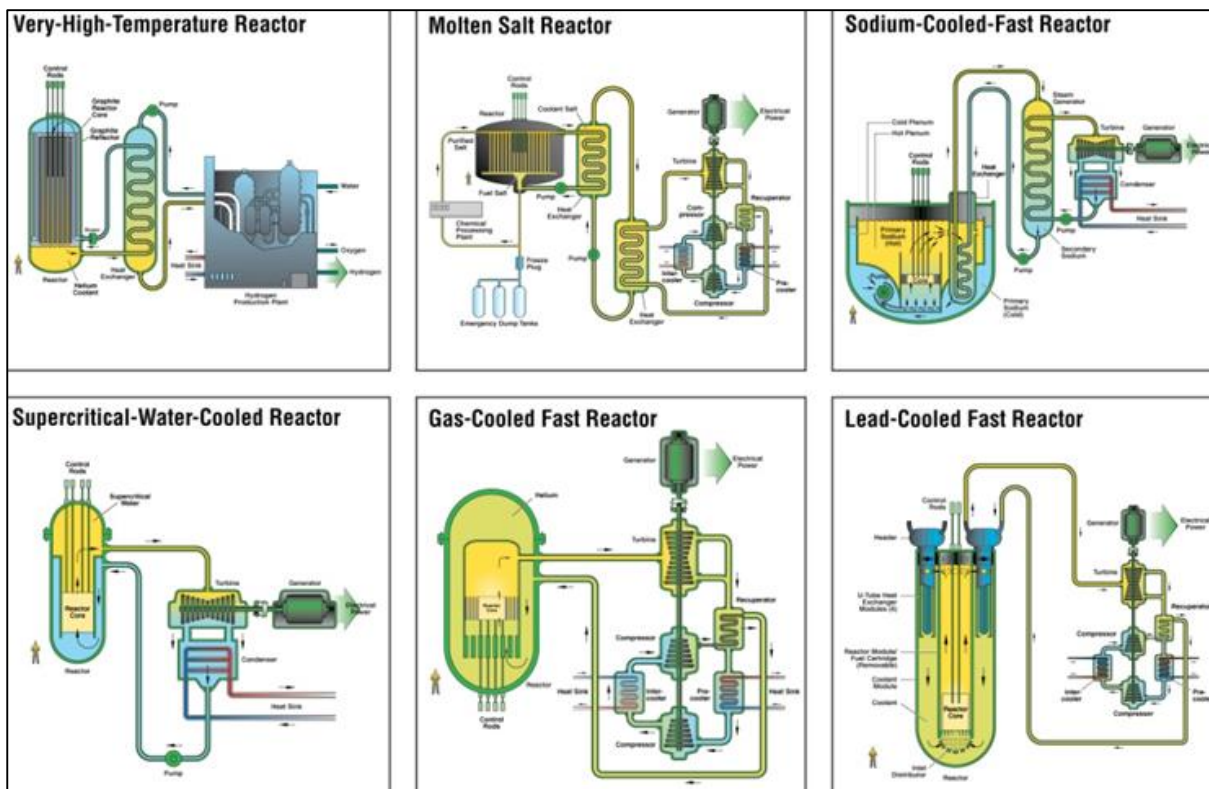
Figure 4. Concepts for 6 Gen-IV reactors (Gen-IV International Forum, 2016).

A variation of the VHTR being developed is the advanced high temperature reactor (AHTR), that utilizes the excellent heat transfer properties of molten salts to transfer nuclear heat for power production and other industrial applications (Sabharwall et al., 2009, 2010). Molten salts are a class of ionic liquids which are solid at standard temperature and pressure and become liquid at higher temperatures. They are mostly comprised of salts with elements from alkali metal (Li, Na, K), alkaline earth metal (Be, Mg, Ca), and halogen (F, Cl, Br) groups (Sohal et al., 2010). Temperatures as high as 700°C can be obtained in the first of a kind AHTR yielding high efficiency of conversion in these applications. These reactors will also be able to produce electricity with a higher efficiency than current reactors using the helium Brayton cycle. A typical AHTR system design involves 3 loops. The coolants in the primary and secondary loops are molten salts, while the process loop contains an inert gas that can be utilized in the Brayton cycle or other applications. A proposed design for the AHTR is shown in Figure 5 (Chen et al., 2015). This is a comprehensive diagram proposed for use as a Gen-IV reactor. The main components include the reactor, the intermediate heat exchanger (IHX), the secondary heat exchanger (SHX), and the direct reactor auxiliary cooling system (DRACS), which is used for passive heat removal. The power conversion unit (PCU) for electricity production is also shown on the right of Figure 5. The AHTR design is comprised of a combination of four existing

technologies 3 of which were stated above including the use of molten salts, Brayton power cycle, and passive safety systems. In addition, coated-particle graphite-matrix fuel is used in the reactor (Forsberg, 2004). This fuel is described in Appendix A. The primary function of the SHX is to transport thermal energy, in the form of heat, from the reactor to the downstream applications while isolating the upstream and downstream coolants from each other and providing a pressure boundary for the system (Sabharwall et al., 2012). Development of high-efficiency heat exchangers for salt-to-salt and salt-to-gas heat transfer is one of key research and development challenges for the AHTR system (Ingersoll et al., 2004). Successful deployment of AHTR systems requires increasing the technology readiness levels of the reactor as well as heat exchange system for stable operation and reliable process heat delivery (Sabharwall et al., 2015).
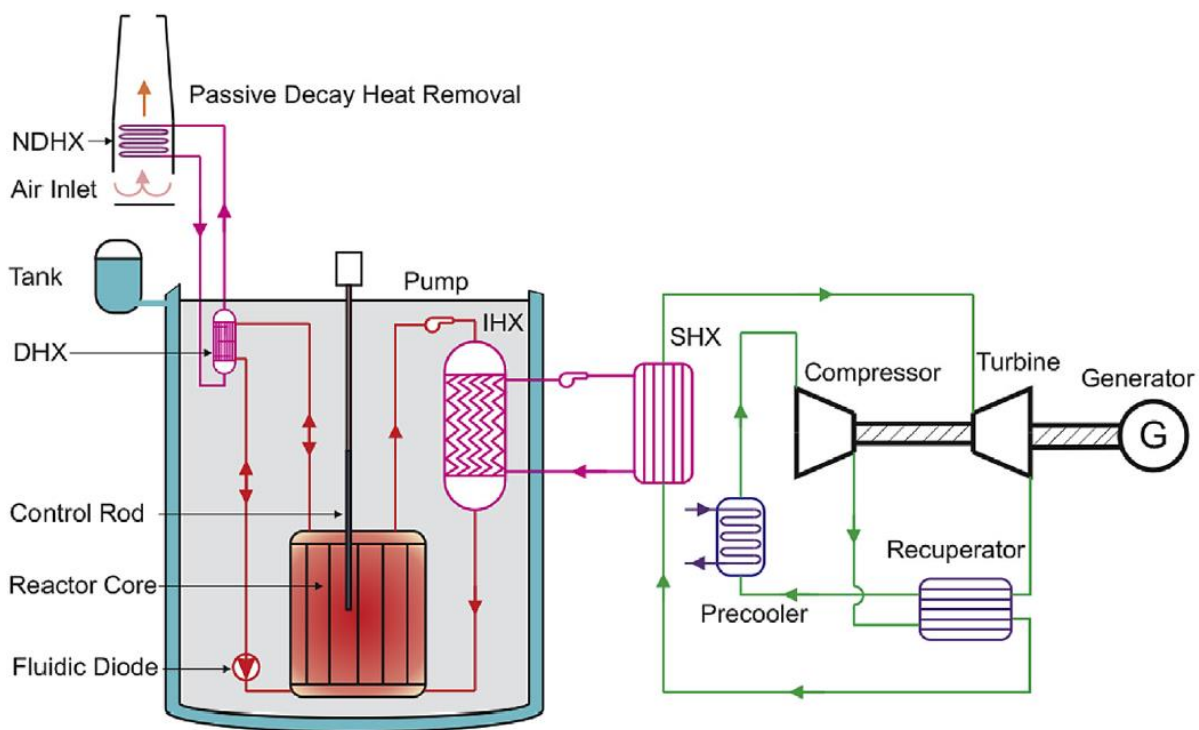
Figure 5. AHTR schematic showing reactor and heat exchangers coupled to Brayton cycle (Chen et al., 2015).

1.2 PROCESS HEAT APPLICATION

One of the improvements of Gen-IV reactors over current reactors is their ability to utilize the energy in additional applications other than electricity production such has hydrogen production. However, electricity production will still be a focus in the design of this reactor. Currently, in the PWR

and BWR a steam Rankine cycle is used. Gen-IV reactors will have the ability to use the helium Brayton cycle which has higher efficiencies than the steam Rankine cycle. Figure 6 shows a simplified schematic of the helium Brayton cycle. The coolant, helium, exits the SHX at a high temperature and enters the turbine. The energy from the turbine spins a generator in which electricity is produced. The pressure drops as the coolant travels through the turbine. The helium enters a recuperator in which the cold side stream exiting the compressor is heated up. Helium then travels through a precooler where water is used to cool down the helium before entering the compressor. Helium enters the compressor where the temperature and pressure of the coolant increase. Compressed helium travels through the recuperator heating up to the desired temperature before entering the SHX again. Control of the helium temperature exiting the SHX is of upmost importance because it has an effect on the overall efficiency of the Brayton cycle.
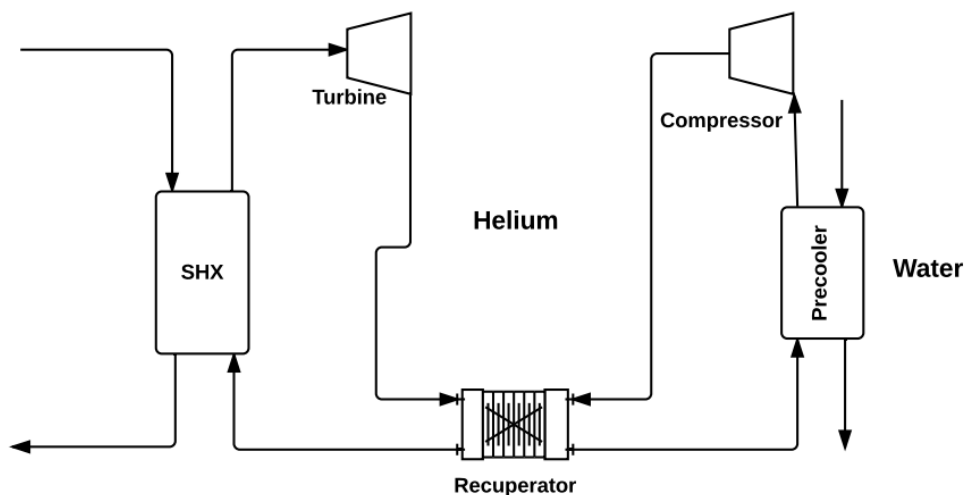
Figure 6. Helium Brayton cycle schematic.

In addition to electricity production, a number of other processes are possible that currently require fossil fuels to operate. Figure 7 shows the temperature ranges required for different processes (Gen-IV International Forum, 2013). Anything to the left of the line for LWRs at 300 °C is a process that is possible using current generation reactors. The line at 800 °C is for VHTRs. It can be seen that a number of other processes are possible when operating at this higher temperature including hydrogen production, cogeneration of electricity and steam, and oil shale processing.
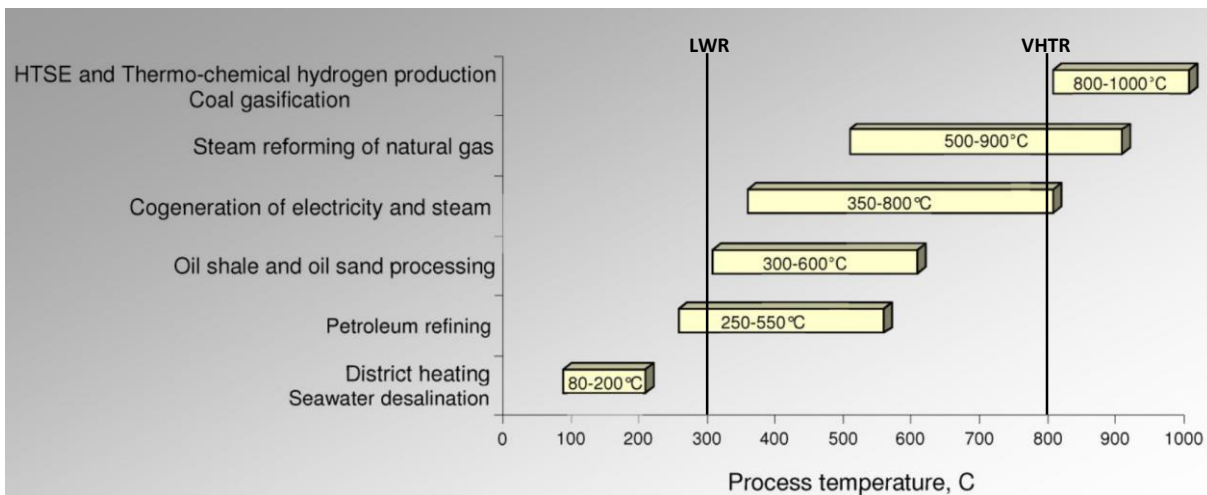
Figure 7. Processes and temperature range necessary to operate (Gen-IV International Forum, 2013).

Hydrogen production is the application that is of most interest for Gen-IV reactors. The production process requires high temperatures and can be achieved in a number of ways including steam reformation, electrolysis, or through thermochemical cycles. Currently, steam reformation of natural gas is the process used for hydrogen production. However, methane is already a high quality fuel and the process produces carbon emissions (Chapin et al., 2004). Therefore, it is expected to be phased out and is not considered as an option for next generation nuclear power plants (NGNP). Other processes include electrolysis or thermochemical cycles. Conventional and steam electrolysis are both being considered as hydrogen production methods. The high temperatures of the system and direct Brayton cycle will produce efficiencies higher than 50% while avoiding carbon emissions that would accompany fossil fuels-based processes (Chapin et al., 2004). In addition, several thermochemical processes are being investigated for sulfur-based cycles. These chemical processes are seen in Figure 8 and include the sulfur-iodine cycle, hybrid sulfur cycle, and sulfur-bromine cycle. The low temperature reactions for each sulfur based method are shown on the right of the figure. Each reaction produces hydrogen (H_2) and sulfuric acid (H_2SO_4). Sulfuric acid is then used in a high temperature reaction seen on the left of Figure 8. The base case requires a chemical reactor and a temperature of 850 °C while the alternative uses a membrane reactor and a temperature of 700 °C. Both produce oxygen (O_2) sulfur dioxide (SO_2) and water (H_2O). SO_2 and H_2O are then used for further hydrogen production. Of these processes the sulfur-iodine cycle is the most attractive because of its potential higher efficiency (Chapin, 2004). This process requires a temperature of around 900 °C for high efficiencies (Ragheb, 2014).
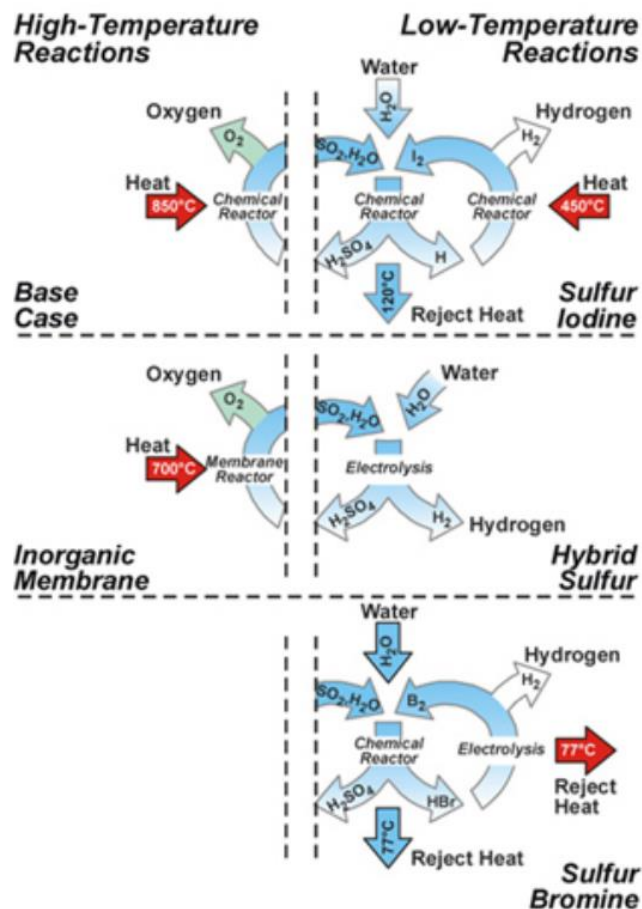
Figure 8. Different sulfur-based thermochemical cycles (Chapin et al., 2004).

1.3 CONTROL OF SYSTEM

The two main reasons for control are for process needs and electricity demand. The process is specifically designed to operate within a narrow range of temperatures and a certain minimum temperature is required to prevent process failure. For this reason certain temperatures must be controlled in order to keep the system running efficiently.

Electricity demand changes throughout the day and seasonally so it is important for electricity producing processes that the system have load following abilities. Load following is the ability for the reactor power to adjust when electricity demand changes throughout the day. This was not an aspect of nuclear reactors that was previously taken into account. If nuclear energy is going to produce a large part of the world's energy, it is necessary for reactors to have this ability. It has however been shown that nuclear reactors can have a great ability to load follow. Many reactors that

have been designed such as the AP600 and AP1000 can load follow up to ±5%/min within the power range of 30-100% (IAEA, 2004).

1.4 OBJECTIVES

The overall goal of this project is to create a control strategy for the AHTR system in order to keep efficiencies of the system high and to avoid any accidents from occurring. However, before getting to this point several objectives must be accomplished.

The design of the system must be determined. This includes the design of the reactor, IHX, and SHX. These designs will be based on system parameters that must first be chosen. Desired temperatures throughout the system can be chosen. From the power of the reactor, temperatures of the system, and design of the units, other system parameters such as flow rates, and heat transfer areas can be determined. Once the parameters of the system are determined analysis can begin.

The first objective of this research is transient analysis of the system. A number of realistic disturbances can be introduced into the system and the response can be analyzed. Disturbances in the system could be caused by breakages in the pipes, problems with the pumps, problems within the reactor, or problems within the process or power conversion unit (PCU). The disturbance will affect the temperatures and flow rates through the system and can have an effect on reactor and heat exchanger performance.

With a good understanding of the dynamics of the AHTR system, a control strategy can be developed. The control strategy can vary but has the goal of keeping the system efficient while also being able to avoid accidents from occurring. This could involve the control of a number of different system temperatures that are important to system efficiency.

The final objective is creating the model and simulating the control of the system. A model for transient analysis can be developed including the dynamics of the reactor, IHX, and SHX. Then the control strategy can be implemented by including controllers in the system. Similar to the transient analysis, different disturbances can be introduced and the system can be analyzed to see if it is desired variables are controlled. From the descriptions above, the three objectives of this research are summarized below.

1. To conduct transient analysis
2. To develop a control strategy
3. To simulate control of AHTR system

The following chapters of this thesis will go over the approach to completing these objectives. Chapter 2 will go over the system architecture and design. This goes over a system description, controlled system architecture and methodology, and controller development. Additionally in this chapter, simulation softwares used for transient analysis are described and differential equations are shown that describe the dynamics of the heat exchangers and reactor. Chapter 3 goes over the transient results of the AHTR system when using simulation software. Chapter 4 looks at the controlled system response of the AHTR system. This includes results for the coupled heat exchangers system and the coupled heat exchangers-AHTR system. Chapter 5 then goes into conclusions and future work for this project.

CHAPTER 2: SYSTEM ARCHITECTURE AND DESIGN METHODS

2.1 SYSTEM DESCRIPTION

A simplified diagram of the system is shown in Figure 9. A number of different molten salts have been researched for the use in the primary and secondary loops (Sohal et al., 2010). The molten salt chosen for the primary loop is FLiBe. This is a combination of LiF and BeF$_2$. For the secondary loop the molten salt chosen is FLiNaK, which is a combination of LiF, NaF, and KF. In the process loop Helium is chosen as the medium. The properties of these can be seen in Table 1.

Table 1. **Properties of FLiNaK, FLiBe, and helium.**

Coolant	Formula Weight (g/mol)	Freezing/ Melting Point (K)	Boiling Point (K)	Density (kg/m^3)	Specific Heat (J/kg.K)	Viscosity (Pa.s)	Thermal Conductivity (W/m.K)
FLiNaK	41.3	727	1843	2020	1882.8	0.0029	0.92
FLiBe	33.0	733	-	1940	2414.2	0.0056	1.0
Helium (P=7.5 MPa)	4	-	-	3.8	5505.3	0.00004	0.29
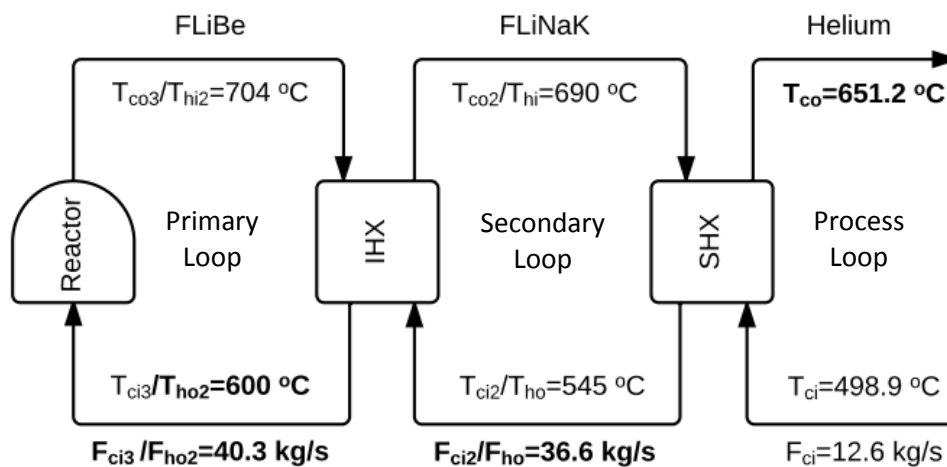
Figure 9. Process flow diagram of AHTR process.

Steady state system parameters are based off of previous work done by Chen et al. (2015) and Bartel et al. (2015). The nuclear reactor is where the fission process occurs and heats up the primary coolant (FLiBe) as it passes through. This coolant travels around the primary loop and enters the intermediate heat exchanger (IHX) where the heat is then transferred to the secondary coolant

(FLiNaK). This coolant travels around the secondary loop and enters the secondary heat exchanger (SHX) where it heats up the process coolant (Helium). This coolant is then utilized for either electricity production in the PCU or for another process (e.g. hydrogen production).

A brief explanation of the steady state design is described here. Temperatures of each of the streams are chosen. With the known temperature and coolant properties, the flow rates of each of the streams can be calculated from Eq. 1. Steady state heat transfer coefficients are based off a paper by Chen et al. (2015), which studies the same system. The IHX design is a fluted tube heat exchanger (FTHX), using spirally-fluted tubes to generate swirling flow to enhance the heat transfer. An example geometry for the FTHX is shown in Appendix B. The tube-side fluid is the primary coolant FLiBe; the shell-side being the secondary coolant FLiNaK. Heat transfer coefficients are based off of a model developed by Garimella (1990). The SHX is an offset strip-fin heat exchanger (OSFHX), a plate-type heat exchanger where flow channels are chemically etched into each plate. The plates are then diffusion bonded with alternate plates providing flow channels for cold and hot fluids. A unit cell of the OSFHX is shown in Appendix B. The offset strips disrupts the flow pattern and prevents large boundary layers from being formed which promotes heat transfer. The SHX cold-side fluid is helium. Heat transfer coefficients are based off a model developed by Manglik and Bergles (1995). With the known steady state heat transfer coefficients and the use of Eq. 3, the heat transfer area required can be calculated from Eq. 2.

$$Q = FC_p\Delta T \tag{1}$$

$$Q = UA\Delta T_{lm} \tag{2}$$

$$\Delta T_{lm} = \frac{(T_{hi}-T_{co})-(T_{ho}-T_{ci})}{ln\left(\frac{T_{hi}-T_{co}}{T_{ho}-T_{ci})}\right)} \tag{3}$$

Where Q is the heat duty, F is the flow rate, C_p is the heat capacity, ΔT is the temperature difference for the fluid, U is the overall heat transfer coefficient, A is the heat transfer area, ΔT_{lm} is the log mean temperature difference between the cold- and hot-side fluids, the subscripts *h, c, i,* and *o* stand for hot, cold, inlet, and outlet, respectively. Table 2 shows the steady state values that are used for the reactor, IHX and SHX in the software simulations and MATLAB codes that will be described. Initially, only models for the heat exchangers were included, adding in models for the reactor in later simulations. Reactor characteristic and heat transfer coefficient equations are described in a paper by Chen et al. (2015).

Table 2. **Steady state design parameters for AHTR.**

Variable	Units	IHX cold	hot	SHX cold	Hot	Reactor
T_{in}	K	818	977	772	963	873
T_{out}	K	963	873	924.5	818	977
ΔT	K	145	104	152.3	145	104
F	kg/s	36.6	40.3	12.6	36.6	40.3
Q	kW	10000		10000		10000
ΔT_{lm}	K	30		42.3		-
U	W/(m^2 K)	775		2181		9309
A	m^2	430.1		108.4		

2.2 CONTROL SYSTEM ARCHITECTURE

The ultimate goal of this research is to create a control strategy that is able to control chosen parameters such that the efficiencies of the system remain high. This involves creating a control system architecture for the system. The variables that we want to control (e.g. temperature) will be controlled by manipulation of another parameter (e.g. flow rate) in the system. After a disturbance the system will be controlled around the set point values that are specified.

Both heat exchanger and reactor control have been researched on a singular basis. Dynamic models were created and a fuzzy logic controller developed for plate type heat exchanger (Al-Dawery et al., 2012). Other investigators employed a model based approach that used the total energy stored in the heat exchanger by the two coolants as the variable of interest rather than the outlet temperatures. These controls were then tested by simulating the models for a single heat exchanger (Michel and Kugi, 2014). It should be noted that the total thermal energy stored in the heat exchanger is a derived quantity which requires the knowledge of inlet and outlet temperatures. No integral action is performed by their control system, as would be when using a PI (Proportional-Integral) or PID (Proportional-Integral-Derivative) controller. Integral action is important for mitigating oscillations and offset in control.

In addition for reactors, fuzzy PID controller were examined for plant control by Pan et al. (2011). Fuzzy logic controllers work well with nonlinear systems, such as a reactor. The controller was optimized and compared with a traditional PID controller. Controller actions for a PID controller were much larger than fuzzy PIDs and it was found that the fuzzy controller performed better in most cases. Das et al. (2013) developed this further by introducing a fractional order PID (FOPID)

controller. This controller has an additional advantage of robustness over a fuzzy PID controller. The fuzzy FOPID is robust when tuned at any variety of power levels while a fuzzy PID must be tuned at the highest power level to serve its optimal purpose. Though the fuzzy PID and fuzzy FOPID controllers are robust and show great ability to control the reactor, the addition of two heat exchangers adds greater complexity to the system. This is the first novel study to have looked at the control of the entire system including the reactor and two heat exchangers. For this reason PID controllers will be used throughout the system. Figure 10 shows a possible control design of the AHTR system and is described in detail in section 2.2.1.
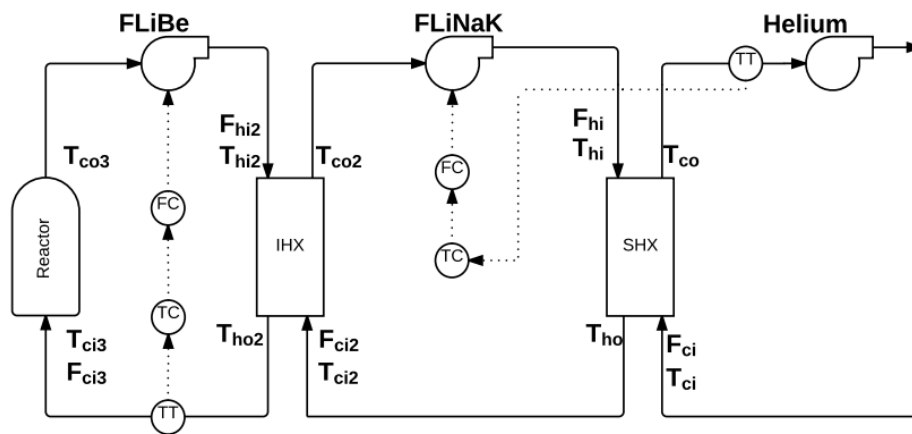
Figure 10. Possible design for control of AHTR system.

2.2.1 Control Methodology

The first step in the design of a control system is the identification and selection of the controlled variables (variables maintained at desired set-point values) and manipulated variables (variables changed in order to maintain the controlled variables at their set points). For the SHX, the controlled variable is chosen to be the cold side outlet temperature (T_{co}) of the process coolant. The process coolant travels through the process loop and is used either to generate electricity or provide thermal energy to drive a chemical process. Processes are designed to operate at specified temperatures, and the temperature difference between the process coolant and design temperature provides the necessary driving force for its operation. Controlling the process coolant temperature (T_{co}) will maintain the necessary driving force at the desired value, enabling the process to operate at the optimum efficiency. This control is accomplished by using the hot side flow rate (F_{hi}) or the cold side flow rate (F_{ci}) as the manipulated variable. Other variables, called load variables, represent

disturbances that will have an effect on the controlled variable. For the SHX, the load variables include the hot and cold inlet temperatures (T_{hi}, T_{ci}) and the flow rate that is not the manipulated variable (F_{ci} or F_{hi}).

The controlled variable for IHX is the hot side outlet temperature (T_{ho2}). This is the temperature of the primary coolant entering the nuclear reactor. Fluctuations in this temperature will have an effect on the reactivity and thus the power of the reactor, which is undesirable. The hot side flow rate (F_{hi2}) or the cold side flow rate (F_{ci2}) is used as the manipulated variable. The load variables include the hot and cold inlet temperatures (T_{hi2}, T_{ci2}) and the flow rate that is not the manipulated variable (F_{ci2} or F_{hi2}). It is important to note that if F_{ci2} is the manipulated variable of the IHX, F_{ci} must be the manipulated variable for the SHX because F_{ci2} and F_{hi} are the same flow rate.

If control using the reactor is desired, as will be seen in section 4.2.4, then a controller for the reactor will also be included. The controlled variable for the reactor is the neutron density (n) which is proportional to reactor power. This is done by manipulating the reactivity with control rod movement (ρ_{rod}). The load variable of the reactor are the coolant mass flow rate (F_c), the reactor inlet temperature (T_i), the reactor outlet temperature (T_e), and the fuel temperature (T_f). Table 3 shows the controlled, manipulated, and load variables for each of the units in the system.

Table 3. **Summary of controlled, manipulated and load variables.**

Process Unit	Controlled Variable	Manipulated Variable	Load Variables
SHX	T_{co}	F_{hi} or F_{ci}	F_{ci} or F_{hi}, T_{ci}, T_{hi}
IHX	T_{ho2}	F_{hi2} or F_{ci2}	F_{ci2} or F_{hi2}, T_{ci2}, T_{hi2}
Reactor	n	ρ_{rod}	F_c, T_i, T_e, T_f

2.2.2 Block Diagrams

Control block diagrams are created to represent the control strategy for each heat exchanger. Figures 11 and 12 show the block diagrams for the SHX and IHX, respectively. Each block in these figures represents a transfer function which relates the variables entering and leaving the block. Each variable within the block is expressed as the deviation from the steady state values of that particular parameter. For example, the topmost block in Figure 11 relates the deviation in the cold stream outlet temperature (ΔT_{co}) from its steady state value to the deviation in the temperature of the hot inlet stream (ΔT_{hi}) from its steady state value. These two deviations are related by the transfer function G_{S4}. The asterisk on a variable (for example, ΔT_{co}*) indicates a set-point value

which is 0. Both the block diagrams are structured identically, differing only in the controlled and manipulated variables, and the transfer functions. For each diagram G_c is the controller transfer function, G_v is the valve or pump transfer function and G_S/G_I are the process transfer functions for the SHX and IHX, respectively.

The process transfer functions (G_S/G_I) represent the mathematical relationships between the controlled variables and the manipulated variable or load variables. Referring to Figure 11, the transfer functions G_{S2}, G_{S3} and G_{S4} represent the transfer functions which effectively convert the deviations (or disturbances) in the load variables F_{ci}, T_{ci} and T_{hi}, respectively, to the deviation in the controlled variable T_{co}. G_{S1} is the transfer function between the controlled (T_{co}) and the manipulated variable (F_{hi}). All the deviations are summed up at the summation point at the right end of the figure, and total deviation is compared to the set-point at the summation junction at the left end of the figure. The error signal (E1) generated is sent to the controller (G_{cS}). Depending on the error and the controller algorithm, the controller sends an output signal (P1) to the valve transfer function block. The manipulated variable F_{hi} is changed based on the valve transfer function (G_{vS}), to keep the controlled variable at its desired value.
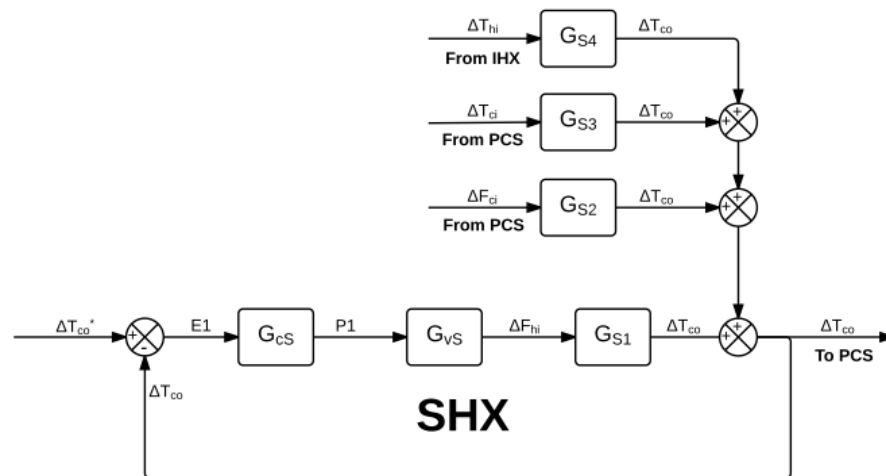
Figure 11. Block diagram for SHX control.
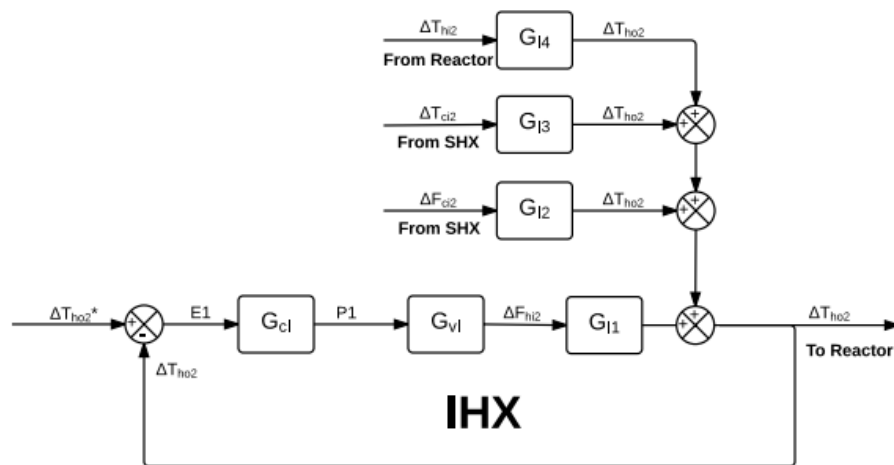
Figure 12. Block diagram for IHX control.

The transfer function for the controller is shown in Eq. 4. It is the characteristic equation for a PID controller, with a proportional, integral, and derivative gain value to control precisely the system based on a given error value.

$$G_c = K_P + K_I \frac{1}{s} + K_D s \tag{4}$$

The transfer function for the valve or pump is shown in Eq. 5. This function has a gain value (K_v), which is just set to 1, and a time constant (τ_v) which determines the time it takes the pump to adjust. This is taken to be 0.05 seconds, which is a near instantaneous response.

$$G_v = \frac{F(s)}{P(s)} = \frac{K_v}{\tau_v s + 1} \tag{5}$$

Eqs. 6-9 show transfer functions for the SHX relating to changes in the cold outlet temperatures based on changes of the other variables. The gain value (K) relates how outlet temperature, in this case the cold side, changes from the initial steady state value with changes in either the manipulated variable or load variables. For example, K_{cFh} is ~1.5 °C/(kg/s) meaning that if the hot side flow rate changes by 1 kg/s the cold side outlet temperature will change by 1.5 °C. The time constant (T) determines the time it takes for the heat transfer. In Eq. 7 there is an extra variable, τ_c, which is a time delay term for the cold side of the SHX. This exists because changes in the cold inlet temperature will not immediately effect the cold outlet temperature. There is a certain amount of time it takes for the coolant to travel through the heat exchanger. Until this occurs effects from changes in the cold inlet temperature will not be seen. The other 4 transfer functions for the SHX and the equations used to calculate the gain and time constant values can be found in Appendix C.

Equations for the IHX are identical to those for SHX. The only difference are different gain values and time constants.

$$G_{S1} = \frac{\Delta T_{co}}{\Delta F_{hi}} = \frac{K_{cFh}}{T_c s+1} \tag{6}$$

$$G_{S2} = \frac{\Delta T_{co}}{\Delta F_{ci}} = \frac{K_{cFc}}{T_c s+1} \tag{7}$$

$$G_{S3} = \frac{\Delta T_{co}}{\Delta T_{ci}} = \frac{K_{ctc}e^{-\tau_c s}}{T_c s+1} \tag{8}$$

$$G_{S4} = \frac{\Delta T_{co}}{\Delta T_{hi}} = \frac{K_{cth}}{T_c s+1} \tag{9}$$

2.2.3 Controller Development

The gain, time constant and time delay values in the transfer functions described above are determined by coolant properties and the system geometry. Designing the controller requires specifying the gain and time constants in the characteristic equation for the controller. A built-in MATLAB function was used called pidtool in order to do this. This function opens a PID tuner graphical user interface (GUI) and chooses proportional, integral, and derivative gain values for the system. The equation used for tuning must first be determined. In this case for each exchanger this will be the valve transfer function (G_v) multiplied by the transfer function that relates how the controlled variable changes with variation of the manipulated variable (G_{S1}/G_{I1}). Eq. 10 and 11 shows the transfer functions used to tune the controllers for the SHX and IHX, respectively. Table 4 and 5 show the tuned controller for P, PI, and PID options. These are tuned parameters when both hot side flow rates are being used as the manipulated variables. If the cold side flow rates are used as manipulated variables, two different controller settings must be used. Eq. 12 and 13 are used for tuning in that case and the resulting controller parameters are shown in Table 6. Initial simulations only look at the control of the coupled IHX and SHX system and thus a controller for the reactor is not implemented. In later results a reactor controller is used to control the system as well. The controller implemented will control neutron density (n) by manipulating the control rods (ρ_{rod}). Similar methods were used for controller tuning and the PID gain values are also shown in Table 6. Stability analysis for the IHX and SHX can be found in Appendix D.

$$G_{vS}G_{S1} = \frac{1}{0.05s+1} * \frac{K_{cFh}}{T_c s+1} \tag{10}$$

$$G_{vI}G_{I1} = \frac{1}{0.05s+1} * \frac{K_{hFh2}}{T_{h2}s+1} \tag{11}$$

Table 4. **SHX controller tuned parameters (Hot side flow rate).**

Controller	K_P (°C*s/kg)	K_I (°C*s/kg)	K_D (°C*s/kg)
P	10.712		
PI	0.7994	0.7680	
PID	0.7976	0.9683	0.1643

Table 5. **IHX controller tuned parameters (Hot side flow rate).**

Controller	K_P (°C*s/kg)	K_I (°C*s/kg)	K_D (°C*s/kg)
P	14.236		
PI	0.4296	0.2054	
PID	0.6163	0.3821	0.2353

$$G_{vS}G_{S2} = \frac{1}{0.05s+1} * \frac{K_{cFc}}{T_c s+1} \tag{12}$$

$$G_{vI}G_{I2} = \frac{1}{0.05s+1} * \frac{K_{hFc2}}{T_{h2}s+1} \tag{13}$$

Table 6. **PID controller parameters for IHX, SHX (Cold side flow rates) and reactor.**

HX	K_P (°C*s/kg)	K_I (°C*s/kg)	K_D (°C*s/kg)
SHX	-0.1695	-0.2057	-0.0349
IHX	-0.6985	-0.4331	-0.2666
Reactor	0.461	0.621	0.0329

2.2.4 Disturbances in System

The need for control is necessary for multiple reasons. First of all the grid demand changes on an hourly, daily, and seasonal basis. For this reason, the reactor power should have the ability to be controlled in order to follow the demand. Secondly, there is a chance that an accident may occur in the system. If this happens there may be changes in flow rates and temperatures throughout the system. Table 7 shows a list of possible disturbances that could occur in the system. These include small or large loss of coolant accidents (LOCA), pump malfunction, process problems causing changes in heat removal, or control rod malfunctions in the nuclear reactor. A small LOCA is defined as a pipe break in which the reactor remains pressurized. This is considered to be a break of up to 12 cm in the primary loop but can vary depending on the system. A large LOCA can be a rupture of a pipe connected to the circulating pump with the reactor vessel. The effect of the large LOCA will depend

on the system as well (Ragheb, 2013). Each has an effect on the system parameters and can be small or large depending on the severity. Table 7 shows how each disturbance would affect each loop in the AHTR system as well as the reactor. For example, a small LOCA in the process loop, seen as the top example of Table 7, would cause the helium flow rate to decrease slightly. That would cause an increase in the temperatures of FLiNaK and FLiBe in the secondary and primary loops, respectively. Due to negative reactivity effects an increase in FLiBe temperature entering the reactor would cause a decrease in the power output of the reactor. This will be seen when looking at the equations for the reactor in section 2.4.2.

Table 7. **Possible disturbances and their effects on the system.**

Disturbance	Process Effect	Secondary Effect	Primary Effect	Reactor Effect
1. Small LOCA in process loop	Lower helium flowrate (T ↑)	Higher FLiNaK temperature	Higher FLiBe temperature	Lower reactor duty
2. Large LOCA in process loop	Much Lower helium flowrate (T ↑)	Much Higher FLiNaK temperature	Much Higher FLiBe temperature	Much Lower reactor duty
3. Small LOCA in secondary loop	Lower helium temperature	Lower secondary flowrate	Higher FLiBe temperature	Lower reactor duty
4. Large LOCA in secondary loop	Much Lower helium temperature	Much Lower secondary flowrate	Much Higher FLiBe temperature	Much Lower reactor duty
5. Small LOCA in primary loop	Lower helium temperature	Lower FLiNaK temperature	Lower primary flowrate	Lower/higher reactor duty
6. Large LOCA in primary loop	Much Lower helium temperature	Much Lower FLiNaK temperature	Much Lower primary flowrate	Much Lower reactor duty
7. Process pump malfunction(2)	Higher helium flowrate (T ↓)	Lower FLiNaK temperature	Lower FLiBe temperature	Higher reactor duty
8. Secondary pump malfunction(2)	Higher helium temperature	Higher secondary flowrate	Lower FLiBe temperature	Higher reactor duty
9. Primary pump malfunction(2)	Higher helium temperature	Higher FLiNaK temperature	Higher primary flowrate	Lower/higher reactor duty
10. Lower process heat removal	Higher helium temperature	Higher FLiNaK temperature	Higher FLiBe temperature	Lower reactor duty
11. Higher process heat removal	Lower helium temperature	Lower FLiNaK temperature	Lower FLiBe temperature	Lower reactor duty
12. Control rod malfunction(ρ_{rod} ↑)	Higher helium temperature	Higher FLiNaK temperature	Higher FLiBe temperature	Initial higher reactor duty.
13. Control rod malfunction(ρ_{rod} ↓)	Lower helium temperature	Lower FLiNaK temperature	Lower FLiBe temperature	Initial lower reactor duty

2.3 SIMULATION SOFTWARE

Modeling and simulation of the dynamic behavior of such a system becomes a challenging task. User-developed computer codes can reach a high level of complexity, and the computational effort can increase significantly. At the same time, several commercial process simulation software packages are available for steady state and dynamic simulation of highly complex processes, and are routinely used in the chemical industry. The softwares used for simulation include PRO-II (steady state behavior) and DYNSIM (dynamic behavior) offered by SimSci Division of Schneider Electric, Lake Forest, CA (www.schneider-electric.com/simsci/)

2.3.1 PRO-II

PRO-II is a professional simulation tool that performs rigorous mass and energy balances for various processes and can be used for process design, operational analysis and optimization. In this work, PRO-II was used to design the components, primarily the IHX and SHX, of the system. The basic procedure consisted of

1. drawing the flowsheet which involved using available equipment components and connecting them with appropriate process streams,
2. specifying the components (chemical species) involved in the process,
3. entering the available data,
4. specifying design constraints, and
5. running the simulation to obtain steady state solution of global mass and energy balance

The resulting flow sheet is shown in Figure 13.
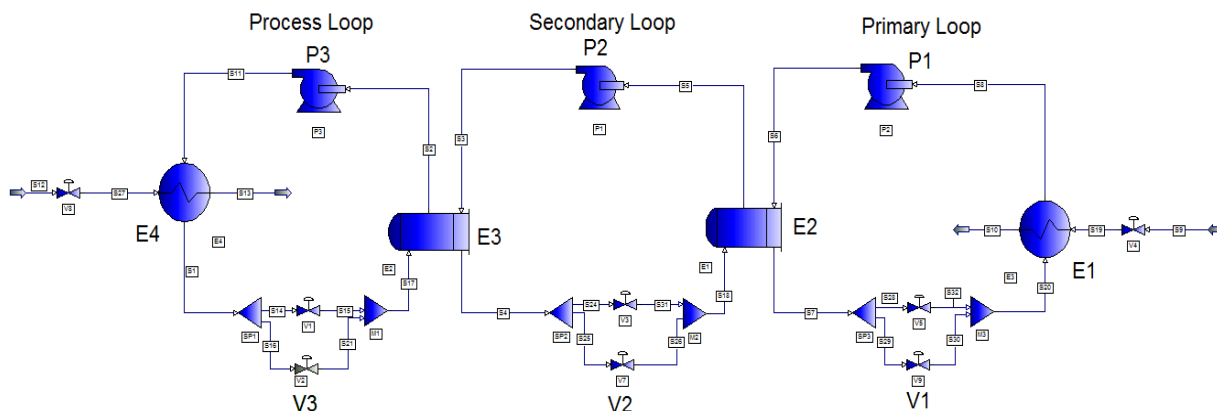
Figure 13. Process flow diagram created in PRO-II.

The main components of the flowsheet are listed in Table 8.

Table 8. **PRO-II process flow diagram description.**

Symbol	Process
E1	Reactor
E2	IHX
E3	SHX
E4	Process or PCS
P1	Primary pump
P2	Secondary pump
P3	Process pump

It should be noted that PRO-II (as any other process simulation software) does not have the nuclear reactor as a process unit, and hence in this simulation it is represented simply by a heat exchanger (E1). The process heat load or power conversion system (PCS) is also modeled as a heat exchanger with a constant duty. FLiBe and FLiNaK are specified as user defined components with appropriate physical property specifications. Helium was added as a component from the list of in-built components.

For each of the two heat exchangers, heat duty, heat transfer area and overall heat transfer coefficient were specified. For each loop, the flow rate, pressure and initial guess for the temperature of one stream was provided. The values entered were calculated as described in Section 2.1. Heat exchanger pressure drop values reported by Chen et al. (2015) were used to specify the pressure rise across the pump in each loop. After all of the values have been entered, the software solves for the steady state temperatures for each of the streams converging to a solution within a few seconds. The flow sheet with converged solution can then be exported to DYNSIM for transient analysis.

2.3.2 DYNSIM

The transient or dynamic behavior of the system is simulated using DYNSIM, a comprehensive dynamic simulator. A dynamic process flowsheet is generated in DYNSIM when the steady-state flowsheet is exported from PRO-II using its command menu. Figure 14 shows the dynamic flowsheet created in DYNSIM, when the flowsheet shown in Figure 13 is exported from PRO-II. The resemblance between the two flowsheets can be seen clearly. DYNSIM automatically adds several units such as valves, splitters and storage tanks that are essential to run the dynamic simulation.
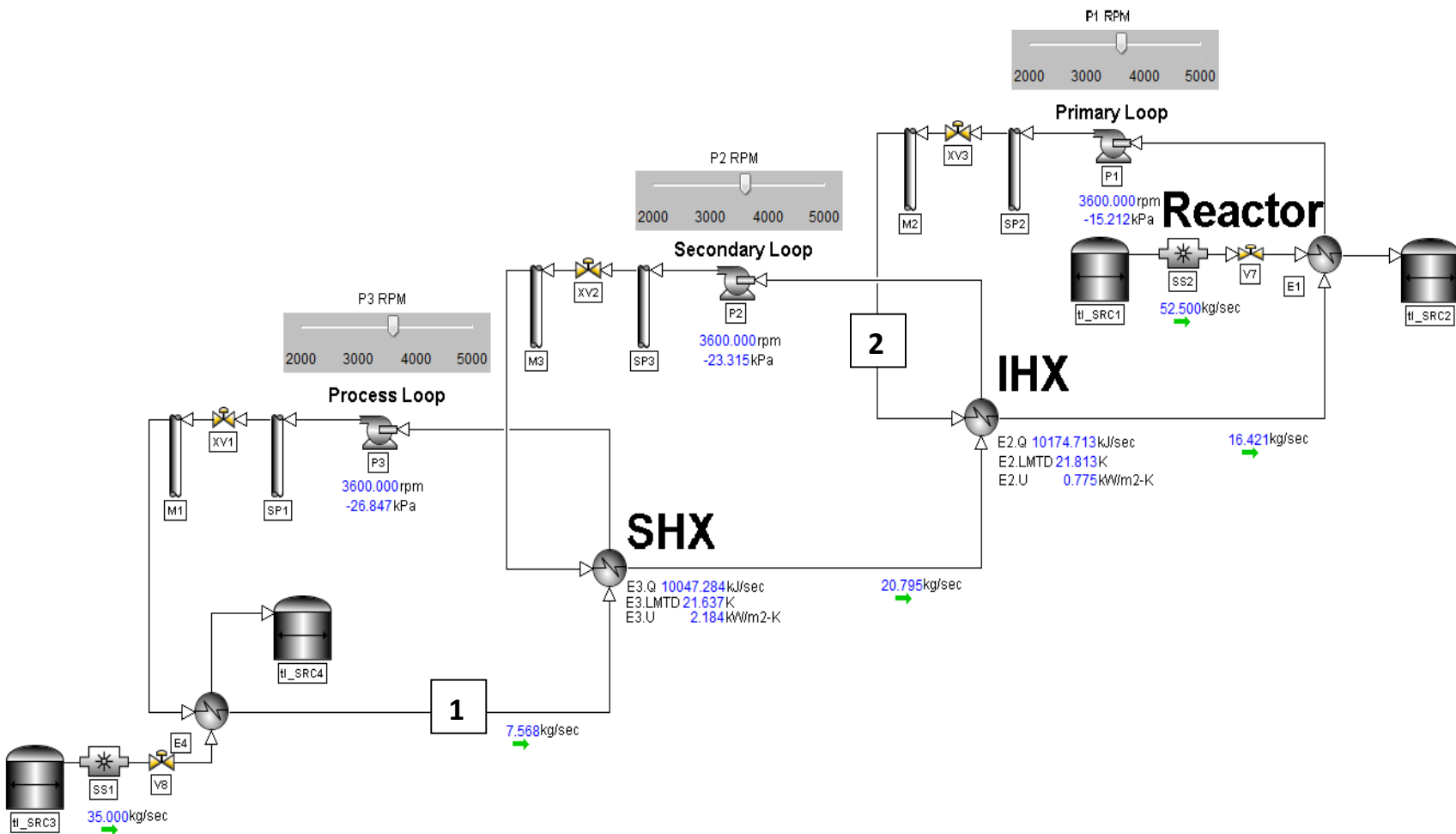
Figure 14. Process flow diagram designed in DYNSIM.

Most of the process unit characteristics and values are automatically imported from the specifications made in the PRO-II flow sheet. However, since this is a dynamic simulator, additional specifications that describe the dependence of parameters on operation variables needs to be fed into the simulator. The most significant of these inputs involves specifying the dependence of the heat transfer coefficients of the heat exchangers on the process stream flow rates. This dependence is obtained from the relevant heat transfer correlations that describe the dependence of the Nusselt number on the Reynolds number. The equations for these are described in the paper by Chen et al., (2014).

The different scenarios shown in Table 7 can then be simulated using DYNSIM. The set-up in Figure 14 can be used for any flow disturbance such as a break in a pipe or pump malfunction by adjusting the RPMs of the pumps. A different program must be created to incorporate temperature disturbance that could be seen from problems in the process or reactor. This is accomplished by incorporating a tank in the system where the disturbance would be seen. At steady state the tanks marked 1 and 2 in Figure 14 have the same inlet and outlet temperature. To incorporate the temperature step entering the cold side of the SHX or hot side of the IHX, an outlet temperature higher or lower than the initial steady-state value is specified in the tank. This then acts as a temperature disturbance entering into the reactors. For example in the process loop the initial value entering the tank is 977 K. In the tank an outlet temperature of 1007 K is specified. This then acts as a +30 K temperature disturbance entering the hot side of the IHX. For the process the tank is added directly before entering the cold side of the SHX, marked 1 in Figure 14. For the reactor the tank is added before entering into the hot side of the IHX, marked 2 in Figure 14.

2.3.3 Simulink Model

Simulink is a useful tool built into MATLAB. It is helpful when dealing with dynamic systems like this one. It can seamlessly combine all of the different elements to simulate the dynamic changes. In addition, a control system can be added to simulate control of the heat exchangers. A model was developed including a control for each heat exchanger, a valve for each loop, and the process transfer functions for the heat exchangers that have been described above. These functions are as described in section 2.2.2. Figure 15 shows a flowchart of the model developed in Simulink. The model takes the block diagrams seen previously and combines them into one system. Changes in one heat exchanger are seen in the other heat exchanger. Because of this control can be quite complicated.
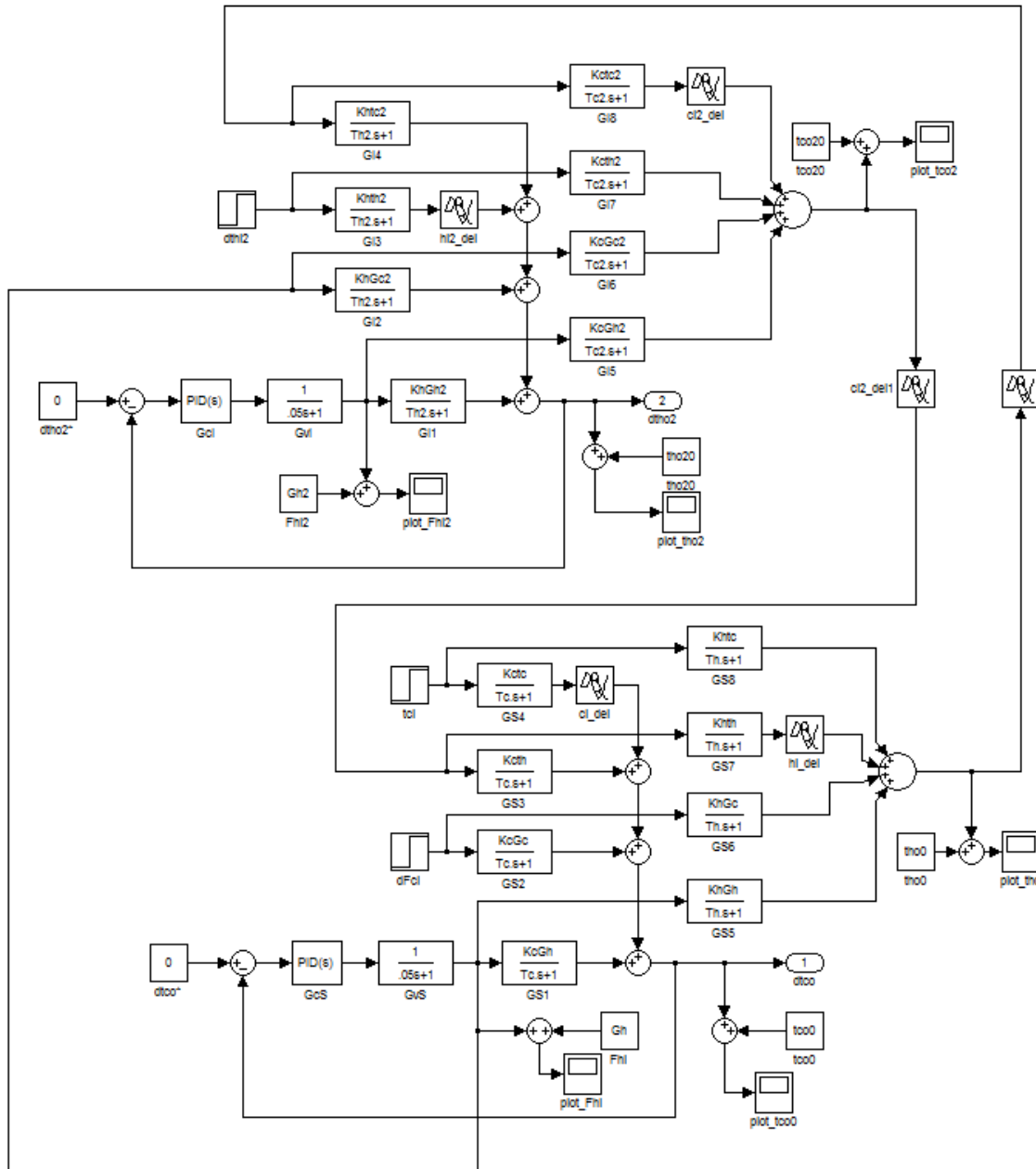
Figure 15. Simulink model developed for IHX/SHX coupled system.

2.4 DYNAMIC VARIABLE CODE

Initially a Simulink model was created to simulate the control of the heat exchangers as shown above. This model would be used as a backbone in creating the code described. Though the Simulink model worked well and was able to simulate the control of the system, it had some limitations. The gain values (K), time constants (T), and time delay values (τ) did not change as the

system changed. In reality all these would change as the flow rate did. Though a variety of different programs could be used to create the model, MATLAB was chosen. A MATLAB code was created using the Simulink model as a backbone. With the created code the system is much more dynamic. Several changes are made including:

- Changing gain values
- Changing time constants
- Changing time delays

These change due to changes in flow rate which in turn effects the velocity of the fluids and the heat transfer coefficients. These heat exchangers are chosen for their compactness and heat transfer capabilities. The MATLAB code can be used to simulate disturbances and control of the system. By comparing with the Simulink model, one can see if the code is accurate.

Simulations were analyzed with the code using the transfer functions for the heat exchangers. However, as work progressed differential equations were substituted for the transfer function in the MATLB code. This was thought to have added accuracy but would result in larger computational load. In addition, at this time the reactor differential equations were also included into the code. The equations and solution method are described in the following sections. The code used for many of the simulations is shown in Appendix E.

2.4.1 System Model: Governing Equations for Heat Exchangers

The representative governing equations for a heat exchanger are obtained by the energy balance and are shown Eqs. 14-16. Eq. 14 is the energy balance for the hot stream, Eq. 15 is the energy balance for the cold stream, and Eq. 16 represents the energy balance for the wall separating the two streams, written for a differential element of the heat exchanger.

$$m_h C_{ph} \frac{dT_h}{dt} + F_h C_{ph}(T_{ho} - T_{hi}) = (hA)_h (T_w - T_h) \tag{14}$$

$$m_c C_{pc} \frac{dT_c}{dt} + F_c C_{pc}(T_{co} - T_{ci}) = (hA)_c (T_w - T_c) \tag{15}$$

$$m_w C_{pw} \frac{dT_w}{dt} = (hA)_h (T_h - T_w) - (hA)_c (T_w - T_c) \tag{16}$$

Where m is the mass of the fluid or metal in the element, C_p is the heat capacity of the fluid or metal, $\frac{dT}{dt}$ is the rate of change in temperature over time, h is the heat transfer coefficient, A is the heat transfer area, and F is the flow rate. The subscripts $h, c, w, i,$ and o stand for hot, cold, wall,

inlet, and outlet, respectively. The first term in each of the equations is the energy accumulation term, which would be zero at steady state. The second term in Eqs. 14 and 15 represents the difference in the energy of the fluid leaving and entering the element by convection. The terms on the right hand side of the equations represent the convective heat transfer between the fluid and the wall. The energy balance for the wall does not involve the convective flow term, but has two heat transfer terms representing convective heat transfer from the hot fluid to the wall and wall to cold fluid. Both IHX and SHX will have a similar set of three equations, with the parameter values that correspond to the properties of the respective streams. Each heat exchanger is discretized and a hot temperature, cold temperature, and wall temperature can be solved for at each node. The node is defined by the uniformity of each temperature at the node (no spatial variation within the node). Again heat transfer coefficients are as described in the system description section.

2.4.2 System Model: Governing Equations for Reactor

The reactor dynamics is described by a series of differential equations that include the neutronics equations with one to six groups of delayed neutrons, as well as energy balances for the fuel, and coolant. In this work the equations based off a paper by Das et al. (2013) have been used, and are reproduced below (Eqs. 17-21). An explanation of the parameters in these equations are described in more detail in Appendix A.

Eq. 17 is for the dynamic neutron density balance,

$$\frac{dn}{dt} = \frac{\rho - \beta}{\Lambda} n + \sum_{i=1}^{G} \lambda_i c_i \tag{17}$$

Where n is the neutron density, ρ is the reactivity (0 at steady-state), β is the delay neutron fraction, Λ is the prompt neutron lifetime, λ_i is the decay constant for group i, and c_i is the precursor concentration for group i. There are up to 6 different precursors. These are the groups that do not emit neutrons instantaneously and only account for a small fraction of the fission products.

The precursor balance is shown by Eq. 18.

$$\frac{dc_i}{dt} = \frac{\beta_i}{\Lambda} n - \lambda_i c_i \quad for\ i=1,2,...,G \tag{18}$$

Where β_i is the delay neutron fraction for delay neutron group i, and G is the number of delay groups. The delay fraction, β from Eq. 17, is the summation of all delay neutron fractions, β_i, and is equal to 0.006502 in all cases. This is the delay neutron fraction for U-235 which is the fuel used in the AHTR. There can be 1 to 6 equations for precursor concentrations depending on how

many delay groups is chosen to be used. For example, if 3 groups are chosen, 3 differential equations for the precursor concentration would be necessary.

Eq. 19 shows the energy balance for the fuel within the reactor.

$$\frac{dT_f}{dt} = \frac{P}{\mu_f}n - \frac{\Omega}{\mu_f}T_f + \frac{\Omega}{2\mu_f}T_i + \frac{\Omega}{2\mu_f}T_e \tag{19}$$

T is the temperature where subscripts, f, i, and e are for fuel, inlet, and exit, respectively. P is the power of the reactor, Ω is the product of the heat transfer area, A, and the heat transfer coefficient, h, and μ_f is defined as the mass of fuel in the reactor, m_f, times the heat capacity of the fuel, C_{pf}. The final differential equation is for an energy balance for the coolant, similar in form to the energy balance for the fuel, and is shown below,

$$\frac{dT_e}{dt} = \frac{2\Omega}{\mu_c}T_f - \left(\frac{2M_c+\Omega}{\mu_c}\right)T_e + \left(\frac{2M_c-\Omega}{\mu_c}\right)T_i \tag{20}$$

The variables are similar, with the addition of M_c which is the product of the coolant mass flow rate, F_c, and the coolant heat capacity, C_{pc}. μ_c is defined as the mass of coolant in the reactor, m_c, times the heat capacity of the coolant, C_{pc}. These differential equations are solved simultaneously to find the values of the dependent variables at each time interval.

In addition, an equation for the reactivity is used which incorporates temperature feedback due to changes in inlet and outlet temperatures. This equation determines the reactivity that is used in Eq. 17.

$$\rho = \rho_{rod} + \alpha_f\left(T_f - T_{f0}\right) + \frac{\alpha_c}{2}(T_i - T_{i0}) + \frac{\alpha_c}{2}(T_e - T_{e0}) \tag{21}$$

The reactivity is dependent on ρ_{rod}, which is the reactivity change due to movement of control rods. In addition, the temperatures of the fuel and coolant affect reactivity. The change depends on the reactivity co-efficient for the fuel, α_f, and the coolant, α_c. The values of these reactivity coefficients used in this study were -3.85x10^{-5} °C^{-1} and -0.34x10^{-5} °C^{-1}, respectively (Galvez, 2011). The significance of the negative reactivity coefficients is that if there is a temperature increase entering the reactor, the power of the reactor will decrease. If the power were to increase, the temperatures of the system would increase until reactor failure.

2.4.3 Numerical Solution Technique

The solution for each set of differential equations require a numerical method. The fourth-order Runge-Kutta method was used in this work to solve each set of differential equations simultaneously. The equations required are shown below (Chapra et al., 2010). There will be one set of the following equations for each dependent variable. For each dependent variable values for *a, b, c,* and *d* are solved for at each time step. *h* is the time step, $f_j(y_1, y_2, ..., y_j)$ is the function of variable *j*, $y_{j,i}$ is the current value of variable *j*, and $y_{j,i+1}$ is the next value for variable *j*. For the IHX and SHX there are 3 dependent variables each (T_h, T_c, T_w) for a total of 6 sets of the equations below. The reactor has from 4 to 9 dependent variable ($n, c_1, c_2, c_3, T_f, T_c$) depending on the number of delay groups used. This equals a total of 10 to 15 sets of the equations below. In total, 10 to 15 sets of the equations will be solved for each of the time steps.

$$a_{j,i} = f_j(y_{1,i}, y_{2,i}, \ldots, y_{m,i}) \tag{22}$$

$$b_{j,i} = f_j((y_{1,i} + {}^h\!/_2 * a_{1,i}), (y_{2,i} + {}^h\!/_2 * a_{2,i}), \ldots, (y_{m,i} + {}^h\!/_2 * a_{m,i}) \tag{23}$$

$$c_{j,i} = f_j((y_{1,i} + {}^h\!/_2 * b_{1,i}), (y_{2,i} + {}^h\!/_2 * b_{2,i}), \ldots, (y_{m,i} + {}^h\!/_2 * b_{m,i}) \tag{24}$$

$$d_{j,i} = f_j((y_{1,i} + h * c_{1,i}), (y_{2,i} + h * c_{2,i}), \ldots, (y_{m,i} + h * c_{m,i}) \tag{25}$$

$$y_{j,i+1} = y_{j,i} + {}^h\!/_6 (a_{j,i} + 2b_{j,i} + 2c_{j,i} + d_{j,i}) \tag{26}$$

Different numerical methods can be used for more accurate results. The fourth-order Runge-Kutta method is a one-step method but there are a number of iterative methods that may be used as well. One such method is the fourth-order Adams method shown in Eqs. 27-28. Eq. 27 is the predictor equations which gives the initial guess. This is then put into Eq. 28, the corrector equation, and iteratively solves for the variables value at the next time step. This model was compared with the Runge-Kutta method and the results can be seen in Figure 16. This is a simulation of only the SHX after a disturbance is introduced. The black and red lines are the hot side duties using the Adams and Runge-Kutta methods, respectively. The brown and blue lines are the cold side duties using the Adam's and Runge-Kutta methods, respectively. As seen the lines match up perfectly. This confirms that the use of the Runge-Kutta method is sufficient in producing accurate results and will be used in the model over the more computationally intensive Adams method.

$$y_{i+1}^0 = y_i^m + h \left(\frac{55}{24} f_i^m - \frac{59}{24} f_{i-1}^m + \frac{37}{24} f_{i-2}^m - \frac{9}{24} f_{i-3}^m \right) \tag{27}$$

$$y_{i+1}^{j} = y_i^m + h\left(\frac{9}{24}f_{i+1}^{j-1} + \frac{19}{24}f_i^m - \frac{5}{24}f_{i-1}^m + \frac{1}{24}f_{i-2}^m\right) \tag{28}$$
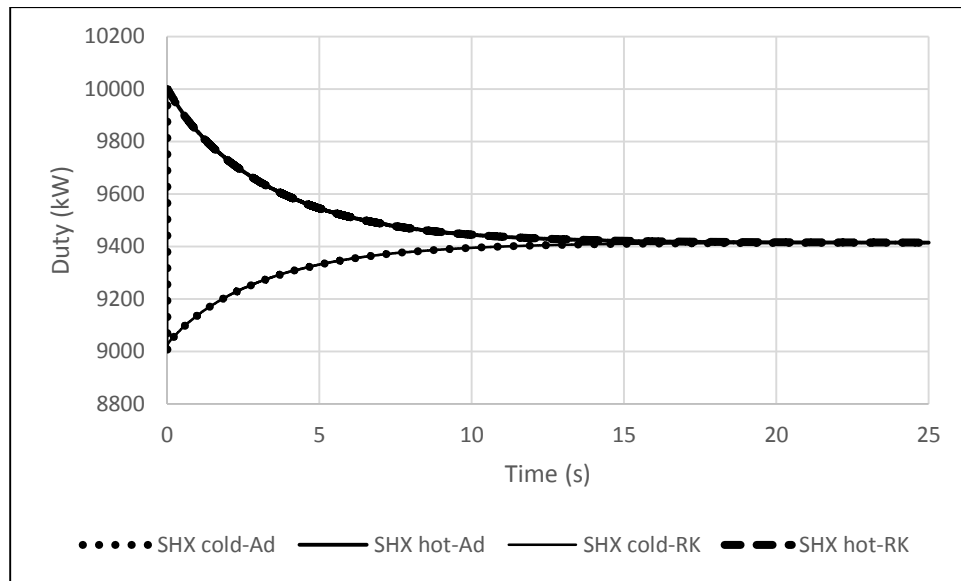
Figure 16. Comparison between fourth-order Runge-Kutta and fourth-order Adams methods.

CHAPTER 3: SIMULATION OF SYSTEM TRANSIENTS

3.1 TRANSIENT ANALYSIS

Process simulation software described in section 2.3.1 and 2.3.2 are used to simulate the dynamics of the AHTR system. Flow rate and temperature disturbances are introduced into the different loops of the system, and the dynamics of the system are analyzed. Because no nuclear reactor exists in the database for these programs, only the coupled IHX and SHX are analyzed.

3.1.1 Process Loop Disturbances

The temperature and flow disturbances were introduced in the process loop before the process stream enters the SHX, representative of a disturbance in the process application that is propagating back through the system to the primary energy source – the nuclear reactor.

The system response to a 30 K decrease in temperature of the cold inlet stream of the SHX is seen in Figure 17. The step decrease can be seen as the thickest solid line on the bottom of Figure 17a. The step decrease in the temperature of stream entering the SHX causes the log mean temperature difference (LMTD) to increase, in turn increasing the thermal duty for the SHX. This increased duty results in the lower outlet temperature for the SHX hot side stream. This stream then travels to the cold side inlet of the IHX, thus propagating the disturbance. The IHX disturbance then feeds back to SHX, and the interplay between the two heat exchangers continues until a new steady state is reached. Ultimately, the decrease in temperature propagates through the system causing temperatures of other streams to drop as well. The largest effect is seen on the medium thick solid line right above. The other temperatures represented by the solid line and dashed lines also decrease but with lesser magnitudes. The SHX hot side outlet temperature decreases by ~27 K and the IHX hot outlet temperature by ~21 K. The new steady state is reached in approximately 35 minutes and the overall duty increases by ~1100 kW as shown in Figure 17c.

The effect of a 30 K increase in the temperature is seen in Figure 17b. The result is similar to that for the step decrease in the temperature, however, in the opposite direction. The thickest solid line on the bottom of Figure 17b shows the step increase in temperature. The LMTD of the SHX decreases causing the duty of the SHX to decrease as well. The hot side outlet stream exits the SHX at a higher temperature and travels to the IHX. The increased temperature causes the IHX to also have a decreased LMTD and duty. In each stream the temperature increases but the magnitude of the increase decreases as the disturbance propagates through the system. The SHX hot side outlet sees

an increase of ~27 K and the IHX hot side outlet sees an increase of ~21 K, the opposite of what was seen in the other case. The time to reach equilibrium is again approximately 35 minutes with an overall duty decrease of ~1100 kW shown in Figure 17d.
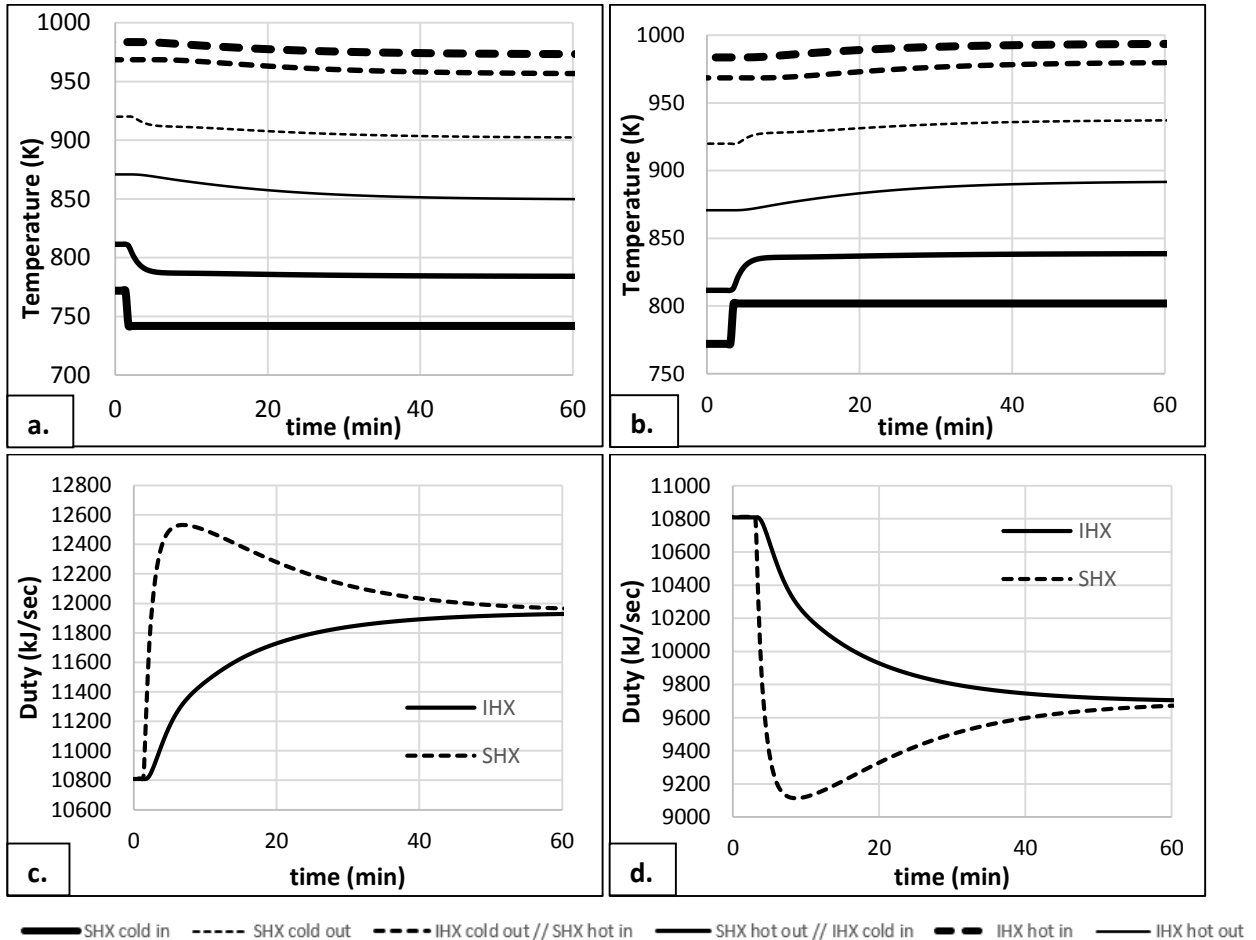
Figure 17. System behavior after temperature disturbance in the process loop. a: Temperatures for -30 K Change, b: Temperatures for +30 K Change, c: Heat Exchange Duties for -30 K Change, d: Heat Exchanger Duties for +30 K Change.

The flow disturbance, which could be caused by a leak in the pipe, a breakage or a pump malfunction. Leakages and breakages would cause a decrease in the flow rate and a pump malfunction could cause either an increase or decrease in the flow rate. A disturbance of ±20% of the initial flow rate was introduced into the system and the system response can be seen in Figure 18. The response time is much faster than that for temperature disturbances. A decrease in the flow rate of the process stream causes the heat transfer coefficient on the cold side of the SHX to decrease, lowering the overall heat transfer coefficient and duty of the SHX. However, the decreased flow rate also results in a higher outlet temperature for both the process stream and the secondary

stream. This temperature disturbance then propagates to the IHX and causes a slight decrease in the LMTD and thus the duty of the IHX. The temperature profiles for this situation are shown in Figure 18a. The effects are minimal causing changes of less than 1 K at steady state for the other streams. The system comes to equilibrium in approximately 10 minutes and the overall duty drop is ~ 50 kW seen in Figure 18c.

The dynamic temperature response to 20% increase in the process flow rate is seen in Figure 18b. The effects are reverse of those observed for the decrease in the flow. The heat transfer coefficient on the cold side of the SHX increases causing the overall heat transfer coefficient to increase. The increase in the flow rate causes the temperature change in the process stream across the heat exchanger to decrease, increasing the LMTD across the SHX. A small initial increase due to the increased flow rate is seen in the thermal duty, which subsequently decreases with time due to the decrease in the LMTD. The increased flow rate causes the temperature rise in the SHX cold stream to decrease from ~151 K to ~124 K. This affects the LMTD which ultimately decreases the duty at the new steady state. The initial increase in duty causes the SHX hot outlet temperature to decrease at first, but the later increase in the duty results in a new steady state temperature that is ~2 K higher than the initial temperature. The small change has little effect on the temperatures of the rest of the system but the slightly decreased LMTD of the IHX causes the duty to gradually decrease. The system comes to equilibrium more gradually taking ~40 minutes and the overall duty decrease is a little more than 100 kW as shown in Figure 18d.
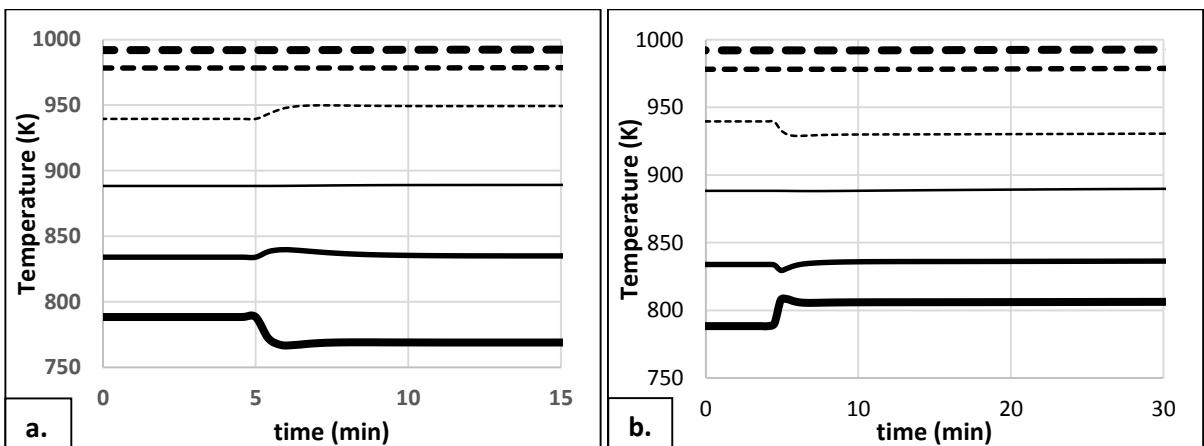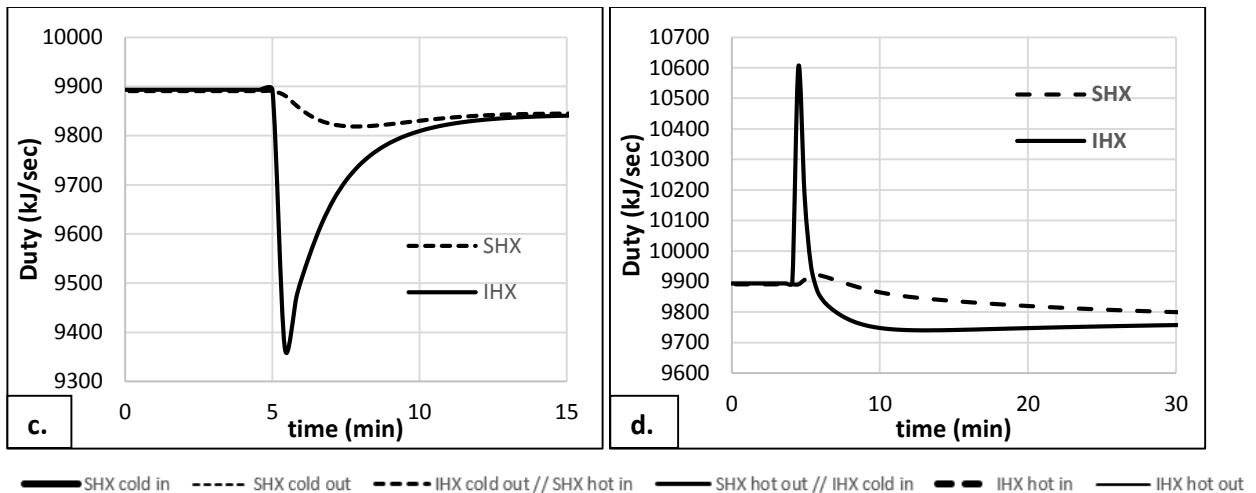
Figure 18. System behavior after flow disturbance in the process loop. a: Temperatures for -20% Change, b: Temperatures for +20% Change, c: Heat Exchange Duties for -20% Change, d: Heat Exchanger Duties for +20% Change.

3.1.2 Secondary Loop Disturbances

Only flow rate disturbances in the secondary loop were analyzed, as unlike the process and primary loop, there are no heat sinks or sources in the secondary loop. The probable causes of the flow disturbances could be pipe breakages, pipe leaks, or a pump malfunction.

A flow rate disturbance of ±20% of the initial flow rate was introduced into the secondary loop of the system and the resulting plots can be seen in Figure 19. The response time is much slower than in the process loop because the disturbances transmit in both directions and are reflected back into the entire system. The temperatures of various streams for the -20% disturbance are seen in Figure 19a. The heat transfer coefficients on the hot side of the SHX and the cold side of the IHX decrease with the drop in flow rate, causing a decrease in the overall heat transfer coefficients and duties of both the SHX and IHX. The decreased flow rate causes the temperature change in the secondary loop to increase, both in the SHX and the IHX. Initial decreases in heat transfer coefficients are partially compensated by increases in the LMTD in both heat exchangers, causing the duties to increase after the initial drop. The process stream SHX outlet temperature decreases by ~24 K and the primary stream IHX outlet temperature increases by ~10 K. Other stream temperatures change in the range of 5 and 10 K. The system comes to equilibrium in ~40 minutes and the overall duty drops by ~650 kW as seen in Figure 19c.

Temperatures of various streams for the +20% disturbance flow rate disturbance are seen in Figure 19b. The heat transfer coefficient on the hot side of the SHX and cold side of the IHX will

increase causing the overall heat transfer coefficient to increase. The increased flow rate causes the temperature change in the secondary loop to decrease, both in the SHX and IHX. This causes the LMTD of the heat exchangers to decrease counteracting the increase in the heat transfer coefficients and causing the duty to decrease after the initial spike. The overall effects on the system are much smaller than with a decrease in the flow rate. No temperature changes by more than 5 K to reach steady state. The system comes to equilibrium in ~50 minutes and the overall duty increase is ~200 kW as shown in Figure 19d.
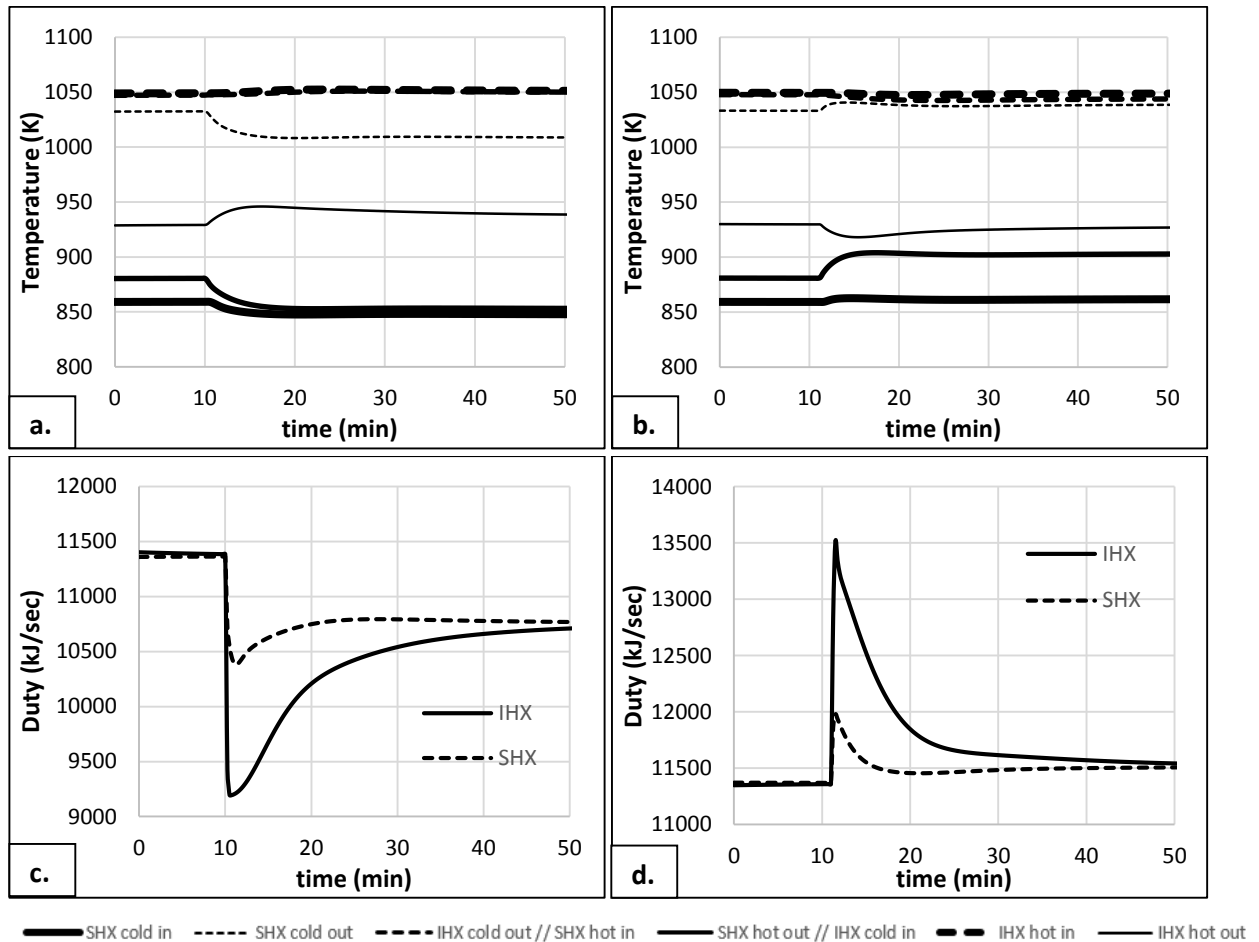
Figure 19. System behavior after flow disturbance in the secondary loop. a: Temperatures for -20% Change, b: Temperatures for +20% Change, c: Heat Exchange Duties for -20% Change, d: Heat Exchanger Duties for +20% Change.

3.1.3 Primary Loop Disturbances

The primary loop is similar to the process loop in the sense that it can experience both the temperature and flow rate disturbances, due to leakages, breakages, equipment malfunctions, or heat addition/removal issues.

A temperature disturbance is introduced with a ±30 K step before the primary stream enters the IHX. Figure 20a shows the resulting stream temperatures for the -30K disturbance. The step decrease in the primary stream entering the IHX causes the LMTD to decrease, resulting in a decreased duty for the IHX. This causes the cold side outlet temperature of the IHX to decrease. This stream then travels to the hot side inlet of the SHX at a decreased temperature, which decreases the LMTD of the SHX and causes a gradual decrease in the duty until its steady state value. Each stream in system experiences a decrease in temperature, however, the magnitude of the decrease is lowered as the disturbance propagates through the system. The IHX cold side outlet sees a decrease of ~14 K and the SHX cold outlet temperature decreases by ~11 K. The system reaches equilibrium in approximately 45 minutes, which is slightly slower than for the process loop disturbances, and the overall duty decrease is ~300 kW as shown in Figure 20c.

The system stream temperatures for a +30K disturbance in the primary stream are shown in Figure 20b. The LMTD of the IHX increases causing the duty of the IHX to increase as well. The cold side outlet stream of the IHX exits at a higher temperature and flows to the SHX. The increased temperature causes the IHX to also have an increased LMTD and duty. The temperature of each stream increases but the magnitude of the increase drops as the disturbance propagates through the system. The IHX cold side outlet sees an increase of ~14 K and the SHX cold side outlet stream increases by ~11 K, the reverse of what was observed for the -30K change. The time to reach equilibrium is again approximately 45 minutes with an overall duty increase of ~300 kW as seen in Figure 20d.
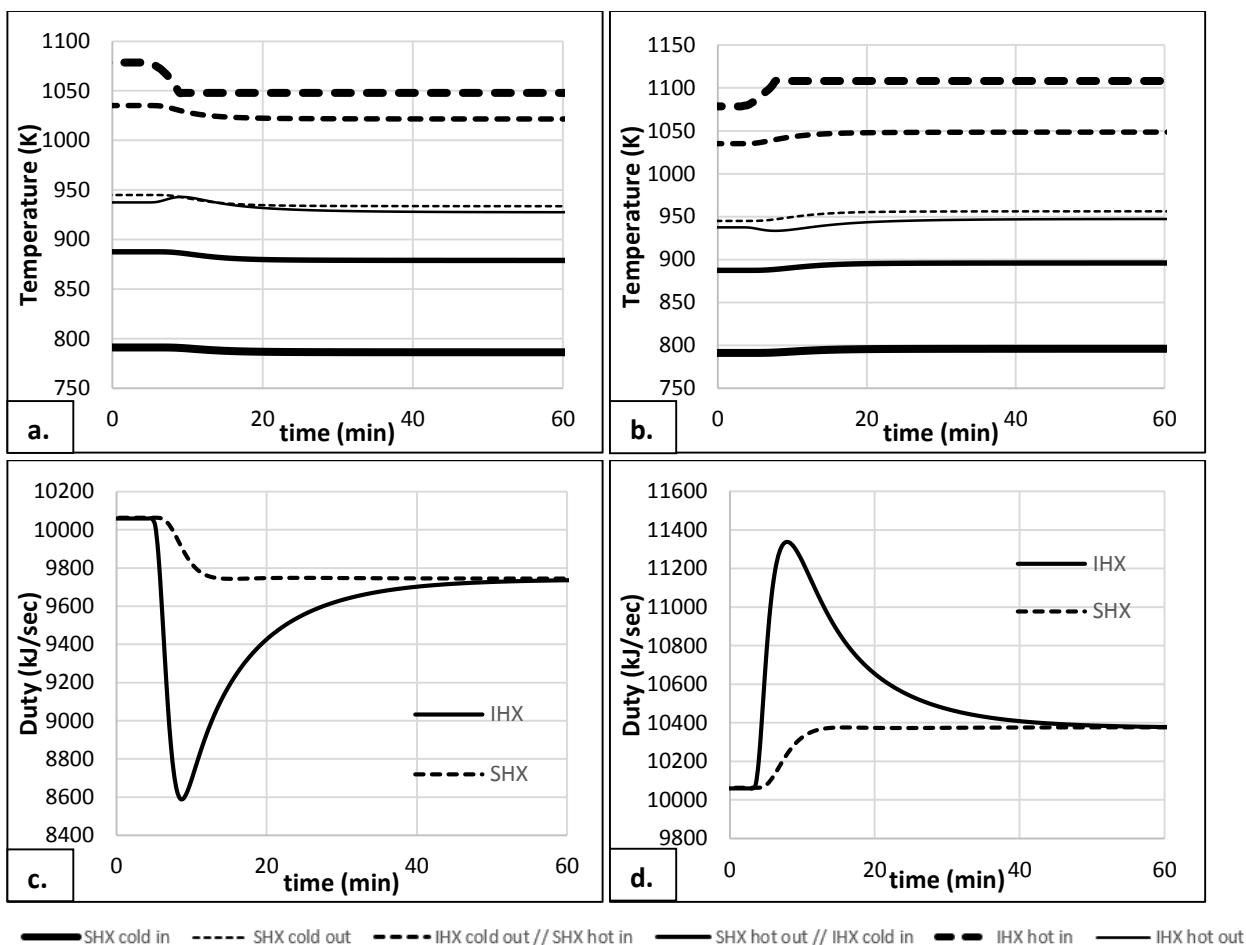
Figure 20. System behavior after temperature disturbance in the primary loop. a: Temperatures for -30 K Change, b: Temperatures for +30 K Change, c: Heat Exchange Duties for -30 K Change, d: Heat Exchanger Duties for +30 K Change.

The system response to the ±20% disturbance in the initial flow rate for the process loop is shown in Figure 21. The stream temperature profiles for -20% flow rate disturbance are seen in Figure 21a. The heat transfer coefficient on the hot side of the IHX will decrease with the flow rate causing a decrease in the overall heat transfer coefficient and duty of the heat exchanger. However, with the decreased primary flow rate, temperature change in the IHX hot side fluid rises from 104 K to 129 K. The decreased duty causes the cold side outlet temperature of the IHX to decrease slightly, ultimately reaching a steady state value ~2 K lower than the initial value. The secondary stream from the IHX transmits the disturbance to the SHX, causing a decrease in the LMTD and thus the SHX duty. Most of the other streams experience a slight (1-2 K) decrease in the temperature. The system comes to equilibrium in ~30 minutes and the overall duty drop is 50 kW as shown in Figure 21c.

The stream temperature profiles for +20% disturbance in the primary loop are shown in Figure 21b. The heat transfer coefficient on the hot side of the IHX will increase causing the overall heat transfer coefficient to increase. An initial spike in the IHX thermal duty is seen immediately. However, the increased flow for the primary stream results in lower change in its temperature through the IHX. This affects the LMTD, causing a decrease in the duty. The disturbances propagate through the system, and the system comes to equilibrium in ~40 minutes with the overall duty decrease of ~50 kW as seen in Figure 21d.
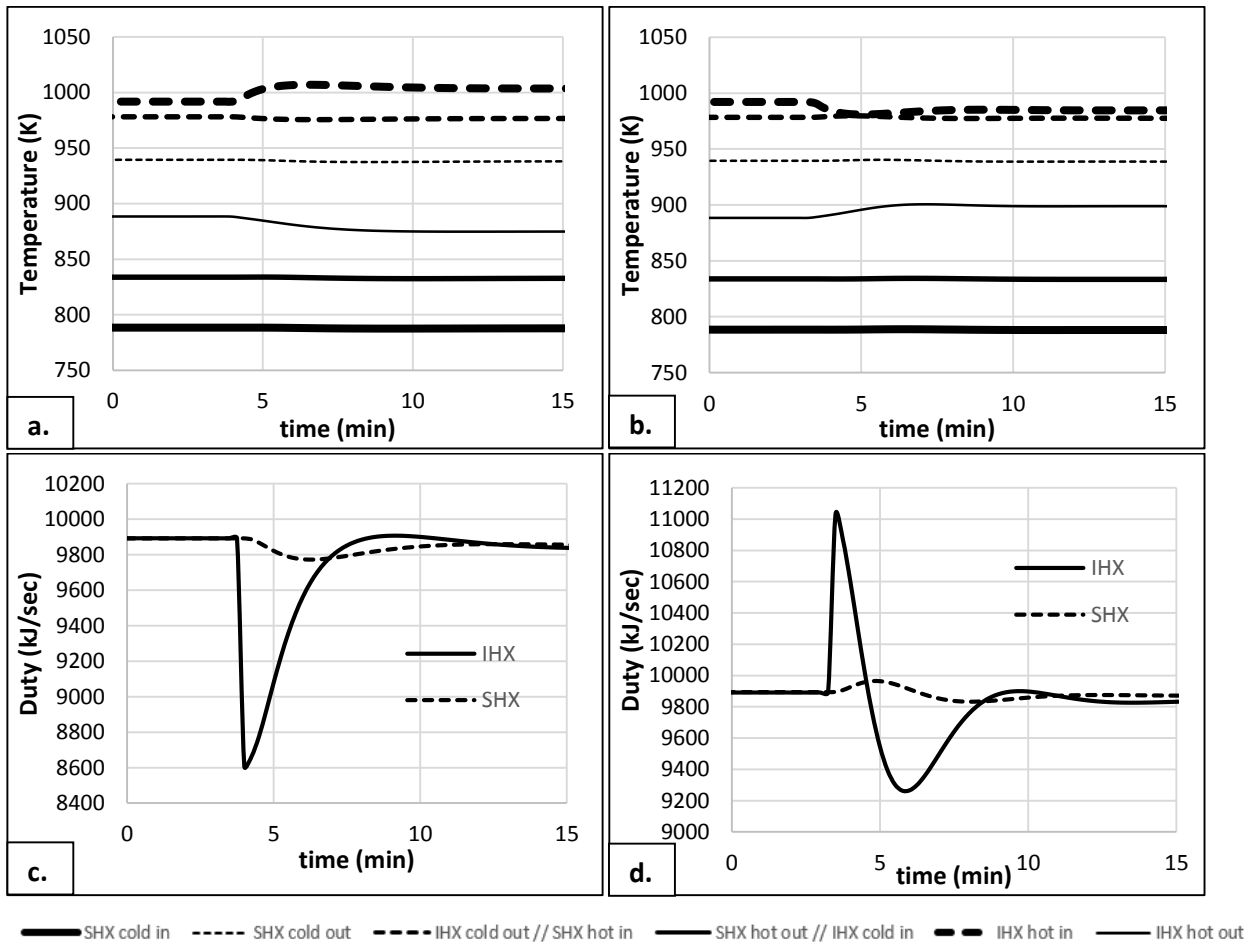
Figure 21. System behavior after flow disturbance in the primary loop. a: Temperatures for -20% Change, b: Temperatures for +20% Change, c: Heat Exchange Duties for -20% Change, d: Heat Exchanger Duties for +20% Change.

3.1.4 Summary of Transient Results

Table 9 presents a summary of the results obtained for the dynamic simulations of various disturbances. The response times needed to reach 95% and 99% of the change to the new steady state values and the change in the thermal duty for each case are shown.

Table 9. **Summary of transient results for different disturbances.**

Loop	Disturbance	Response Time 95% Change min	Response Time 99% Change min	Change in Thermal Duty kW
Temperature Disturbances				
Process	-30 K	35	53	1121
	+30 K	35	55	-1115
Primary	-30 K	43	57	-319
	+30 K	43	54	317
Flow Rate Disturbances				
Process	-20%	11	17	-52
	+20%	41	50	-115
Secondary	-20%	38	47	-651
	+20%	49	54	171
Primary	-20%	31	46	-50
	+20%	42	50	-36

As can be seen from the above table, the system responds to a positive temperature disturbance to stabilize at a higher thermal duty, while a negative temperature disturbance results in a lower overall duty. The magnitudes of the changes for the positive and the negative disturbances are similar. The magnitude of the change for a 30K disturbance in temperature of the process stream is greater than that for the same disturbance in the primary stream, possibly due to the fact that 30K represents a much greater relative change in the temperature of the process stream as compared to the primary stream. The time needed for the system to arrive at a new steady state is slightly less than an hour, with the response to the flow disturbances slightly faster than that for temperature disturbances.

The complexity of the system can be clearly seen from the system response to flow disturbances. In almost all the cases, the net effect is a decrease in the thermal duty, whether the disturbance is positive or negative. In case of the flow disturbances in the primary and the process loop, the change in the thermal duty is marginal (<1% in most cases), due to the complex interplay

between the various factors as described above. The largest change is observed for a negative disturbance in the secondary loop, where the thermal duty decreases by ~6%. A positive disturbance, on the other hand results in ~1.7% increase in the thermal duty.

The dynamic simulations described above provide information about the nature and the magnitude of the system response to various disturbances well as the time needed to reach a new steady state. This information is useful in designing the control system to minimize the effects of such disturbances.

CHAPTER 4: SYSTEM DYNAMICS UNDER CONTROLLER ACTION

4.1 CONTROLLED RESPONSE OF COUPLED HEAT EXCHANGERS SYSTEM

Once the transients of the system are fully understood a control strategy can be included. Transfer functions were used for controller tuning and dynamic simulation in MATLAB as described in section 2.2.2 and 2.2.3. Again, the nuclear reactor dynamics are not included at this time. Only the control of the coupled IHX and SHX are simulated. The cold outlet temperature of the SHX (T_{ci}) and the hot outlet temperature of the IHX (T_{ho2}) are the controlled variables in each of the cases shown in this section.

4.1.1 Process Loop Disturbances

Figure 22 shows the controller system response after a +10 ^{o}C step change in the temperature of the stream entering the cold side of the SHX (T_{ci}). Figures 22a and 22d show the time profiles for the controlled variables for the SHX (T_{co}) and IHX (T_{ho2}), respectively. As can be seen these two temperatures are successfully controlled around their set-point values. Figure 22e shows the change in the manipulated variables (F_{hi}/F_{hi2}) as a function of time. An increase in the inlet temperature of the cold stream implies a lower heat duty requirement in the heat exchanger when the outlet temperature of that stream is controlled. This lower heat duty is achieved by decreasing the flow rate of the stream on the hot side of the heat exchanger. The hot side flow rates for the IHX (F_{hi2}) and SHX (F_{hi}) shown in Figure 22e change by -6.5% and -5.0%, respectively. Figures 22b and 22c show the increas in the uncontrolled variables for the SHX (T_{ho}) and the IHX (T_{co2}), respectively. The hot side outlet temperature of the SHX (T_{ho}) increases by 3.5 ^{o}C and the cold side outlet temperature of the IHX (T_{co2}) increases by a little more than 1 ^{o}C. After the disturbance occurs, it takes the system about 400 seconds to come to a controlled equilibrium at a new steady state. Due to the drop in the flow rates the duty of the heat exchangers drop to about 9350 kW, which is ~6.5% less than the initial duty of 10 MW as shown in Figure 22f.
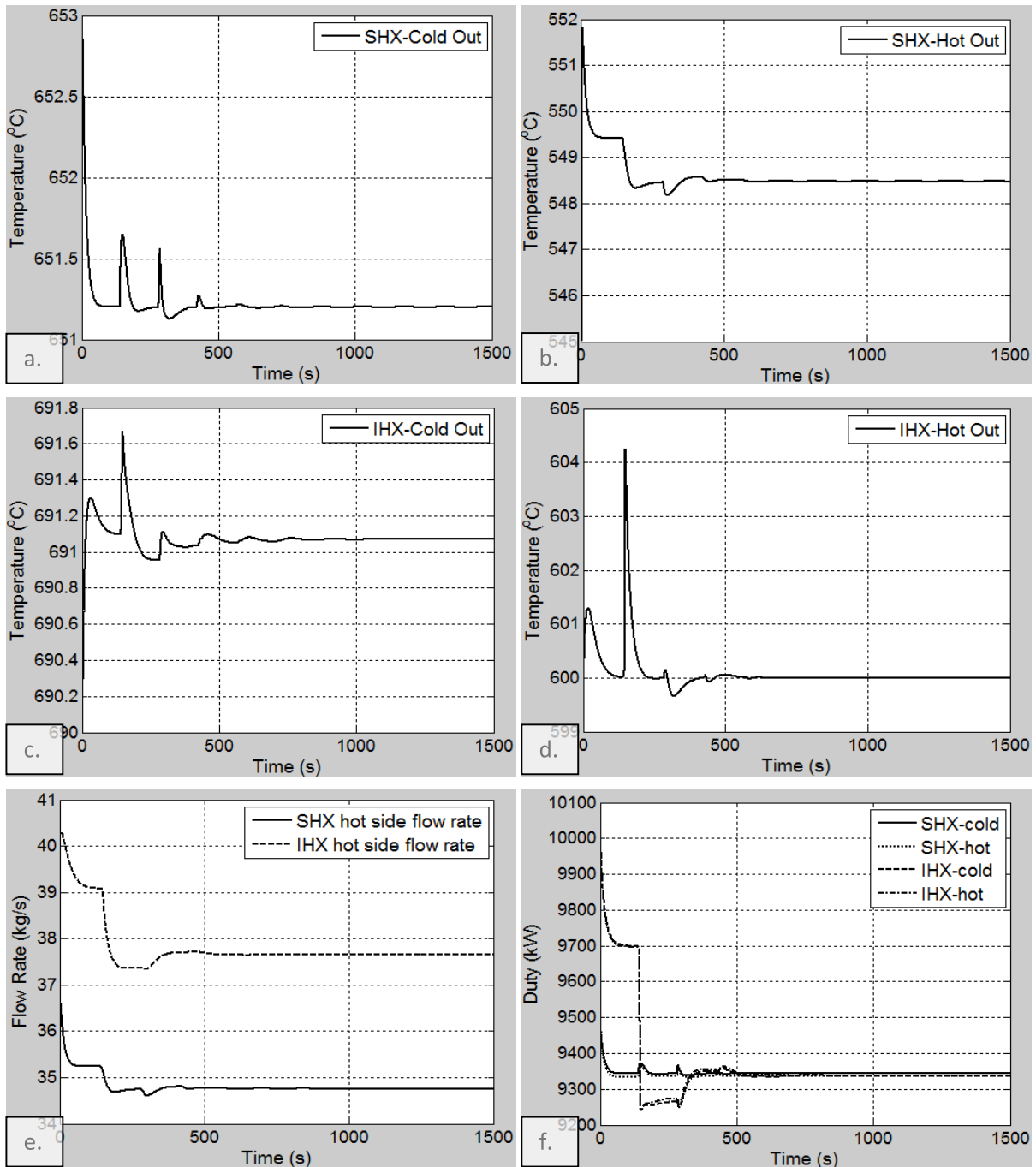
Figure 22. Control of IHX and SHX after +10 °C step change entering the cold side of the SHX. a: SHX cold outlet temperature, b: SHX hot outlet temperature, c: IHX cold outlet temperature, d: IHX hot side outlet temperature, e: hot side flow rates of SHX and IHX, f: Duties of the hot and cold side of SHX and IHX.

Figure 23 shows the system response for the control of the IHX and SHX after a -10 °C step change in the temperature of the stream entering the cold side of the SHX (T_{ci}). Figures 23a and 23d show the response as a function of time for the controlled variables for the SHX (T_{co}) and IHX (T_{ho2}),

respectively. As before, these variables are controlled successfully around their set-point values by manipulating the hot side flow rates. In this case, the increased heat duty requires increasing the flow rates of the streams on the hot side of the heat exchangers. The change in the hot side flow rates for the IHX (F_{hi2}) and SHX (F_{hi}) are 6.7% and 6.8%, respectively as seen in Figure 23e. Figures 23b and 23c show the uncontrolled variables for the SHX (T_{ho}) and IHX (T_{co2}) and they are seen to decrease. The hot side outlet temperature of the SHX (T_{ho}) decreases by ~1.4 °C and the cold side outlet temperature of the IHX (T_{co2}) decreases by ~1.7 °C. After the disturbance occurs, it takes the system about 700 seconds to come to a controlled equilibrium. Due to the increase in the flow rates, the duty of the heat exchangers rises to about 10650 kW, which is about 6.5% higher than the initial duty as shown in Figure 23f.
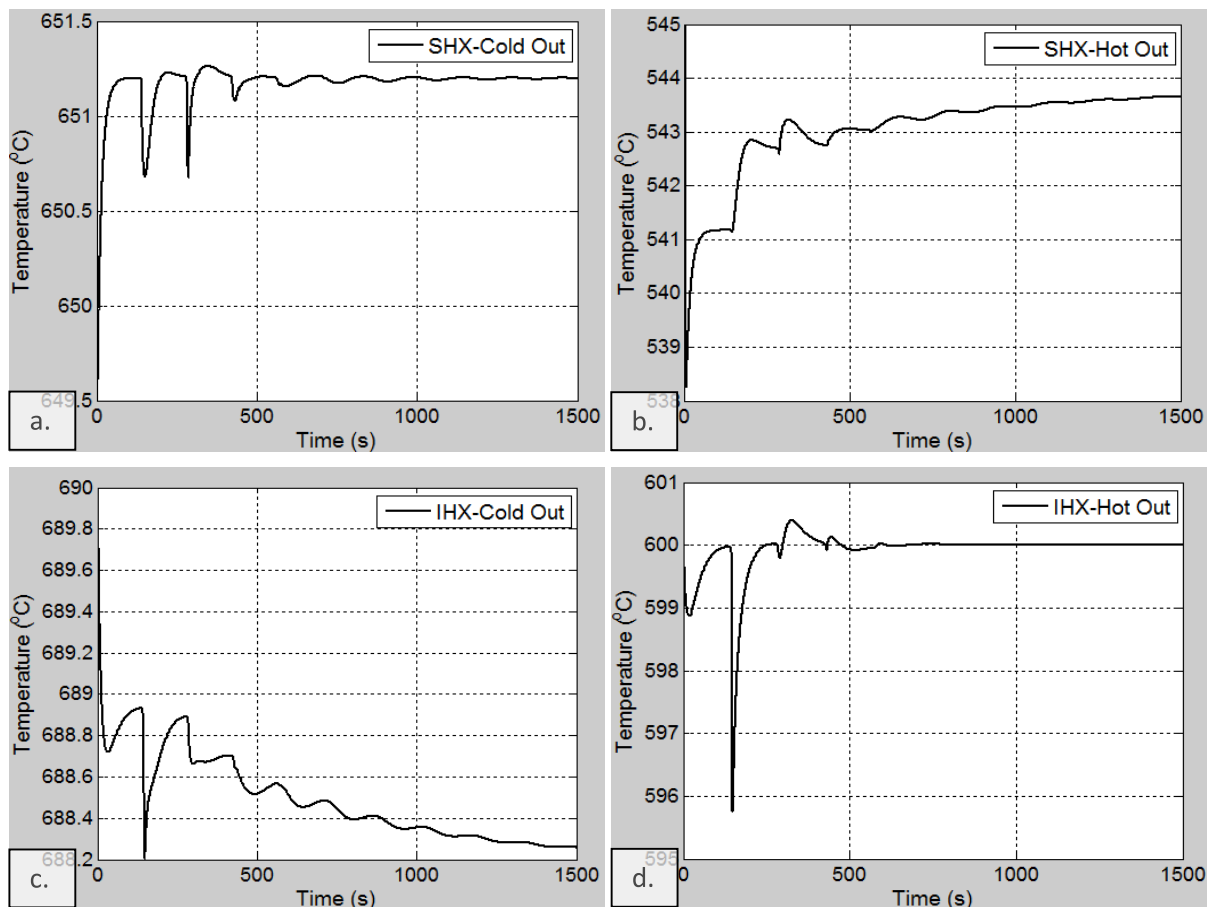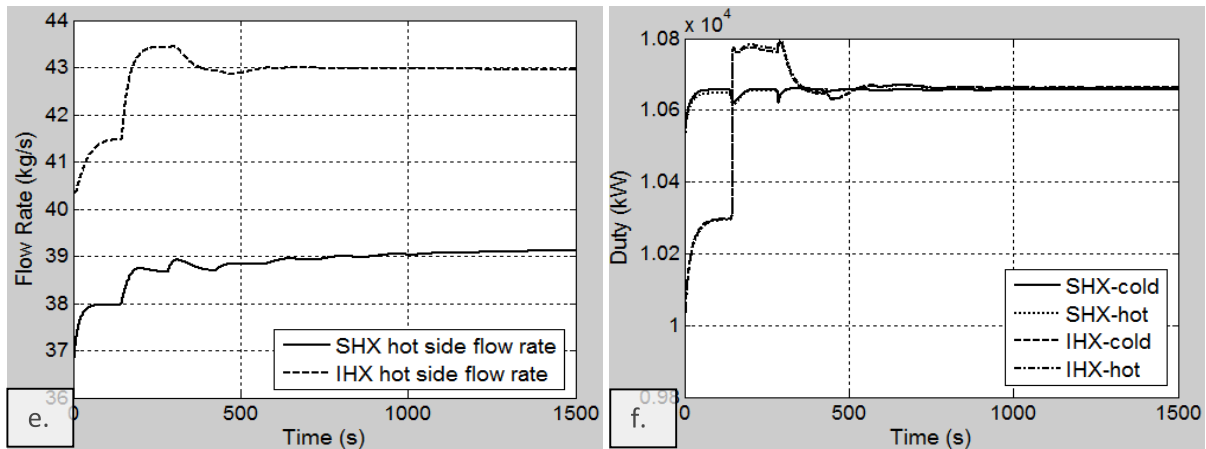
Figure 23. Control of IHX and SHX after -10 °C step change entering the cold side of the SHX. a: SHX cold outlet temperature, b: SHX hot outlet temperature, c: IHX cold outlet temperature, d: IHX hot side outlet temperature, e: hot side flow rates of SHX and IHX, f: Duties of the hot and cold side of SHX and IHX.

4.1.2 Primary Loop Disturbances

Figure 24 shows the system control after a -10 °C step change in the temperature of the stream entering the hot side of the IHX (T_{hi2}). To look at other manipulated variable options, the cold side flow rates are used as the manipulated variables rather than the hot side flow rates. The controlled variables for the SHX (T_{co}) and IHX (T_{ho2}) are unchanged, as shown in Figures 24a and 24d. The decrease in the temperature of the hot stream entering the heat exchanger implies lowering the amount of heat transferred to the cold stream. In order to maintain a constant outlet temperature of the hot stream, the cold side flow rates are decreased. The cold side flow rates of the IHX (F_{ci2}) and SHX (F_{ci}) shown in Figure 24e decrease by 6.3% and 9.5%, respectively. Figures 24b and 24c show the uncontrolled variables for the SHX (T_{ho}) and IHX (T_{co2}), respectively. Both of these temperatures decrease, with the decrease being more severe for the temperature of the cold outlet stream (T_{co2}) of the IHX. It decreases by ~7 °C and the temperature of the hot outlet stream of the SHX (T_{ho}) decreases by ~1°C. The system exhibits oscillatory behavior, stabilizing at a new equilibrium in ~1000 seconds. The thermal duty decreases to about 9000 kW, 10% lower than the initial duty as seen in Figure 24f.
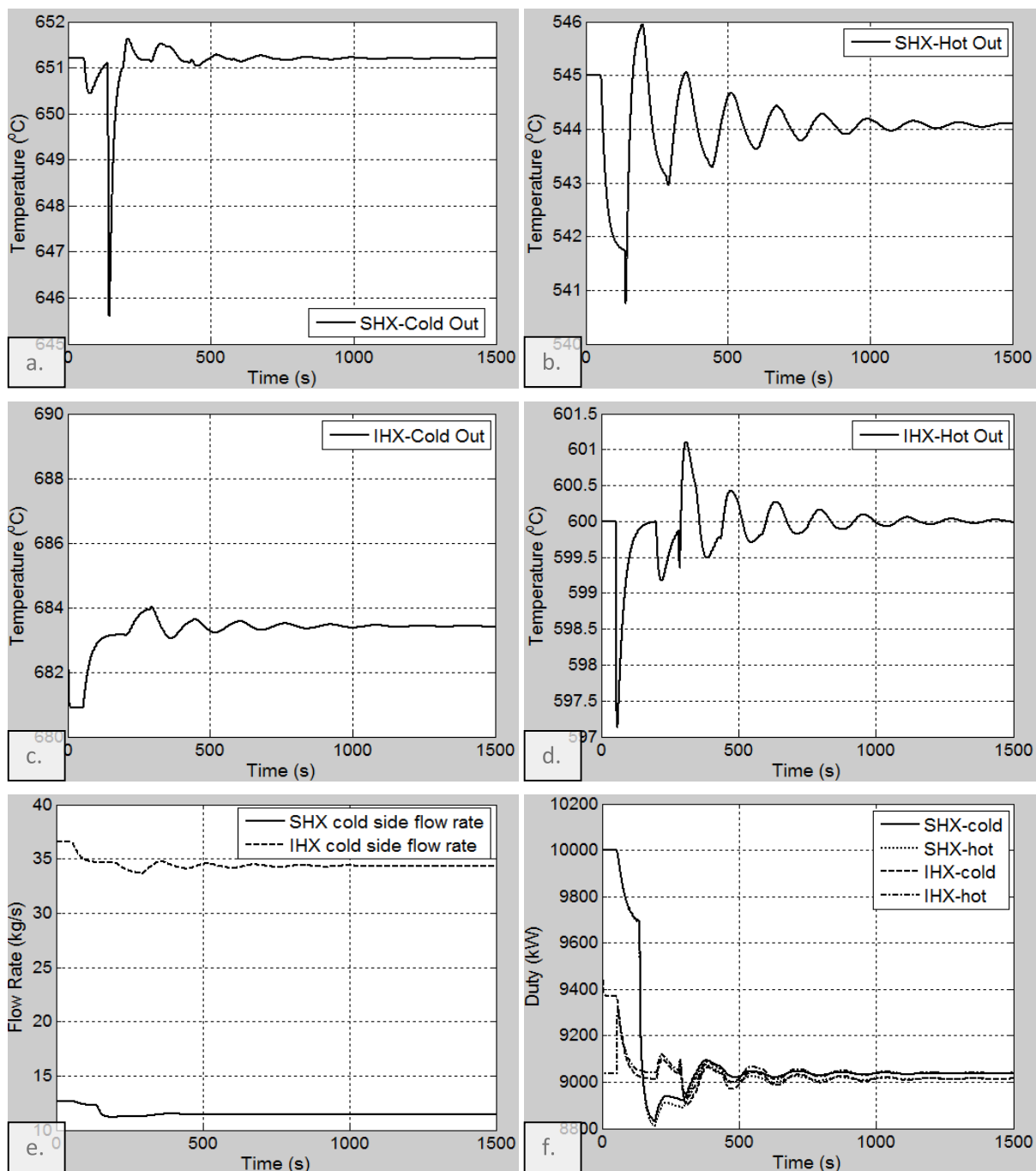
Figure 24. Control of IHX and SHX after -10 °C step change entering the hot side of the IHX. a: SHX cold outlet temperature, b: SHX hot outlet temperature, c: IHX cold outlet temperature, d: IHX hot side outlet temperature, e: cold side flow rates of SHX and IHX, f: Duties of the hot and cold side of SHX and IHX.

Figure 25 shows the system control after a +10 °C step change in the temperature of the stream entering the hot side of the IHX (T_{hi2}). Again, the cold side flow rates are used as the manipulated variables rather than the hot side flow rates. Figures 25a and 25d show the time profiles

of the controlled variables for the SHX (T_{co}) and IHX (T_{ho2}), respectively. After the disturbance, the temperatures are controlled at their desired values by changing the cold side flow rates(F_{ci}/F_{ci2}). The system exhibits oscillatory behavior. The initial drop in the cold outlet temperature is compensated by increasing the flow rate as seen in Figure 25e. This causes the temperature rise across the SHX to decrease and thus keeps the temperature at its desired value. The hot outlet temperature of the IHX (T_{ho2}) also rises initially. The cold side flow rate increases in order to make the heat transfer greater and increase the temperature drop across the hot side. The cold side flow rates of the IHX (F_{ci2}) and SHX (F_{ci}) rise by 8.5% and 10.3% respectively. Figures 25b and 25c show the uncontrolled variables for the SHX (T_{ho}) and IHX (T_{co2}), respectively. Both temperatures increase, with the increase being slightly greater for the cold outlet stream of the IHX. The cold outlet of the IHX (T_{co2}) rises by about 4.5 °C and the hot outlet of the SHX (T_{ho}) rises by about 3.2°C. A new equilibrium is established in ~800 seconds and the duty rises to about 11000 kW, 10% higher than the initial value as seen in Figure 25f.
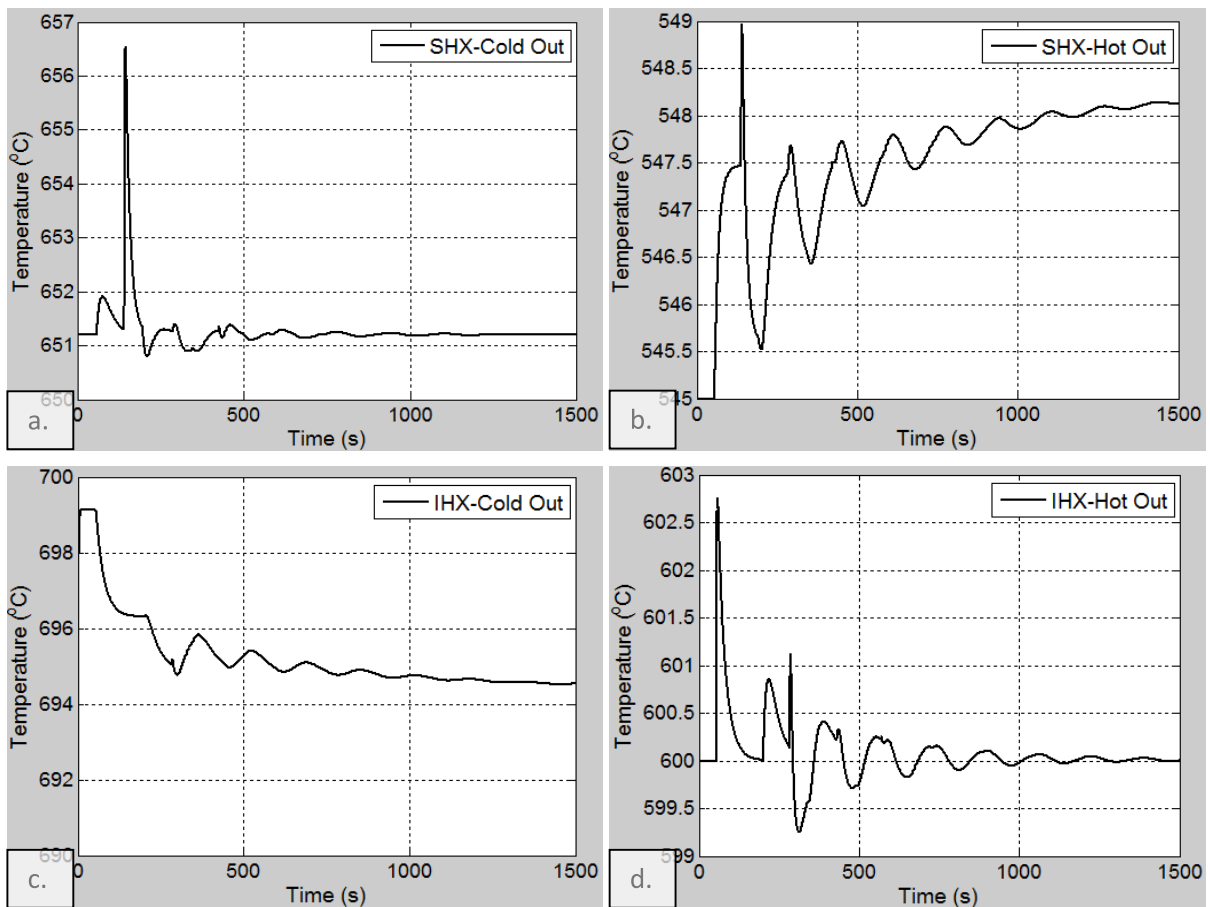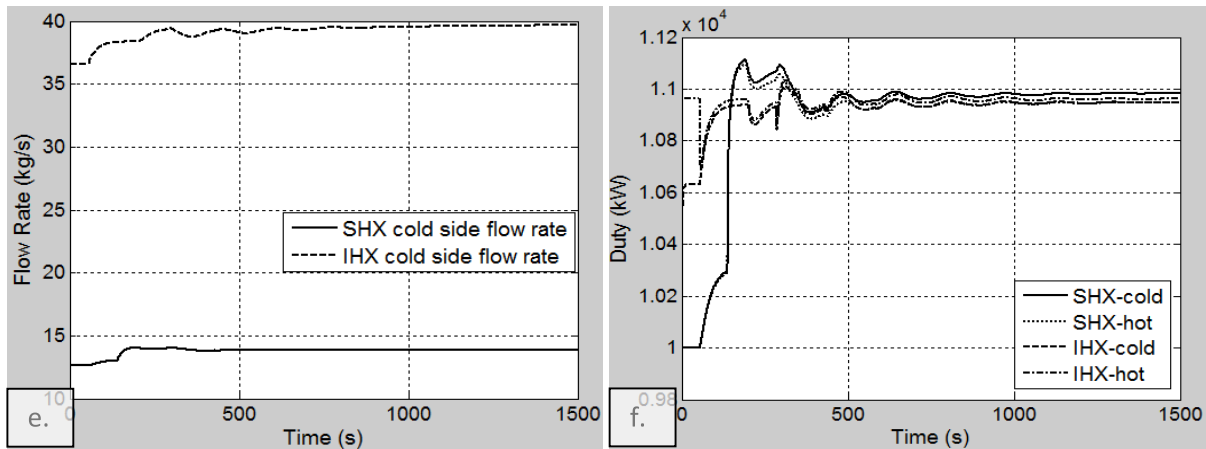
Figure 25. Control of IHX and SHX after +10 °C step change entering the hot side of the IHX. a: SHX cold outlet temperature, b: SHX hot outlet temperature, c: IHX cold outlet temperature, d: IHX hot side outlet temperature, e: cold side flow rates of SHX and IHX, f: Duties of the hot and cold side of SHX and IHX.

4.1.3 Alternative Control Method

Larger disturbances in load variables require progressively larger adjustments in the manipulated variables for system control. However, the range of a manipulated variable may be subject to other constraints arising from limitations in other components of the system. For example, the pump capacity may limit the maximum flow rate of a manipulated variable. The flow rate may also be constrained by a limit on the acceptable pressure drop. Conversely, a minimum limit may be specified on the flow rate, arising from the equipment constraints. In such cases where the system disturbances result in reaching limiting condition of a manipulated variable, the control system design must provide for switching to using another combination of manipulated variables for further control. In the present work, the limits of manipulated variables are specified at ±20% of its initial flow rates. Once a manipulated variable reaches its limit, further control requires manipulation of another variable. Figure 26 shows the controller system response after a -22 °C step decrease in the temperature of the stream entering the cold side of the SHX (T_{ci}). Figures 26a and 26d show the controlled variables for the SHX (T_{co}) and IHX (T_{ho2}), respectively. Both the controlled temperatures show an immediate decrease after the disturbance is introduced. Both the manipulated variables – the SHX the hot side flow rate (F_{hi}) and the hot side flow rate of the IHX (F_{hi2}) – increase in response, causing the controlled temperatures to increase to their set points. Figures 26b and 26c show the uncontrolled variables for the SHX (T_{ho}) and IHX (T_{co2}). The hot side outlet temperature of the SHX (T_{ho}) decreases by about 15 °C initially before rising to a temperature of 547 °C, which is 2 °C higher than the initial value. The cold outlet temperature of the IHX (T_{co2}) drops by about 6 °C. At about 650

seconds the hot side flow rate of the SHX reaches the limit (120% of initial flow) as seen in Figure 26f. At this point the system switches to using the cold side flow rate of the SHX (F_{ci}) as the manipulated variable, as seen in Figure 26g. The hot side flow rate of the IHX seen in Figure 26e never reaches the limit and is used as the manipulated variable for the IHX for the entirety of the control. This flow rate increases by about 13%. The hot and cold side flow rates of the SHX change by +20% and -1%, respectively. The system takes around 1100 seconds to come to equilibrium and the duty increases by around 13% to ~11300 kW as shown in Figure 26h.
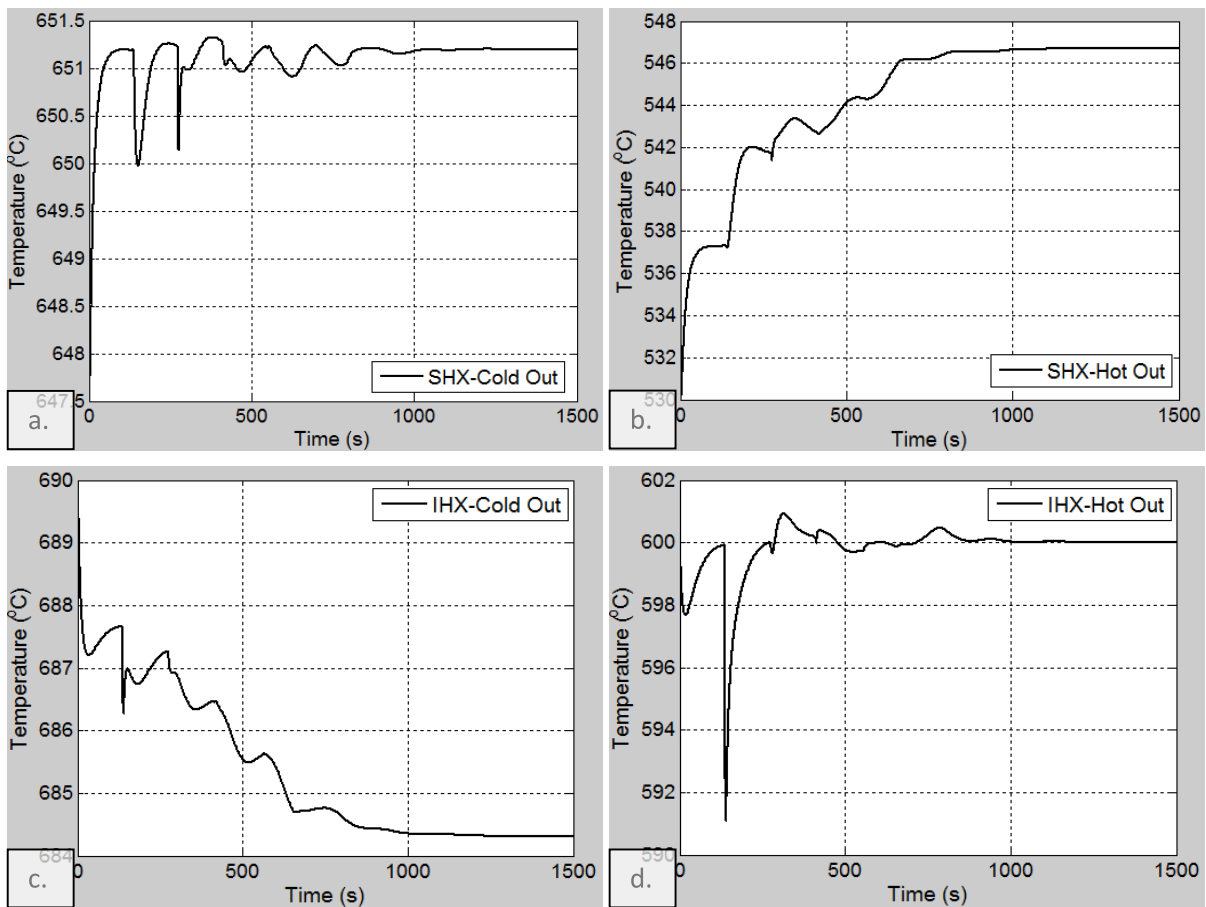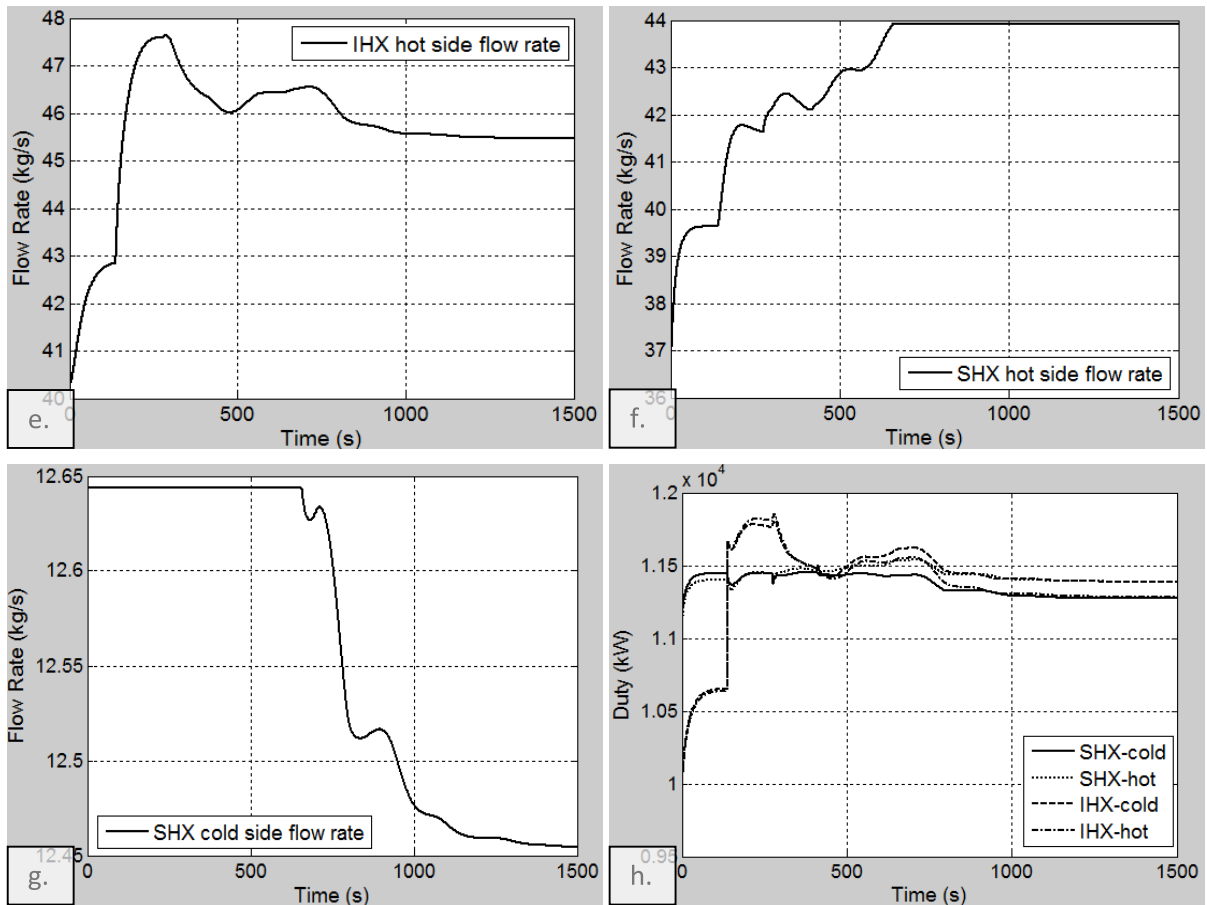
Figure 26. Control of IHX and SHX with changing manipulated variables after -22 °C step change entering the cold side of the SHX. a: SHX cold outlet temperature, b: SHX hot outlet temperature, c: IHX cold outlet temperature, d: IHX hot side outlet temperature, e: hot side flow rate IHX, f: hot side flow rate of SHX, g: cold side flow rate of SHX, h: Duties of the hot and cold side of SHX and IHX.

Figure 27 shows the system response to a +30 °C step increase in the temperature of the stream entering the cold side of the SHX (T_{ci}). Figures 27a and 27d are the controlled variables for the SHX (T_{co}) and IHX (T_{ho2}), respectively. As shown, both the temperatures spike immediately after the disturbance. The manipulated variables – the hot side flow rate of SHX (F_{hi}) and the hot side flow rate of IHX (F_{hi2}) – decrease in response. Figures 27b and 27c show the uncontrolled temperatures for the SHX (T_{ho}) and IHX (T_{co2}), respectively. The hot outlet temperature of the SHX (T_{ho}) increases by ~14 °C. After an initial increase of roughly 3.6 °C, the temperature of cold outlet stream of the IHX (T_{co2}) stabilizes at a temperature 2.5 °C higher than the initial value. Again, the manipulated variables are changed once a flow rate has reached the constraint of a change of ±20% in the initial value. In this scenario, the hot side flow rate of the IHX reaches this limit first (80%) at approximately 150 seconds as seen in Figure 27e. At this time, the IHX switches to using the cold side flow rate (F_{ci2}) as

the manipulated variable. This is the same variable as the hot side flow rate of the SHX (F_{hi}) and thus the SHX must also switch to using the cold side flow rate (F_{ci}) because both controllers can not use the same manipulated variable. Figure 27f shows the IHX cold side (SHX hot side) flow rate. It decreases by ~16.4% during the initial phase of control when employed for the control of the SHX, but then increases by 2.5% when it is switched to control the IHX. The overall change in the flow rate of this stream is -13.9%. The cold side flow rate of the SHX, seen in Figure 27g, has an initial spike but eventually decreases by 0.4%. The system is in equilibrium at ~700 seconds after the disturbance is introduced, with a decrease in the thermal duty of ~2000 kW or -20% of the initial duty as seen in Figure 27h.
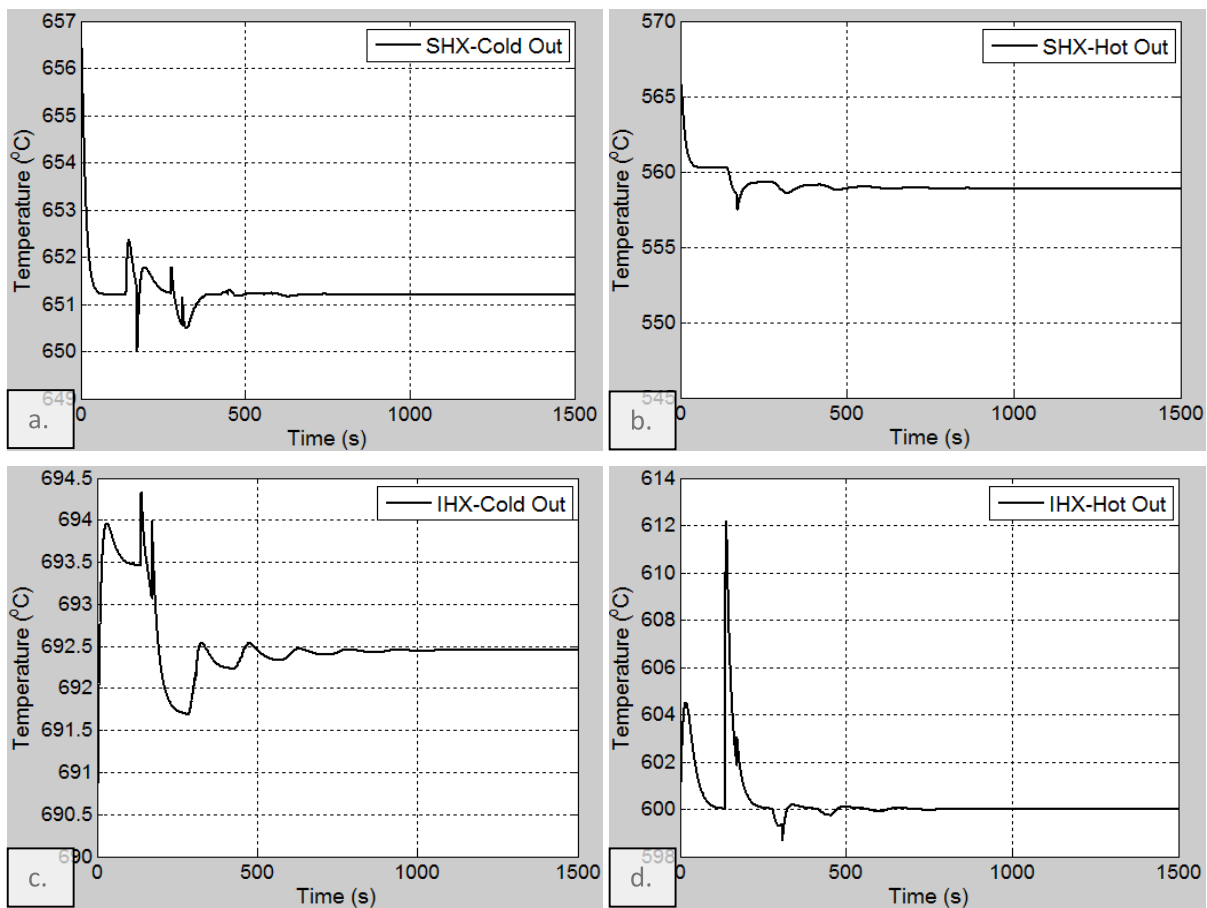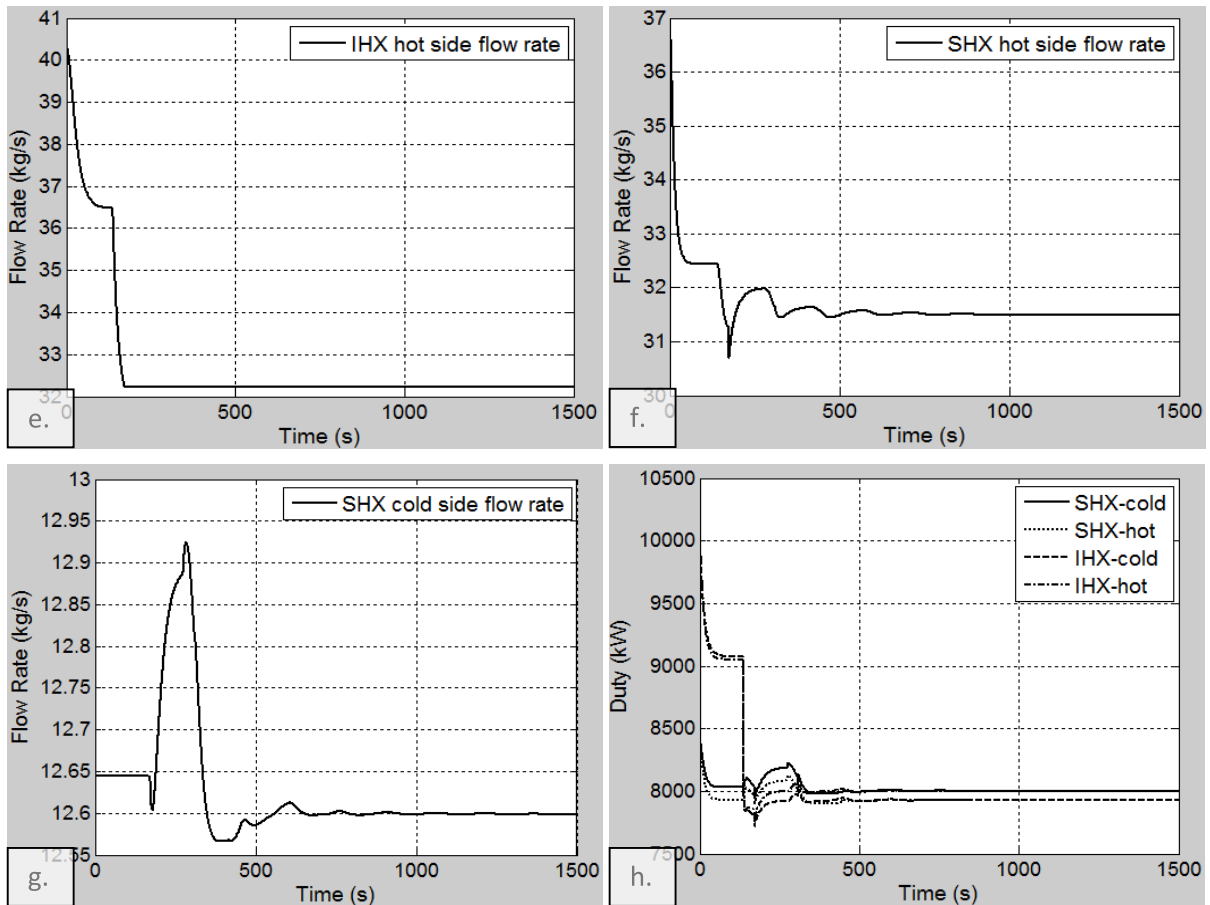
Figure 27. Control of IHX and SHX with changing manipulated variables after +30 °C step change entering the cold side of the SHX. a: SHX cold outlet temperature, b: SHX hot outlet temperature, c: IHX cold outlet temperature, d: IHX hot side outlet temperature, e: hot side flow rate IHX, f: hot side flow rate of SHX, g: cold side flow rate of SHX, h: Duties of the hot and cold side of SHX and IHX.

4.1.4 Summary of Control Results

The control system response to various disturbances is summarized in Table 10. As seen from the table, the system is able to establish a new steady state for step temperature disturbances in the process and primary streams.

Other potential system disturbances involve changes in flow rates of various streams, arising from leakages or breakages in the piping system or a pump malfunction, etc. The control system described above does not include the dynamics of the nuclear reactor and its control. The next section describes the control system response incorporating the flow disturbances and the reactor dynamics along with feedback effects.

Table 10. **Summary of control results for different disturbances**

Loop	Disturbance	SHX flow rate change %	IHX flow rate change %	Change in Thermal Duty kW
		Temperature Disturbances		
Process	-10 °C	F_{hi}= +6.8%	F_{hi2}= +6.7%	+650 (+6.5%)
	+10 °C	F_{hi}= -5.0%	F_{hi2}= -6.5%	-650 (-6.5%)
	-22 °C*	F_{ci}= -1.0% F_{hi}= +20%	F_{hi2}= +13%	+1300 (+13%)
	+30°C**	F_{ci}= -0.4% F_{hi}= -16.4%	F_{hi2}= -20% F_{ci2}=+2.5%	-2000 (-20%)
Primary	-10 °C	F_{ci}= -9.5%	F_{ci2}= -6.3%	-1000 (-10%)
	+10 °C	F_{ci}= +10.3%	F_{ci2}= +8.5%	+1000 (+10%)

*System changes from using F_{hi2}/F_{hi} → F_{hi2}/F_{ci} **System changes from using F_{hi2}/F_{hi} → F_{ci2}/F_{ci}

4.2 CONTROLLED RESPONSE OF COUPLED HEAT EXCHANGERS-AHTR SYSTEM

While previous results were done using transfer functions, differential equations described in section 2.4.1 were chosen to be used for their higher accuracy. In addition, the reactor model described in section 2.4.2 was incorporated into the code as well completing the system for the AHTR.

4.2.1 Optimization of Number of Delayed Neutron Groups

As noted in section 2.4.2, 1 to 6 delayed neutron groups may be used in the model. The six groups come from 6 precursors. These are certain fission products with specific half-lives. When the fission products decay they release a neutron which are called the delayed neutrons. Though using 6 groups gives the highest accuracy the groups can be lumped together according to their half-lives creating fewer groups. Table 11 shows the neutron fractions and decay constant when 1, 2, 3, or 6 groups of delayed neutrons are considered in the model. The values for the 6 groups was acquired from Lamarsh and Baratta (2001). The β_i values for the situations where delayed neutrons fractions are grouped into 1, 2, and 3 groups are found by summing the β_i values of the fractions in that group. For example, when the fractions are combined into 3 groups, the 3 β_i values are the sum of group 1 and group 2, the sum of group 3 and group 4, and the sum of group 5 and group 6. The λ_i values to be used in Eqs. 17 and 18 are found using Eq. 29, where the summation is carried over the delayed neutron fractions combined in that group.

$$\lambda_i = \frac{\sum \beta_i}{\sum \beta_i/\lambda_i} \tag{29}$$

Table 11. **Neutron fraction and decay constant for 1, 2, 3, and 6 groups of delayed neutrons.**

	6 Groups		3 Groups		2 Groups		1 Group	
Group	β_i	λ_i (s^{-1})	β_i	λ_i (s^{-1})	β_i	λ_i (s^{-1})	β_i	λ_i (s^{-1})
1	0.000215	0.0124	0.001639	0.0256	0.002913	0.0386	0.006502	0.0767
2	0.001424	0.0305						
3	0.001274	0.111	0.003842	0.192				
4	0.002568	0.301			0.003589	0.387		
5	0.000748	1.14	0.001021	1.37				
6	0.000273	3.01						

Eq. 18, in reality, is not a single equation, but represents as many equations as the number of delay groups used. As seen from Table 11, there are 6 distinct groups of delayed neutrons, and the greatest accuracy will be obtained by using 6 distinct equations. However, this will result in an increased computation load and complexity in programming as well as an increased possibility of introducing rounding errors in computation. Combining all the distinct delayed neutrons into a single delay group will result in lower computation load and simplified programming, but may introduce inaccuracies in the results. To optimize the number of delay groups to be used in the computations, the 6 delay neutron groups were lumped into 1, 2 and 3 group and the resultant effective neutron fraction and delay constant calculated for each grouping. These values can be seen in Table 11. Then the simulations for the 1, 2, and 3 group models were compared to the simulation where all 6 distinct groups were used in the model. A disturbance of -0.2 $ was introduced in the reactor. For each situation the reactor power was found as a function of time. The reactor power error of the 1, 2, and 3 group models from the 6 group model was then found and is shown in Figure 28. The error is defined as the deviation of the results for the 3 different models from the results for the simulation involving 6 groups. The model combining all 6 delay neutrons into a single group of delayed neutrons had the largest error while the model using 3 delayed groups had minimal error. The largest errors were seen during the initial period, with the errors becoming vanishingly small for all combinations at around 600 s. The largest error seen between 1 group and 6 groups was just over 6%, which was the largest error of the 3 models. The 2 delay group model involves a maximum error of just over 2% and with 3 groups the maximum error is roughly 0.5%. For this reason, the delayed neutrons were combined into 3 groups in subsequent simulations as it reduces the computational burden by 50% with respect to Eq. 18 while only introducing minor error. With the number of delay groups decided the code can then be developed and simulation of temperature and flow rate disturbances analyzed.
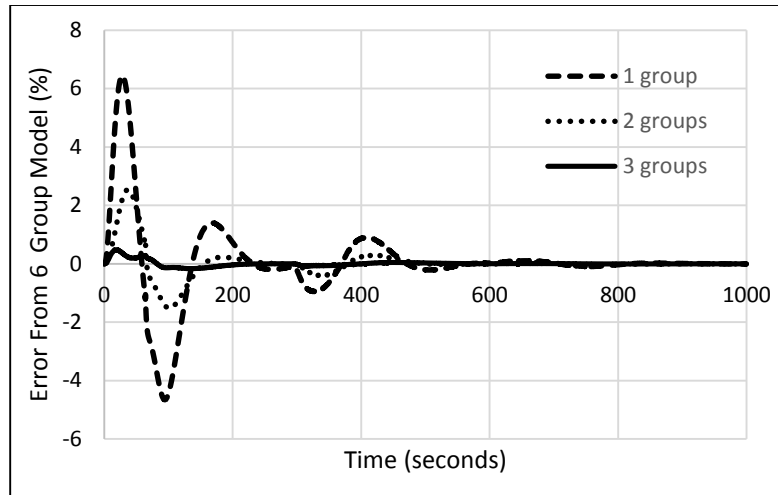
Figure 28. Error from model using 6 groups of delayed neutrons.

4.2.2 Temperature Disturbances

Figure 29 shows the response of the system after a +10 °C step increase in the temperature of the stream entering the cold side of the SHX (T_{ci}). Figures 29a and 29d show the time trajectories of the controlled variables for the SHX (T_{co}) and IHX (T_{ho2}), respectively. As can be seen these figures, the disturbance causes the temperatures to increase initially, followed by the controller action that manages to return the temperatures to their set-point values indicated by the dashed lines. Figures 29b and 29c, respectively, show the time trajectories of temperatures of other streams of SHX (T_{ho}) and IHX (T_{co2}) that are not controlled. T_{ho} increases by 5.7 °C while T_{co2} decreases by ~0.9 °C. To counteract the increase in temperature seen in the controlled variables both hot side flow rates (F_{hi}/F_{hi2}) are manipulated, with both the flow rates ultimately decreasing: F_{hi} by 0.8 kg/s (-2.2%) and F_{hi2} by 3.0 kg/s (-7.4%) as seen in Figures 29f and 29g. Due to a decrease in flow rate going through the reactor an increase in outlet temperature of ~1.0 °C is seen in Figure 28e. The system comes to a new equilibrium in approximately 1200 seconds with an overall decrease in the heat duty of ~650 kW (6.5%) as seen in Figure 29h.
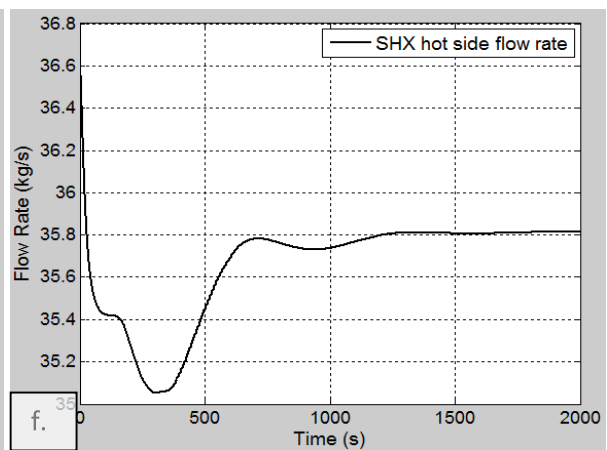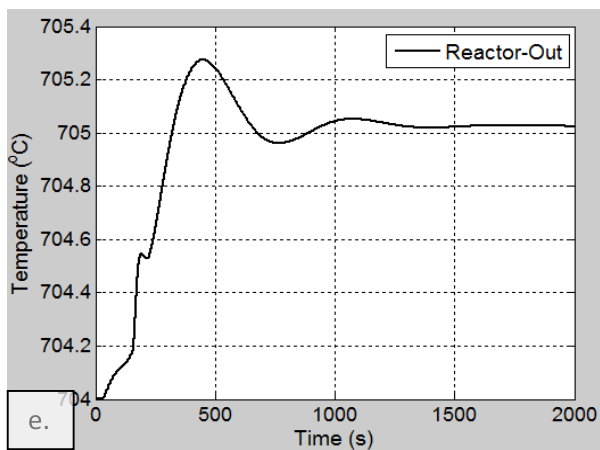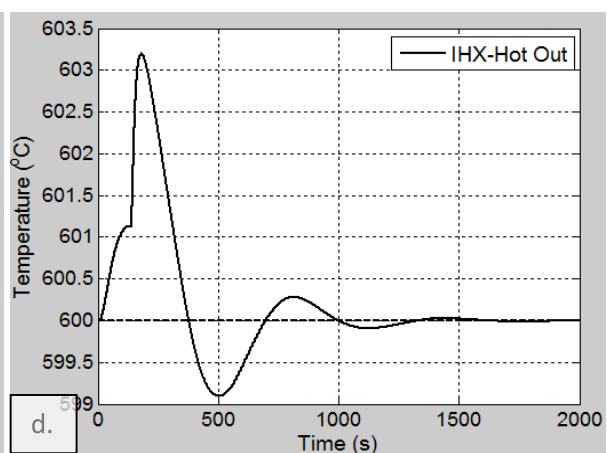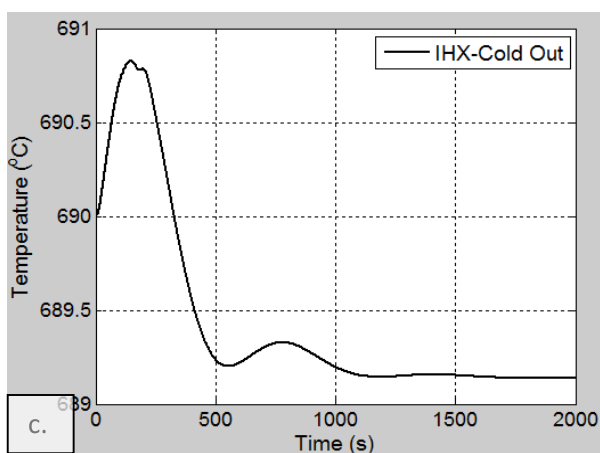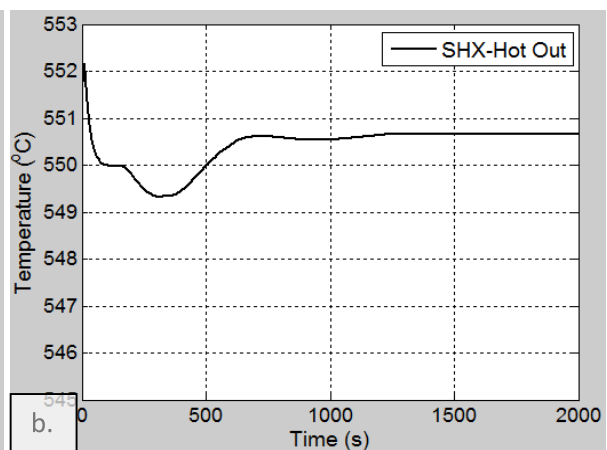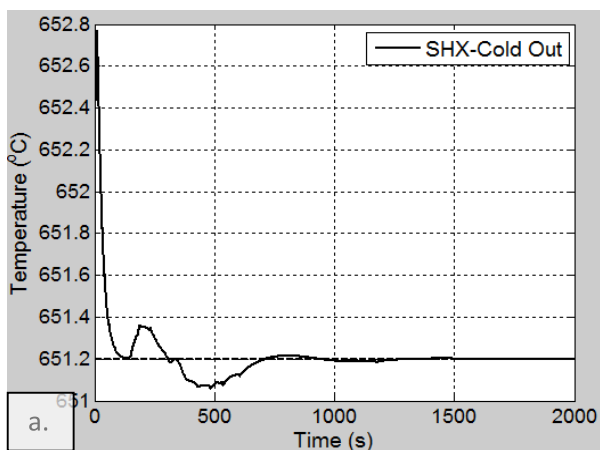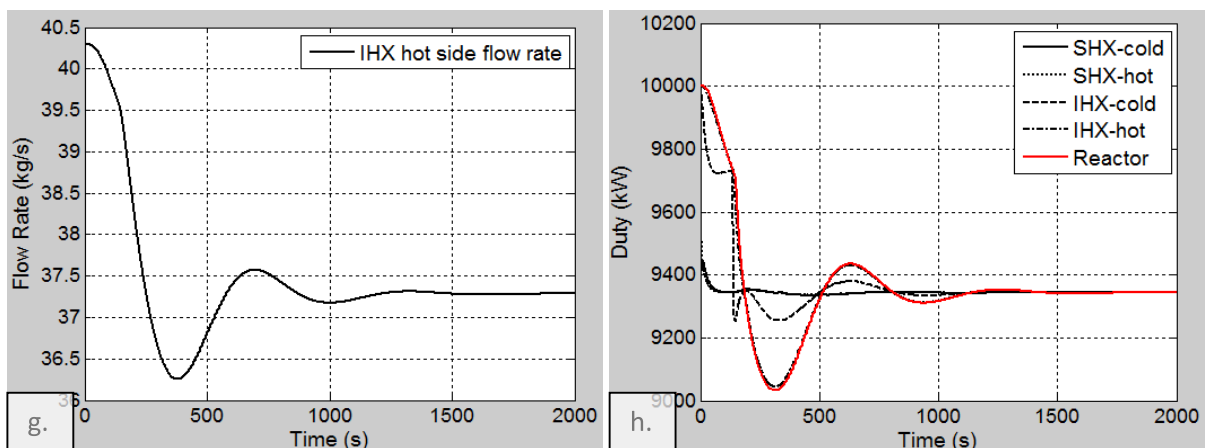
Figure 29. Controlled response of system after disturbance of +10 °C entering cold side of SHX. a: SHX cold outlet temperature, b: SHX hot outlet temperature, c: IHX cold outlet temperature, d: IHX hot side outlet temperature, e: Reactor outlet temperature, f: SHX hot side flow rate, g: IHX hot side flow rate h: Duties of SHX, IHX, and reactor.

Figure 30 shows the opposite case in which a temperature disturbance of -10 °C is introduced in the stream entering the cold side of the SHX (T_{ci}). Figures 30a and 30d show the controlled variables for the SHX (T_{co}) and IHX (T_{ho2}), respectively, returning to their set-point values by manipulating the hot side flow rates. Figures 30b and 30c, respectively, show the other temperatures not being controlled in the SHX (T_{ho}) and IHX (T_{co2}). At equilibrium T_{ho} increases by ~5.3 °C while T_{co2} increases by a little over 0.5 °C. To counteract the decrease in temperature of the controlled variables, both hot side flow rates (F_{hi}/F_{hi2}) increase: F_{hi} by ~0.9 kg/s (+2.5%) and F_{hi2} by ~3.1 kg/s (+7.7%) as seen in Figures 30f and 30g. The increase in the flow rate in the primary loop causes a decrease in the outlet temperature of the reactor of just under 1.0 °C as seen in Figure 30e. Again, the system is in equilibrium in ~1200 seconds with an overall duty increase of ~650 kW (6.5%) as seen in Figure 30h.
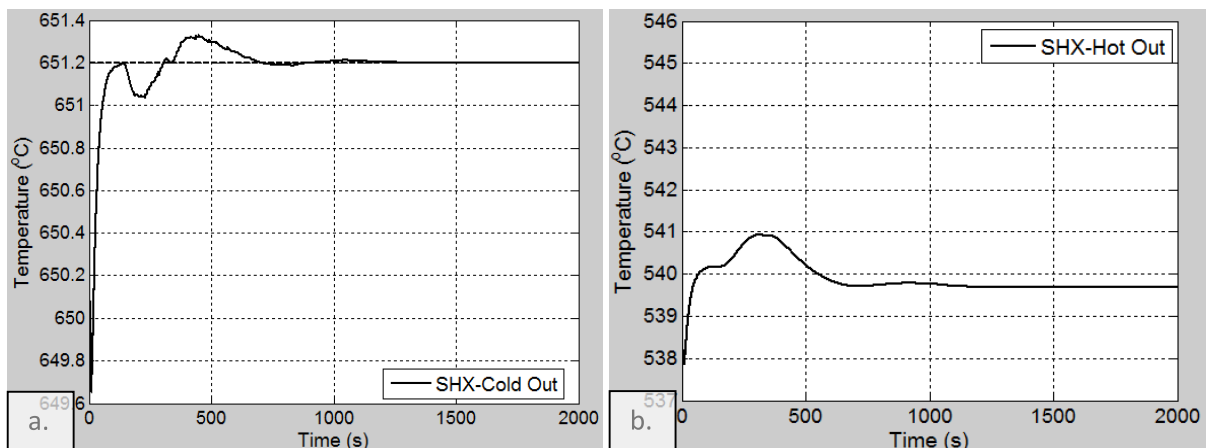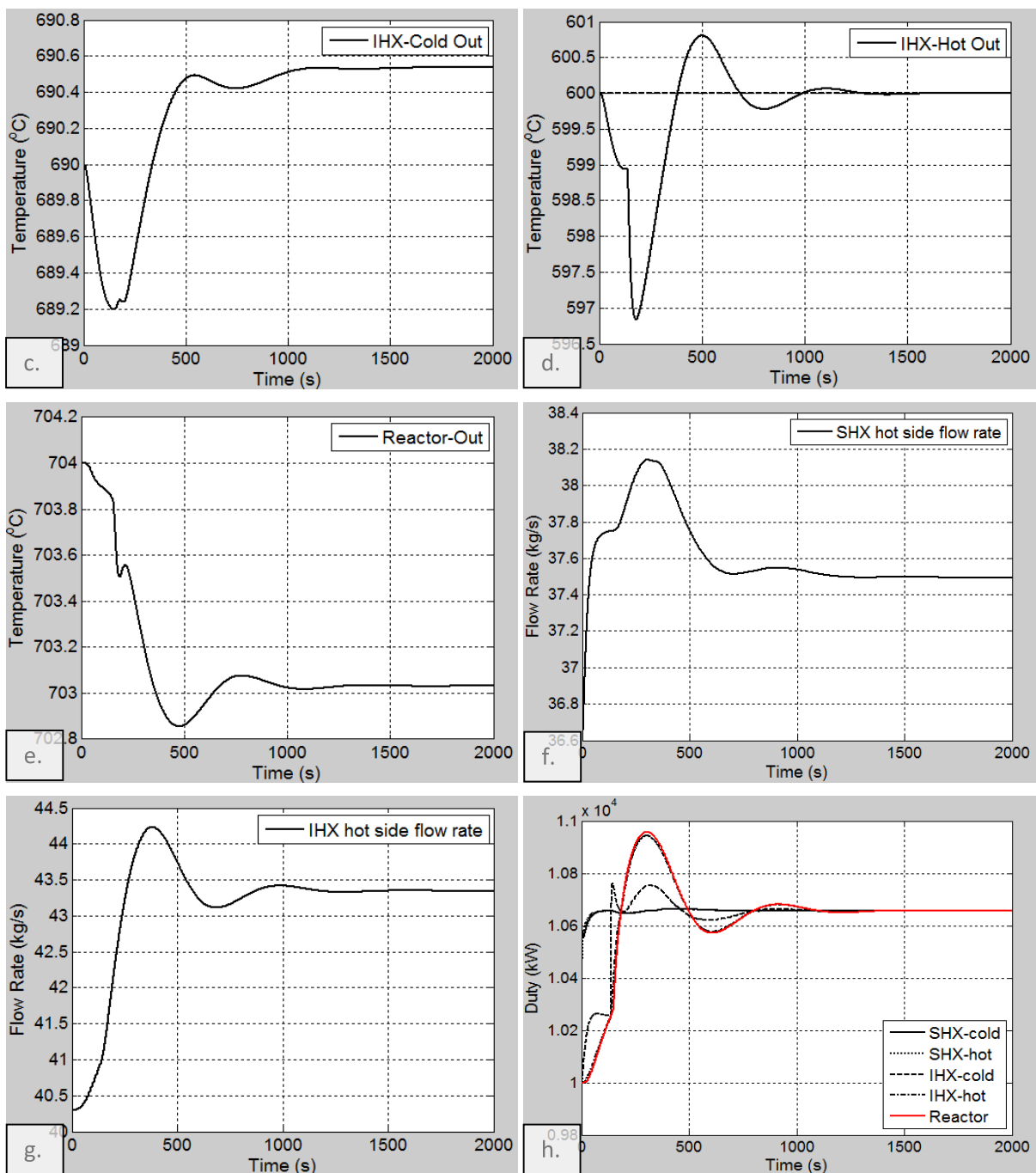
Figure 30. Controlled response of system after disturbance of -10 °C entering cold side of SHX. a: SHX cold outlet temperature, b: SHX hot outlet temperature, c: IHX cold outlet temperature, d: IHX hot side outlet temperature, e: Reactor outlet temperature, f: SHX hot side flow rate, g: IHX hot side flow rate h: Duties of SHX, IHX, and reactor.

4.2.3 Flow Rate Disturbances

Figure 31 shows the system response after a -10 % step change in the cold side flow rate of the SHX (F_{ci}). Figures 31a and 31d show the controlled variables for the SHX (T_{co}) and IHX (T_{ho2}), respectively. The decrease in the flow rate causes an initial spike in the controlled temperature, triggering the control system to decrease the manipulated hot side flow rates (F_{hi}/F_{hi2}). The controlled temperatures return to their set-point values as seen in Figures 31a and 31d. Figures 31b and 31c show the other temperatures not being controlled in the SHX (T_{ho}) and IHX (T_{co2}), respectively. T_{ho} decreases by ~5.0 °C while T_{co2} increases by ~3.1 °C. F_{hi} decreases by 5.4 kg/s (-14.7%) and F_{hi2} decreases by 4.5 kg/s (-11.2%) as seen in Figures 31f and 31g. After the decrease in flow rate going through the reactor an increase in outlet temperature of ~1.6 °C is seen exiting the reactor, shown in Figure 31e. The system is at equilibrium within ~1000 seconds with an overall decrease in the thermal duty of 1000 kW or 10% of the initial duty as seen in Figure 31h.
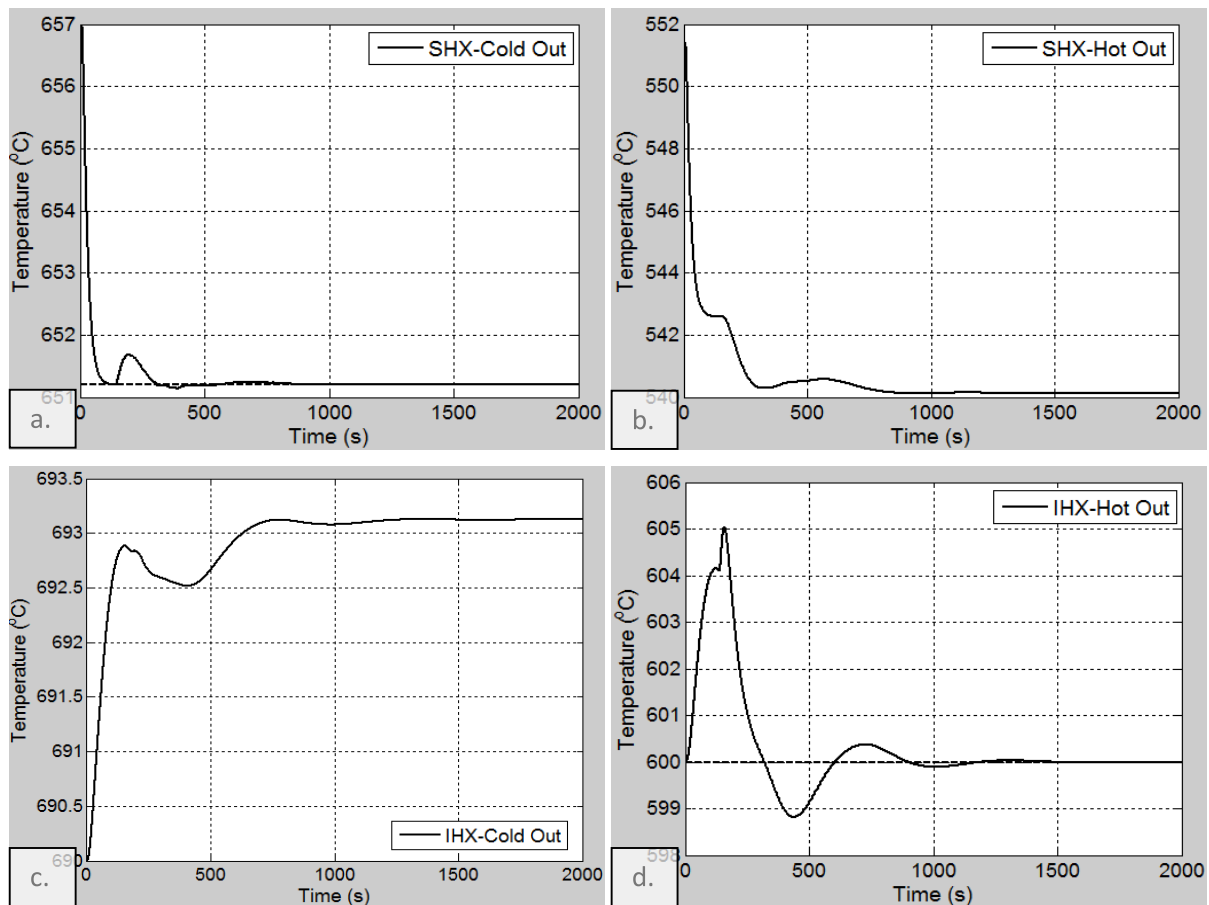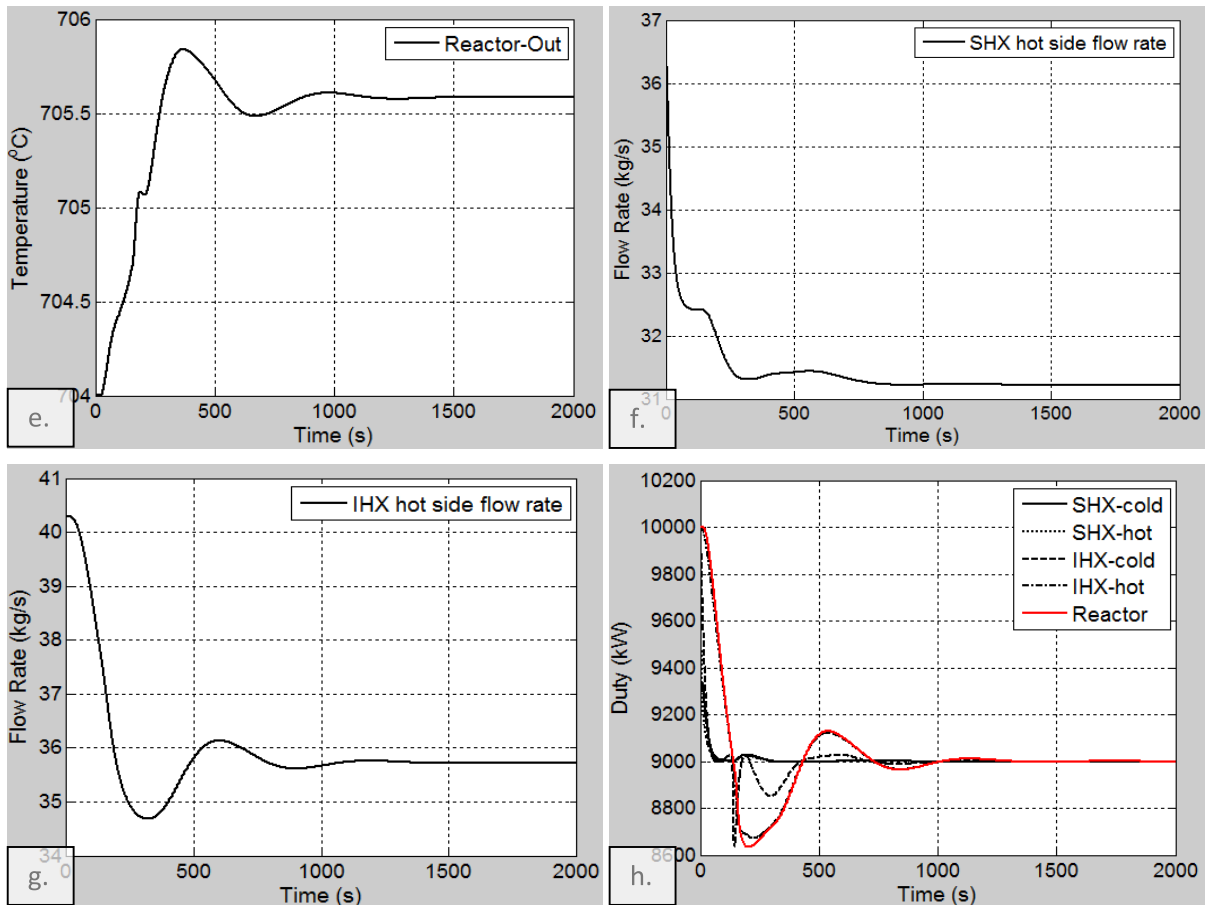
Figure 31. Controlled response of system after disturbance of -10% in the cold side flow rate of the SHX. a: SHX cold outlet temperature, b: SHX hot outlet temperature, c: IHX cold outlet temperature, d: IHX hot side outlet temperature, e: Reactor outlet temperature, f: SHX hot side flow rate, g: IHX hot side flow rate h: Duties of SHX, IHX, and reactor.

Figure 32 shows the system response after a +10 % step increase in the cold side flow rate of the SHX (F_{ci}). Figures 32a and 32d shows the controlled variables for the SHX (T_{co}) and IHX (T_{ho2}), respectively. Again, these are controlled around their set-point values after manipulation of the hot side flow rates. To counteract the decrease in temperature seen in the controlled variables both hot side flow rates (F_{hi}/F_{hi2}) must increase. F_{hi} increases by ~6.5 kg/s (+17.8%) and F_{hi2} increases by ~5.0 kg/s (+12.4%) as seen in Figures 32f and 32g. Figures 32b and 32c show the other temperatures not being controlled in the SHX (T_{ho}) and IHX (T_{co2}), respectively. T_{ho} increases by ~5.6 °C while T_{co2} decreases by ~3.7 °C. Due to the increase in flow rate going through the reactor, a decrease in outlet temperature of ~1.7 °C is seen exiting the reactor, seen in Figure 32e. The system is at equilibrium within ~1000 seconds with an overall duty increase of 1000 kW or 10% if the initial duty as seen in Figure 32h.
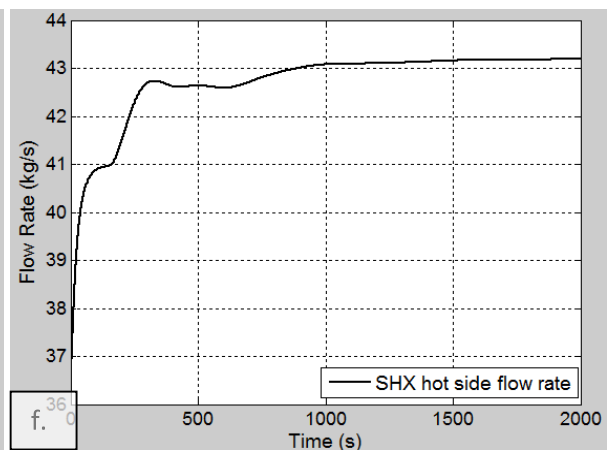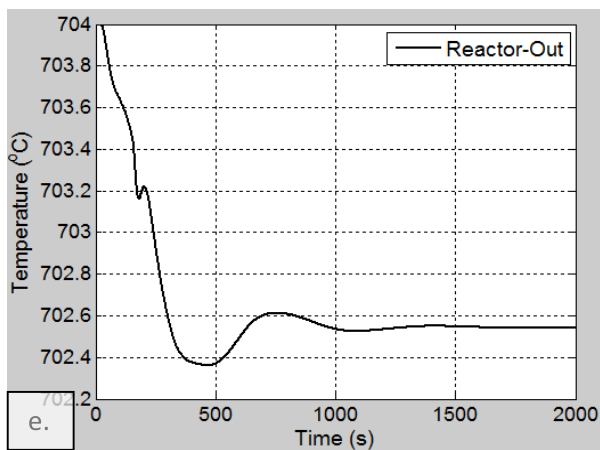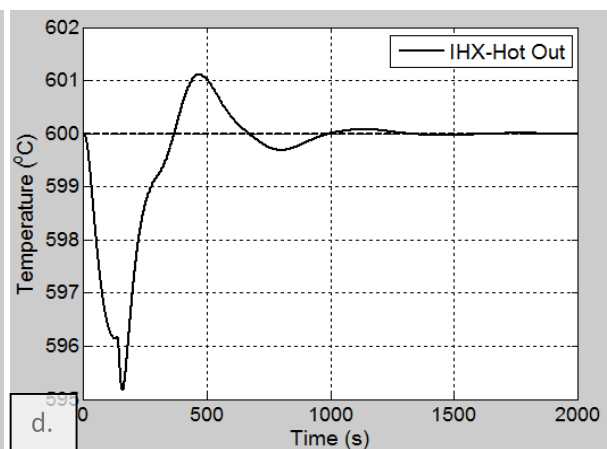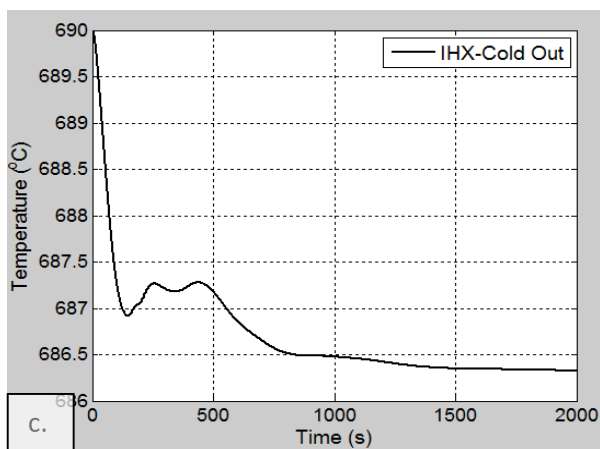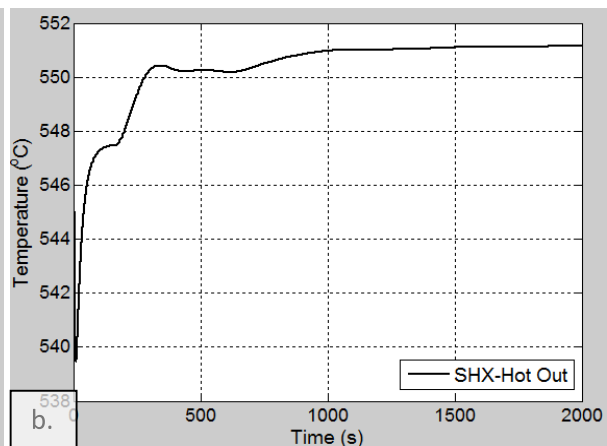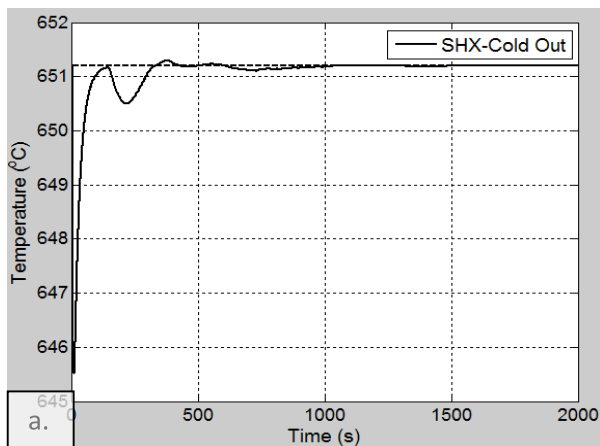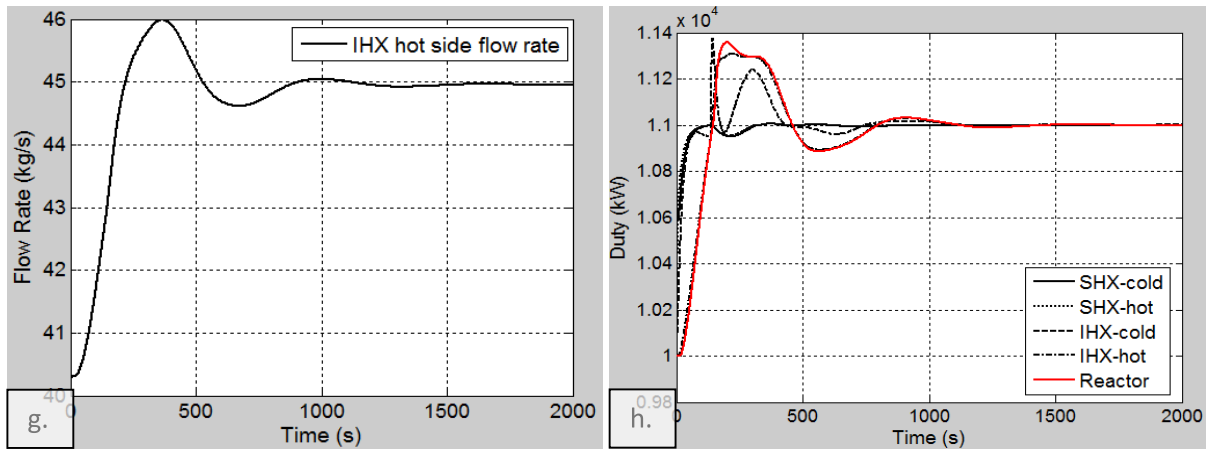
Figure 32. Controlled response of system after disturbance of +10 % in the cold side flow rate of the SHX. a: SHX cold outlet temperature, b: SHX hot outlet temperature, c: IHX cold outlet temperature, d: IHX hot side outlet temperature, e: Reactor outlet temperature, f: SHX hot side flow rate, g: IHX hot side flow rate h: Duties of SHX, IHX, and reactor.

4.2.4 Alternate Control Method

Control of both the cold side outlet temperature of the SHX (T_{co}) and the hot side outlet temperature of the IHX (T_{ho2}) by manipulation of hot side flow rate of both heat exchangers (F_{hi}/F_{hi2}) has been described above. However, there are other alternatives available for control as described below for the control of the cold outlet temperature of the SHX (T_{co}), which is the temperature of the stream providing the driving force for energy production in the power conversion unit or an alternate process, and hence considered to be the controlled variable of primary significance. The control options are:

- Control of T_{co} by manipulation of flow rate (could be F_{hi} or F_{ci})
- Control of T_{co} by controlling reactor power
    - Changing reactor power to equal the change in duty seen on the cold side of the SHX such that T_{co} will end up at its original value.
- A combination of reactor control and flow rate control
    - Initially reactor power is used to control T_{co}. As the temperature comes close to the set-point value, the system switches to using the hot side flow rate of the SHX to control T_{co}.

A comparison of the three alternatives for a disturbance of +20 °C in the temperature of the cold inlet stream of the SHX (T_{ci}) is described below.

Figure 33 shows the system response when the hot side flow rate of the SHX (F_{hi}) is manipulated to control the cold side outlet temperature (T_{co}). The initial increase in cold outlet temperature is mitigated by decreasing the hot side flow rate. As seen from Figure 33a, the controlled temperature T_{co} returns to its set point at ~600 seconds. The reactor outlet temperature decreases by about ~3.5 °C as shown in Figure 33b. The manipulated variable, the hot side flow rate (F_{hi}), changes by approximately -2.6 kg/s (-7.1%) shown in Figure 33c. Figure 33d, shows that the duties throughout the system decrease by approximately 1300 kW or 13% of the initial duty.
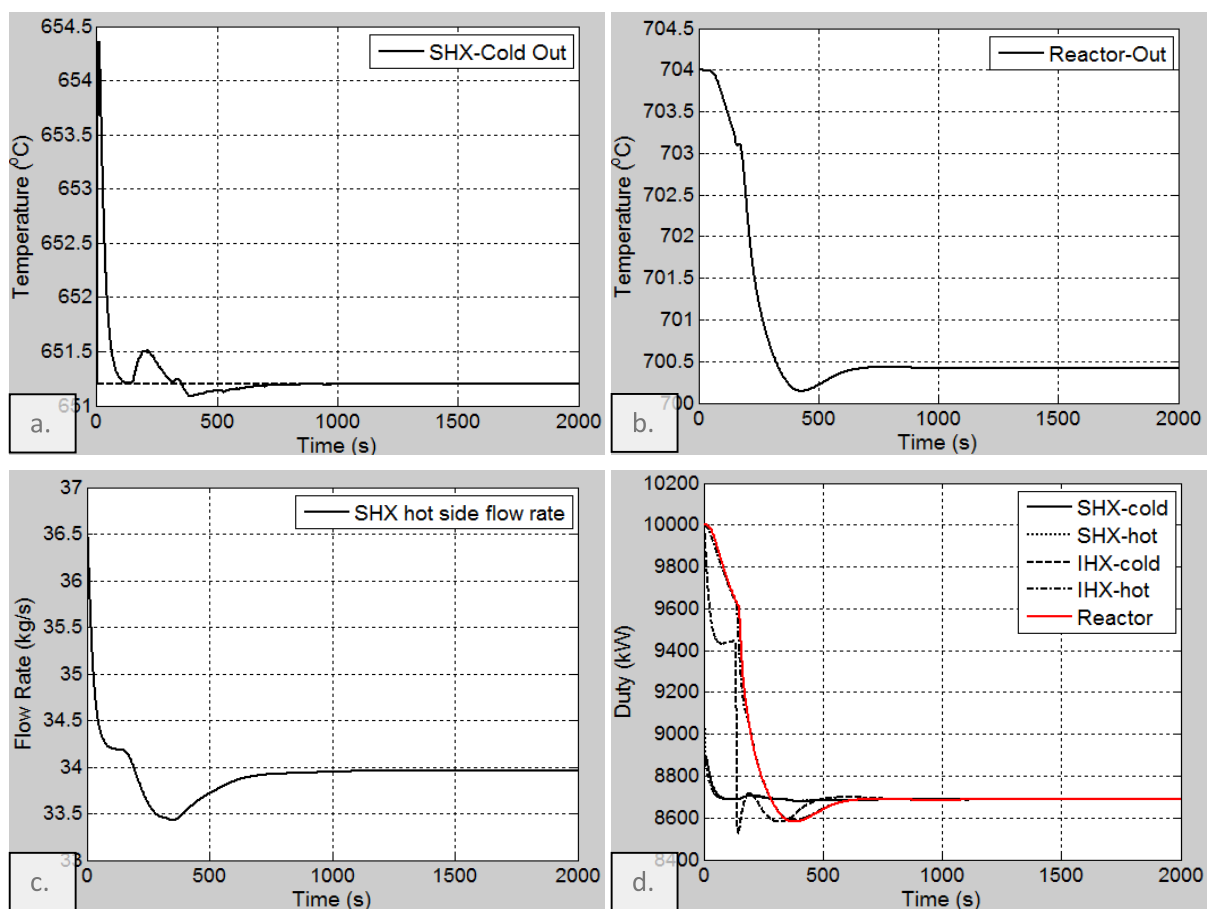
Figure 33. Controlled response of system after disturbance of +20 °C entering cold side of SHX using flow rate for control. a: SHX cold outlet temperature, b: Reactor outlet temperature, c: SHX hot side flow rate, d: Duties of SHX, IHX, and reactor.

Figure 34 shows the transients for the same disturbance when the reactor power is used to control the cold side outlet temperature (T_{co}). In this case, the reactor power is controlled to equal the duty of the cold side of the SHX such that the cold outlet temperature will equal its set point value. Figure 34a shows that it takes ~1800 seconds to reset the controlled temperature to its set point. The reactor outlet temperature decreases by ~7 °C as (Figure 34b), while the flow rate remains

unchanged (Figure 34c). The final duty of the system will be the same as for the first option, decreasing by about 1300 kW or 13%, as seen in Figure 34d.
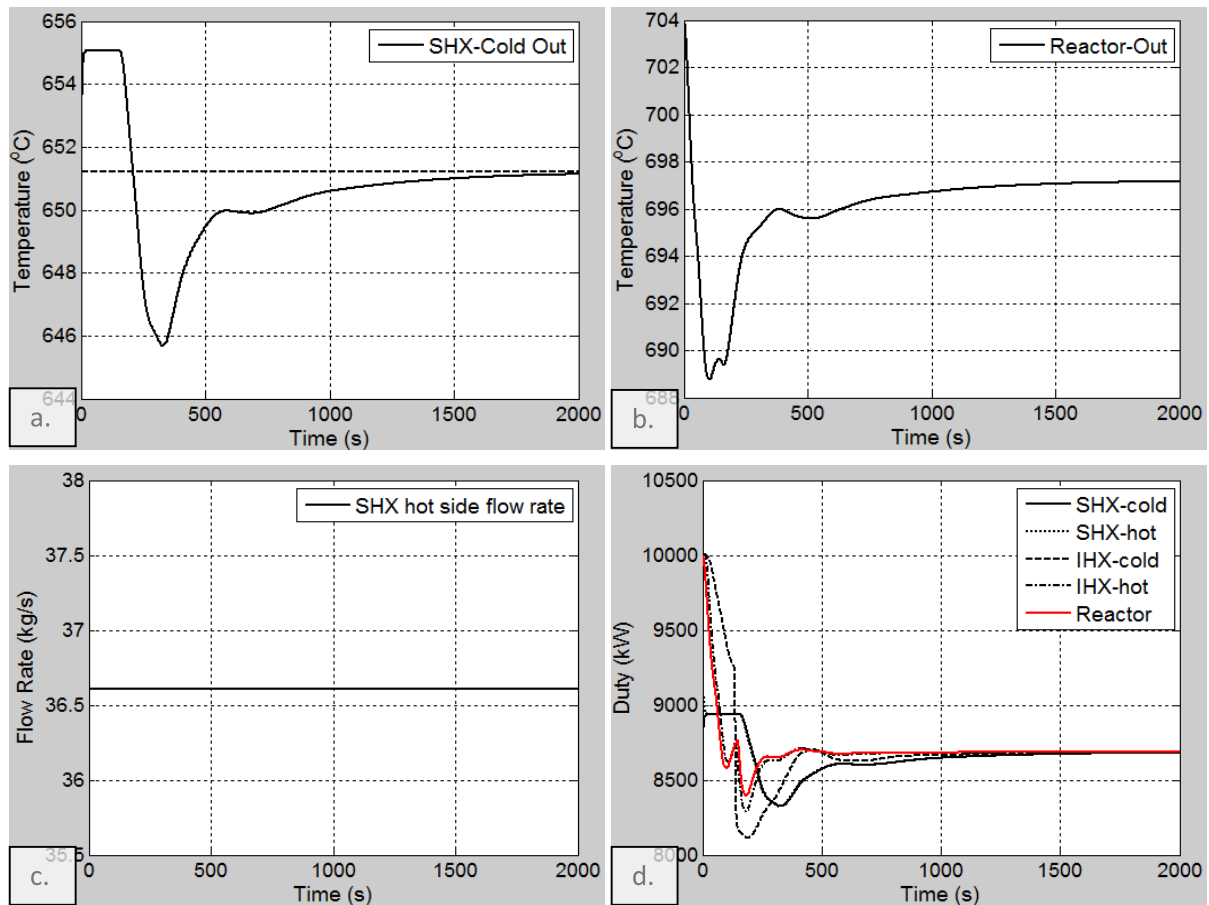
Figure 34. Controlled response of system after disturbance of +20 °C entering cold side of SHX using reactor for control. a: SHX cold outlet temperature, b: Reactor outlet temperature, c: SHX hot side flow rate, d: Duties of SHX, IHX, and reactor.

Figure 35 shows the transients when the reactor power is manipulated followed by flow rate manipulation for controlling the cold side outlet temperature (T_{co}) for the same disturbance (20 °C increase in the temperature of cold inlet stream of the SHX (T_{ci})). Initial control is accomplished by manipulating the reactor power until the controlled temperature T_{co} is within 1 °C of the set point (at ~800 s), when the system switches to manipulating hot side flow rate (F_{hi}) for the final part of the control. Figure 35a shows that T_{co} is reset in ~900 seconds, while the reactor outlet temperature decreases by ~7.5 °C (Figure 35b). As seen in Figure 35c, a small flow rate change of +0.75 kg/s or +2.0% is required. Again, the final duty of the system will be the same as seen previously decreasing by ~1300 kW or -13%, as seen in Figure 35d.
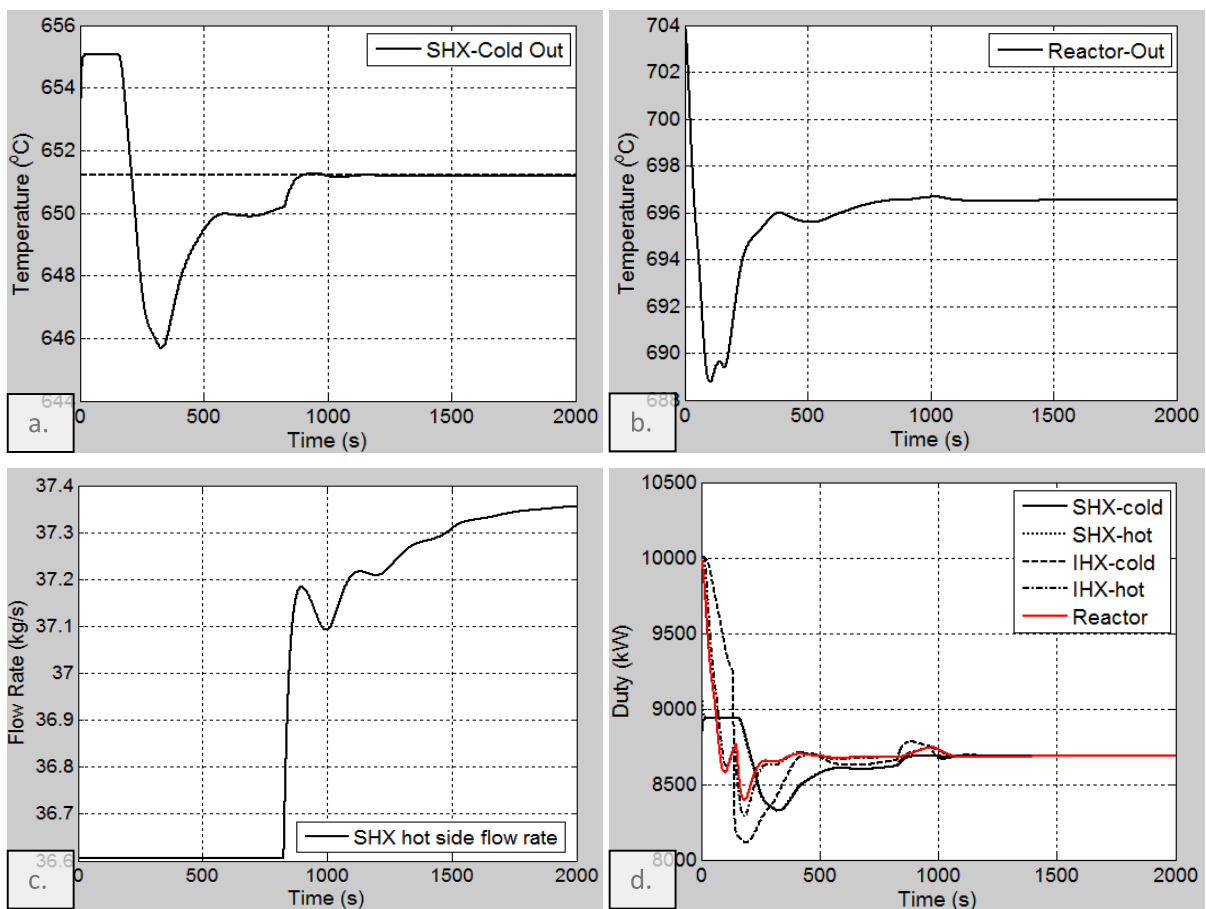
Figure 35. Controlled response of system after disturbance of +20 °C entering cold side of SHX using reactor power followed by flow rate manipulation for control. a: SHX cold outlet temperature, b: Reactor outlet temperature, c: SHX hot side flow rate, d: Duties of SHX, IHX, and reactor.

It can be seen by using just the flow rate for control (the first option) the response is much quicker – new equilibrium is reached in ~600 s. However, a large change in flow rate - -7.1% in F_{hi} – is necessary. When using the reactor power only for control (the second option), the response is much slower (time to new equilibrium state tripled to ~1800 s) but no flow rate change is necessary. With the last scheme (the third option), the response time is between the two (response time ~900 s) and only a small change in flow rate (+2%) is necessary for the control. Depending on the situation, one of these schemes may be preferred over the others.

4.2.5 Summary of Control Results

The control system response to various disturbances is summarized in Table 12. As seen from the table, the system is able to establish a new steady state for step temperature disturbances and step flow rate disturbances coming from the process loop.

Table 12. **Summary of control results for different disturbances with reactor.**

Loop	Disturbance	SHX flow rate change %	IHX flow rate change %	Change in Thermal Duty kW
		Temperature Disturbances		
Process	-10 °C	F_{hi}= +2.5%	F_{hi2}= +7.7%	+650 (+6.5%)
	+10 °C	F_{hi}= -2.2%	F_{hi2}= -7.4%	-650 (-6.5%)
		Flow Rate Disturbances		
	-10% F_c	F_{hi}= -14.8%	F_{hi2}= -11.2%	-1000 (-10%)
	+10% F_c	F_{hi}= +17.8%	F_{hi2}= +12.4%	+1000 (+10%)

It can be seen that flow rate disturbances require a larger manipulation of the hot side flow rates than temperature disturbances for control. Normalizing the disturbances on the basis of the disturbance in the thermal duty indicates similar level of changes in the hot side flow rate of the IHX ($F_{hi2,}$ column 4) for both flow rate and temperature disturbances. However, for the SHX, a much larger change in the hot side flow rate ($F_{hi,}$ column 3) is necessary for flow rate disturbances than temperature disturbances. Apart from the magnitude of changes in flow rate, another factor of importance is the time period for which the cold side outlet temperature of the SHX (T_{co}) is not around its set point value. The simulation results show that at any given time the temperature does not exceed ~±5 °C from the design value with these disturbances due to the quick responses of the tuned PID controllers. In addition, the SHX responds quickly and within 100 seconds the temperature does not exceed 1 °C. Controlling the cold outlet temperature of the SHX allows for the process to run at high efficiencies. The SHX is much more compact compared to IHX, thus changes in the exchanger affect the parameters at a quicker rate. The larger IHX takes more time to react to changes in the flow rate. This can be seen in the plots from sections 3.3.2 and 3.3.3. . The alternate control strategy results are summarized in Table 13.

Table 13. **Equilibrium time and flow rate change for alternate control strategy.**

Control Option	Disturbance	SHX flow rate change %	Equilibrium time s	Change in Thermal Duty kW
1	+20 °C	F_{hi}= -7.1%	600	-1300 (-13.0%)
2	+20 °C	F_{hi}= +0.0%	1800	-1300 (-13.0%)
3	+20 °C	F_{hi}= +2.0%	900	-1300 (-13.0%)

As can be seen from the table, control option 3 (reactor power manipulation followed by flow rate manipulation) response, while 50% slower than option 1 (flow rate manipulation only) is twice as fast as the option 2 (reactor power manipulation only). Further, the flow rate change needed for option 1 is more than 3 times as high as that for option 3. The third control method has a quick response and only a small change in the flow rate is necessary. However, the controlled temperature is far from the set point value for ~300 seconds longer than control option 1. This could have an effect on the efficiency of the process. The process is designed to operate for a narrow range of temperature and a minimum temperature must be present to prevent process failure. A larger disturbance may cause the temperature to dip below the minimum value so a quick response, as seen in control option 1, may be desired. If only minimal changes in the temperature are seen entering the process, control option 3 may be favored in order to prevent large flow rate changes in the secondary loop.

CHAPTER 5: CONCLUSION AND FUTURE WORK

5.1 CONCLUSION

In this work dynamic simulations for the AHTR system were accomplished using simulation softwares PRO-II and DYNSIM, as well as using MATLAB. PRO-II and DYNSIM were successfully used to simulate and analyze the coupled IHX and SHX system after numerous disturbances were introduced into the system. It was found that temperature disturbances in the process loop had the largest effect on duty. Additionally, the system takes more time to arrive at a new steady-state operational point after temperature disturbances. In general, flow rate disturbances took less time to come to equilibrium and had an overall lower impact on the thermal duties in the system.

A MATLAB code was created and used to simulate the dynamics and control of the AHTR system. Two controllers were incorporated into the code to control the temperatures of the cold side outlet stream of the SHX (T_{co}) and hot side outlet stream of the IHX (T_{ho2}) by manipulating either the hot side flow rates (F_{hi}/F_{hi2}), cold side flow rates (F_{ci}/F_{ci2}), or combination of these. Transfer functions were used to tune the controllers and simulate the transient response of the control system to temperature disturbances in the process and primary loops, representing either a problem in the process or the reactor. For a 10 °C step change in the process, the hot side flow rates (F_{hi}/F_{hi2}) changed between 5% and 7% of the initial flow rate and the duty changed by ±650 kW or ±6.5% to maintain the controlled temperatures at their set points. For the same disturbances in the primary loop, the cold side flow rates (F_{ci}/F_{ci2}) changed between 6% and 10% of the initial flow rate and the overall duty change was approximately ±1000 kW, or 10% of the initial duty. The disturbances in the primary loop had an overall greater impact on the system. It may be best to have a control strategy in which the manipulated variables depend on where the disturbance occurs. For example, if the disturbance is from the process side then the hot side flow rates (F_{hi}/F_{hi2}) may be the desired manipulated variables. However, if the disturbance comes from the primary loop then using the cold side flow rates (F_{ci}/F_{ci2}) may produce better control. In addition, switching of the manipulated variable after a certain pre-set limit ($\pm$20% change in the manipulated variable) was reached for that variable was investigated. This limit is reached for larger temperature disturbances in the system, which triggered a switching of the manipulated variables. The system was able to come to a new equilibrium state relatively quickly while successfully maintaining the controlled temperatures at their set points.

The final part of this research transitioned from using transfer functions to using differential equations to model the heat exchangers. In addition differential equations for the nuclear reactor were included, completing the AHTR system. The reactor model included the point kinetic equations with 3 groups of delayed neutrons. 3 groups was chosen over 6 groups for the lower computational load while minimizing the error. The system response was simulated using MATLAB codes for a number of different temperature and flow disturbances introduced into the system. Two types of control strategies were implemented into the model. The first was identical to the first MATLAB model and involved 2 controllers in which the cold side outlet temperature of the SHX (T_{co}) and hot side outlet temperature of the IHX (T_{ho2}) are controlled by manipulation of the hot side flow rate of the SHX (F_{hi}) and hot side flow rate of the IHX (F_{hi2}). Temperature disturbances of ±10 ^{o}C required flow rate changes of ±2-8% of their initial value to properly control the system. Flow rate disturbances of ±10% F_c required a larger change in flow rate of ±11-18% of their initial values for control. The second control strategy involved the control of the cold outlet temperature of the SHX (T_{co}) using 3 different control options. The first involved manipulating the flow rate, the second controlling the reactor power and the third a combination of the first two options. The final control option combines the advantages from the other two control options – rapidity of the response from option one, and minimal flow rate change from option two – and is potentially a superior option compared to the first two.

5.2 FUTURE WORK

Continued development of the MATLAB code for the AHTR system should be done for increased accuracy of the results. One addition that must be made to the system is the inclusion of the helium Brayton cycle into the model. With this inclusion, we will be able to see how changes in the cold side temperature exiting the SHX (T_{co}) affect the efficiency of the power cycle. Once a sufficient Brayton cycle has been developed, it can be included into the AHTR system model. Then looking at realistic problems that may occur in the system, situations can be modeled and analyzed.

REFERENCES

Al-Dawery, S., Alrahawi, A., Al-Zobai, K., "Dynamic Modeling and Control of Plate Heat Exchanger," Int. J. Heat Mass Transfer, 55, 6873-6880, 2012.

Averill, B., Eldredge, P., "Principles of General Chemistry," Flatworld Knowledge Books, Irvington, NY, 2012.

Bartel, N., Chen, M., Utgikar, V., Sun, X., Kim, I.-H., Christensen, R., Sabharwall, P., "Comparative analysis of compact heat exchangers for application as the intermediate heat exchanger for advanced reactors," Ann. Nucl. Energy, 81, 143-149, 2015.

Chapin, D., Kiffer, S., Nestell, J., "The very high temperature reactor: A technical summary," MPR Associates, Alexandria, VA, 2004.

Chapra, S., Canale, R., "Numerical Methods for Engineers," sixth ed., McGraw-Hill, New York, 2010.

Chen, M., Lv, Q., Kim, I.-H., Sun, X., Christensen, R., Utgikar, V., Sabharwall, P., "Dynamic analysis of a fluoride salt-cooled high-temperature reactor coupled to a helium Brayton power system via an intermediate loop," Prog. Nucl. Energy, 83, 283-293, 2015.

Das, S., Pan, I., Das, A., "Fractional order fuzzy control of nuclear reactor power with thermal-hydraulic effects in the presence of random network induced delay and sensor noise having long range dependence," Energy Conv. Manage., 68, 200-218, 2013.

European nuclear society, "Fuel comparison," https://www.euronuclear.org/info/encyclopedia/f/fuelcomparison.htm, Accessed April 15, 2016.

Forsberg, C., "The advanced high-temperature reactor: High-temperature fuel, liquid salt coolant, and liquid-metal-reactor plant," Prog. Nucl. Energy, 47, 32-43, 2004.

Galvez, C., "Design and transient analysis of passive safety cooling systems for advanced nuclear reactors," Doctoral dissertation, University of California, 2011.

Garimella, S., "Experimental investigation of heat transfer and pressure drop characteristics of annuli with spirally-fluted inner tubes," Doctoral dissertation, The Ohio State University, 1990.

Gen-IV International Forum, "Annual Report." 2013.

Gen-IV International Forum, "Gen-IV Systems," https://www.gen-4.org/gif/jcms/c_59461/generation-iv-systems, Accessed April 15, 2016.

Guomin, C., Jinyang, W., Tao, J., Xiangbai, H., "Transfer behavior of heat exchanger," Adv. Mater. Res., 233-235, 1281-1287, 2011.

Ingersoll et al., "Status of Preconceptual Design of the Advanced High-Temperature Reactor (AHTR)," ORNL Report # ORNL/TM-2004/104, 2004.

International Atomic Energy Agency, "Status of advanced light water reactor designs," IAEA-TECDOC-1391, Vienna, 2004.

Kessler, G., Veser, A., Schlüter, F.-H., Raskob, W., Landman, C., Päsler-Sauer, J., "The risks of nuclear energy technology: Safety concepts of light water reactors," Science Policy Reports, Springer, Verlag Berlin Heidelberg, 2014.

Lamarsh, J., Baratta, A., "Introduction to Nuclear Engineering," third ed., Prentice Hall, Upper Saddle River, 2001.

Manglik, R., Bergles, A., "Heat transfer and pressure drop correlations for the rectangular offset strip fin compact heat exchanger," Exp. Therm. Fluid Sci., 10, 171-180, 1995.

Michel, A., Kugi, A., "Model based control of compact heat exchangers independent of the heat transfer behavior," Journal of Process Control, 24, 286-298, 2014.

Nuclear Energy Institute, "US nuclear power plants," http://www.nei.org/Knowledge-Center/Nuclear-Statistics/US-Nuclear-Power-Plants, Accessed April 20, 2016.

Nuclear Regulatory Commission, "The boiling water reactor (BWR)," http://www.nrc.gov/reading-rm/basic-ref/students/animated-bwr.html, Updated September 2015.

Nuclear Regulatory Commission, "The pressurized water reactor (PWR)," http://www.nrc.gov/reading-rm/basic-ref/students/animated-pwr.html, Updated September 2015.

Pan, I., Das, S., Gupta, A., "Tuning of an optimal fuzzy PID controller with stochastic algorithms for networked control systems with random time delay," ISA Trans., 50, 28-36, 2011.

Peterson, F., "Liquid-salt cooled Advanced High Temperature Reactors," GoNERI Seminar, University of California, Berkeley, CA, 2008.

Peterson, F., "The pebble-bed AHTR liquid salt cooled reactor," Forum on Small and Medium Reactors, University of California, Berkeley, CA, June 18, 2010.

Ragheb, M., "Loss of coolant accident, LOCA," University of Illinois at Urbana-Champaign, IL, 2013.

Ragheb, M., "Thermochemical iodine sulfur process for hydrogen production," University of Illinois at Urbana-Champaign, IL, 2014.

Sabharwall, P., Utgikar, V., Tokuhiro, A., Gunnerson, F., "Design of liquid metal phase change heat exchanger for next generation nuclear plant process heat application," J. Nucl. Sci. Technol., 46(6), 534-544, 2009.

Sabharwall, P., Patterson, M., Utgikar, V., Gunnerson, F., "Phase change heat transfer device for process heat application," Nucl. Eng. Des., 240, 2409-2414, 2010.

Sabharwall, P., Collins, J., Clark, D., Siahpush, A., Phoenix, W., McKellar, M., and Patterson, M., "Technology Development Roadmap for the Advanced High Temperature Reactor Secondary Heat Exchanger," INL/EXT-12-26219, Idaho National Laboratory, Idaho, September 2012.

Sabharwall, P., O'Brien, J.E., Yoon, S.-J., Sun, X. "Experimental facility for development of high-temperature reactor technology: instrumentation needs and challenges," EP J. Nucl. Sci. Technol., 1, 14-23, 2015.

Sohal, M. S., Ebner M. A., Sabharwall, P., Sharpe, P., "Engineering database of liquid salt thermophysical and thermochemical properties," INL/EXT-10-18297, Idaho National Laboratory, Idaho Falls, ID, March 2010.

World Nuclear Association, "Three Mile Island Accident," http://www.world-nuclear.org/information-library/safety-and-security/safety-of-plants/three-mile-island-accident.aspx, Updated January 2012.

World Nuclear Association, "Outline history of nuclear energy," http://www.world-nuclear.org/information-library/current-and-future-generation/outline-history-of-nuclear-energy.aspx, Updated March 2014.

World Nuclear Association, "Chernobyl Accident 1986," http://www.world-nuclear.org/information-library/safety-and-security/safety-of-plants/chernobyl-accident.aspx, Updated April 2016.

APPENDIX A: ADVANCED REACTOR FUEL AND REACTOR DYNAMICS

A.1 TRISO FUEL DESCRIPTION

The coated-particle graphite-matrix is shown in Figure 36 also known as TRISO fuel. Four outer layers consist of pyrolytic carbon, silicon carbide, another layer of pyrolytic carbon, and a porous carbon buffer. In the center lies the fuel kernel which has all of the fissionable material. The exact geometry of the particle will be optimized depending on the design trade-offs for performance, costs, safety, and more (Ingersoll et al., 2004). These particles are packed into rods and put into an assembly. The coolant travels through the reactor and heats up as the fission process occurs within the assemblies.
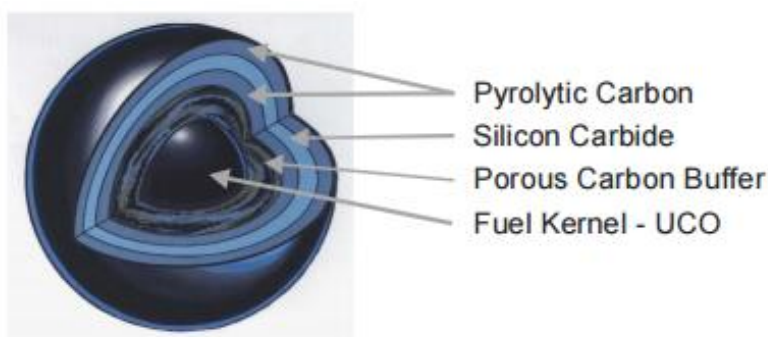
Figure 36. TRISO coated-particle graphite-matrix (Ingersoll et al., 2004).

A.2 REACTOR DYNAMICS FUNDAMENTALS

In section 2.4.2 equations describing the dynamics of the reactor are described. More details on these equations will be described here. There are two types of neutrons that emit during the fission process in a nuclear reactor. There are prompt neutrons and delayed neutrons. Prompt neutrons are neutrons released within ~10^{-14} seconds after fission occurs. After this point the neutrons are considered delayed. The majority of neutrons released are prompt neutrons but the actual percentage is dependent on the fuel being used. For example with U-235 about 99.35% of the neutrons are prompt meaning the other 0.65% of the neutrons are delayed. However, as fuel becomes depleted these percentages will change. Without the existence of delayed neutrons reactor power control would be very difficult. The power change would be too quick if only prompt neutrons were to exist.

Delayed neutrons can be split into a number of groups depending on their half-lives. Each of these neutron groups is called a precursor and has a specific half-life and group fraction. In general the precursors are split into 6 groups. Eq. 18 shows the equations for each precursor group and Eq. 17 shows the equations for the neutrons in the reactor. These are both considered point kinetic equations and don't take into account the spatial effects that may be seen in an actual nuclear reactor. Eqs 17-21 are repeated and described below.

$$\frac{dn}{dt} = \frac{\rho - \beta}{\Lambda} n + \sum_{i=1}^{G} \lambda_i c_i \tag{17}$$

Eq. 17 is the neutron density balance. The term on the left is the change in neutron density (n: number of neutrons per unit volume) with time. On the right side of the equation several parameters exist however only some will vary or may be altered with changes in the system. ρ is the reactivity of the reactor. At steady-state the value of this is 0 but changes in temperature or control rod position can alter this. The units of reactivity are $. The value is dependent on the delayed neutron fraction (β) and thus dependent on the fuel used. The reactivity in $ is equal to ρ/β. For example a reactivity insertion of 1$ mean that ρ=β. As noted β is the delayed neutron fraction for a specific fuel, which is 0.006502 for U-235. Below those two parameters is the parameter for prompt neutron lifetime (Λ). This parameter is in seconds and is equal to the average time it takes a prompt neutron to either be absorbed or escape the system. The right side of the equations shows the sum of the precursor concentrations (c_i: precursor amount per unit volume) times their respective decay constants (λ_i). The decay constant is related to the half-life as follows: $\lambda_i = 0.693 / h_i^{1/2}$. 1 to 6 terms can be included in the equation depending on the number of precursor groups that are chosen to be included in the model.

$$\frac{dc_i}{dt} = \frac{\beta_i}{\Lambda} n - \lambda_i c_i \quad \textit{for i=1,2,...,G} \tag{18}$$

Eq. 18 is the precursor concentration balance. The term on the left is the change in precursor concentration (c_i) with time. Several of the parameters in this balance are the same as in Eq. 17. One additional parameter is β_i which is the delay neutron fraction for precursor group *i*. The summation of all of the individual delay neutron fractions (β_i) is equal to the total delay neutron fraction (β). One of these equations is necessary for every precursor group that is included in the model. As can be seen in these two equations the neutron density (n) and precursor concentration (c) are dependent on one another. Changes in the neutron density will affect the precursor concentration and changes in the precursor concentration will affect the neutron density.

$$\frac{dT_f}{dt} = \frac{P}{\mu_f}n - \frac{\Omega}{\mu_f}T_f + \frac{\Omega}{2\mu_f}T_i + \frac{\Omega}{2\mu_f}T_e \tag{19}$$

$$\frac{dT_e}{dt} = \frac{2\Omega}{\mu_c}T_f - \left(\frac{2M_c+\Omega}{\mu_c}\right)T_e + \left(\frac{2M_c-\Omega}{\mu_c}\right)T_i \tag{20}$$

Eqs. 19 and 20 show the energy balances for the fuel and the coolant, respectively. Changes in the fuel temperature are dependent on the fuel temperature and coolant temperature, as well as the neutron density in the system. Changes in the fuel temperature and inlet coolant temperature of the reactor will have an effect on the coolant exiting temperature as seen in Eq. 20.

$$\rho = \rho_{rod} + \alpha_f\left(T_f - T_{f0}\right) + \frac{\alpha_c}{2}(T_i - T_{i0}) + \frac{\alpha_c}{2}(T_e - T_{e0}) \tag{21}$$

Eq. 21 is an equation for reactivity (ρ). The first term on the right (ρ_{rod}) is the change in reactivity due to control rod movement. The other 3 terms on the right are how the reactivity changes with change in inlet and exit coolant temperatures and fuel temperature. It can be seen that the reactivity is 0 if ρ_{rod} is 0 and the temperatures of the reactor are at their original design values. If there are changes in coolant or fuel temperatures then there will be a change in reactivity due to the reactivity coefficients (α) described in section 2.4.2.

APPENDIX B: FTHX AND OSFHX DESIGNS

The IHX is a fluted tube heat exchanger (FTHX). A cross-section of one of the tubes is shown in Figure 37. The tubes are straight but are twisted to give the geometry shown below. A different number of fluted starts can be done giving different geometries and flow patterns. The design makes swirling flow patterns which promote heat transfer.
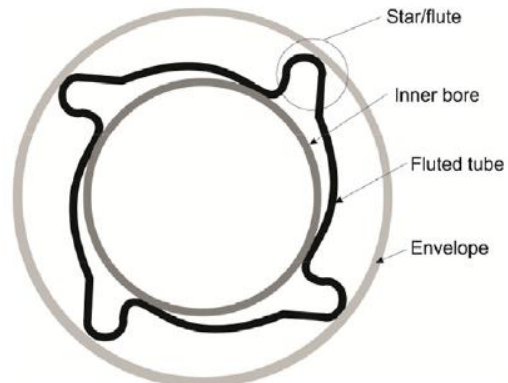
Figure 37. Cross-section of fluted tube in FTHX (Chen et al., 2015).

The SHX is an offset strip-fin heat exchanger (OSFHX). The design of the fins on each plate is shown in Figure 38. The fins can have different thickness, pitches, lengths and heights. The fins prevent large boundary layers from being formed which increases heat transfer in the heat exchanger.
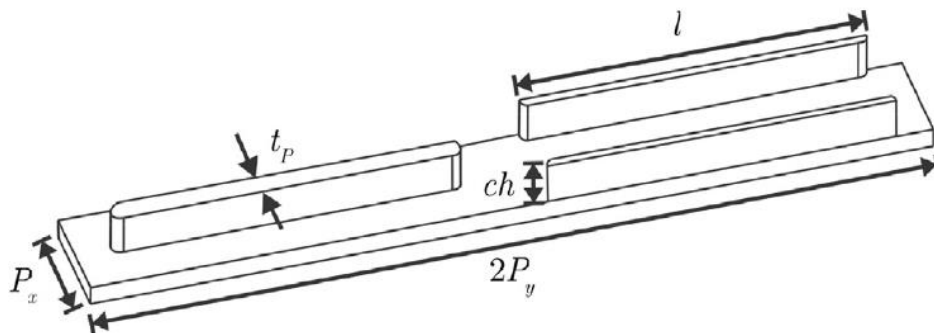
Figure 38. Offset strip-fin design in OSFHX (Chen et al., 2015).

APPENDIX C: TRANSFER FUNCTIONS, GAINS, AND TIME CONSTANTS

Transfer functions for the hot side of the heat exchangers are shown below.

$$G_{s5} = \frac{\Delta T_{ho}}{\Delta F_{hi}} = \frac{K_{hFh}}{T_h s + 1} \tag{30}$$

$$G_{s6} = \frac{\Delta T_{ho}}{\Delta F_{ci}} = \frac{K_{hFc}}{T_h s + 1} \tag{31}$$

$$G_{s7} = \frac{\Delta T_{ho}}{\Delta T_{ci}} = \frac{K_{htc} e^{-\tau_h s}}{T_h s + 1} \tag{32}$$

$$G_{s8} = \frac{\Delta T_{ho}}{\Delta T_{hi}} = \frac{K_{hth}}{T_h s + 1} \tag{33}$$

The gains to changes are calculated by methods developed previously based on simple energy balance for various streams (Guomin et al., 2011). Temperature gains are as follows.

$$K_{ctc} = \frac{\Delta t_{co}}{\Delta t_{ci}} = \frac{\frac{F_c Cp_c}{F_h Cp_h} - 1}{\frac{F_c Cp_c}{F_h Cp_h} - B_c} \tag{34}$$

This is the gain for change in cold side outlet temperature due to changes in cold side inlet temperature.

$$K_{cth} = \frac{\Delta t_{co}}{\Delta t_{hi}} = \frac{1 - B_c}{\frac{F_c Cp_c}{F_h Cp_h} - B_c} \tag{35}$$

This is the gain for change in cold side outlet temperature due to changes in hot side inlet temperature.

$$K_{hth} = \frac{\Delta t_{ho}}{\Delta t_{hi}} = \frac{B_h - B_h \frac{F_h Cp_h}{F_c Cp_c}}{1 - B_h \frac{F_h Cp_h}{F_c Cp_c}} \tag{36}$$

This is the gain for change in hot side outlet temperature due to changes in hot side inlet temperature.

$$K_{htc} = \frac{\Delta t_{ho}}{\Delta t_{ci}} = \frac{1 - B_h}{1 - B_h \frac{F_h Cp_h}{F_c Cp_c}} \tag{37}$$

This is the gain for change in hot side outlet temperature due to changes in cold side inlet temperature.

These gains describe the change in outlet temperature with changes in the inlet temperatures. B_c and B_h are shown below.

$$B_h = e^{\frac{k_h A_h}{F_c C p_c} - \frac{k_h A_h}{F_h C p_h}} \tag{38}$$

$$B_c = e^{\frac{k_c A_c}{F_c C p_c} - \frac{k_c A_c}{F_h C p_h}} \tag{39}$$

In these equations k is the heat transfer coefficient, A is the heat transfer area, G is the flow rate and C_p is the heat capacity. Additionally there are gains to changes in flow rates and those are shown below.

$$K_{cFc} = \frac{dt_{co}}{dF_c} = \frac{t_{hi} - t_{ci}}{\left(B_c - \frac{F_c C p_c}{F_h C p_h}\right)^2} \left(B_c \frac{k_c A_c}{F_c F_h C p_h} + B_c \frac{C p_c}{F_h C p_h} - B_c \frac{k_c A_c}{F_c^2 C p_c} - \frac{C p_c}{F_h C p_h}\right) \tag{40}$$

This is gain for change in cold side outlet temperature due to changes in cold side flowrate.

$$K_{cFh} = \frac{dt_{co}}{dF_h} = \frac{t_{hi} - t_{ci}}{\left(B_c - \frac{F_c C p_c}{F_h C p_h}\right)^2} \left(B_c \frac{k_c A_c}{F_h^2 C p_h} + \frac{F_c C p_c}{F_h^2 C p_h} - B_c \frac{k_c A_c F_c C p_c}{F_h^3 C p_c^2} - B_c \frac{F_c C p_c}{F_h^2 C p_h}\right) \tag{41}$$

This is gain for change in cold side outlet temperature due to changes in hot side flowrate.

$$K_{hFh} = \frac{dt_{ho}}{dF_h} = \frac{t_{hi} - t_{ci}}{\left(B_h \frac{F_h C p_h}{F_c C p_c} - 1\right)^2} \left(B_h \frac{k_h A_h}{F_h^2 C p_h} + B_h^2 \frac{C p_h}{F_c C p_c} - B_h \frac{k_h A_h}{F_h F_c C p_c} - B_h \frac{C p_h}{F_c C p_c}\right) \tag{42}$$

This is gain for change in hot side outlet temperature due to changes in hot side flowrate.

$$K_{hFc} = \frac{dt_{ho}}{dF_c} = \frac{t_{hi} - t_{ci}}{\left(B_h \frac{F_h C p_h}{F_c C p_c} - 1\right)^2} \left(B_h \frac{k_h A_h F_h C p_h}{F_c^3 C p_c^2} + B_h \frac{F_h C p_h}{F_c^2 C p_c} - B_h \frac{k_h A_h}{F_c^2 C p_c} - B_h^2 \frac{F_h C p_h}{F_c^2 C p_c}\right) \tag{43}$$

This is gain for change in hot side outlet temperature due to changes in cold side flowrate.

The time constant (T) is described below. And the time delay is simply the time it takes for the fluid to flow through the heat exchanger or simply L/v where L is the flow length and v is the velocity.

$$T = \frac{M_w C_w}{\frac{C p_c \alpha_c A_c}{C p_c + \frac{\alpha_c A_c}{2 F_c}} + \frac{\alpha_h A_h F_h}{F_h + \frac{\alpha_c A_h}{2 C p_h}}} \tag{44}$$

APPENDIX D: STABILITY ANALYSIS

Stability of the system with the tuned control parameters can be seen by looking at the step response and Nyquist plots for each of the heat exchangers. Figure 39 shows step responses and Nyquist plots for the SHX and IHX. The PID controller tunings are used as seen in Table 4 and 5. Figure 39a shows the step response for the SHX with the PID controller. The rise time is 1.75 seconds with a settling time of 2.44 seconds. The slight overshoot seen is 1.53%. Figure 39b shows the Nyquist plot for the SHX. The plot shows the closed-loop stability of the system. The point (-1, 0) can be seen on the left as a red cross. Because the loop does not circle around this point, the system is considered closed-loop stable. Figure 39c shows the step response for the IHX with the PID controller previously tuned. A slightly slower response is seen due to the larger size of the IHX. The rise time is 3.23 seconds with a settling time of 4.79 seconds. In this case the overshoot is just 0.66%. Figure 39d shows the Nyquist plot for the IHX. Again this is testing the closed-loop stability. The loop does not encircle the point (-1,0) and thus the system is considered closed-loop stable.
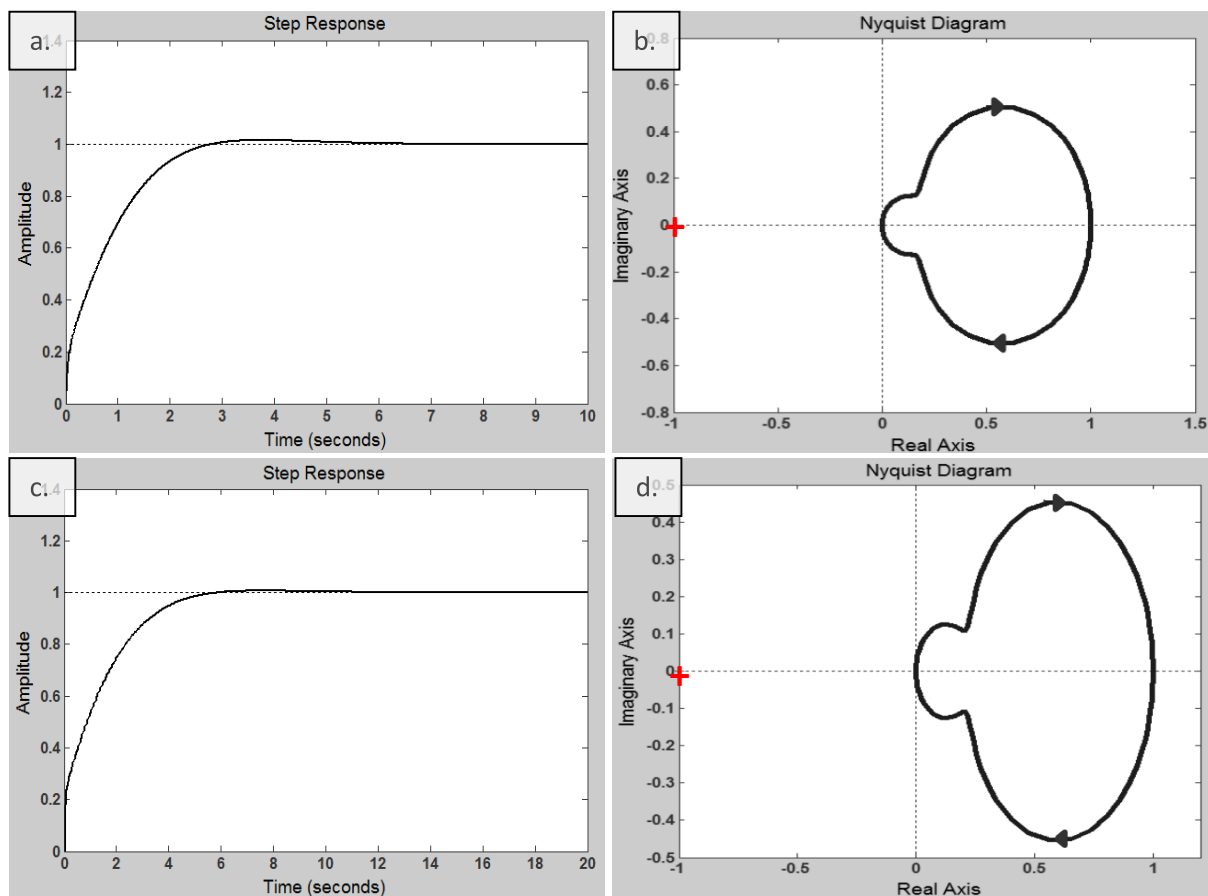
Figure 39. Step response and Nyquist plots for SHX and IHX. a: step response for SHX, b: Nyquist plot for SHX, c: step response for IHX, d: Nyquist plot for IHX.

APPENDIX E: MATLAB CODE

```matlab
close
clear all
clc

for z=1:1

Q=10000; %initial duty
P0=Q;
ft=2000; %total run time
dt=.001; %time step
t=(0:dt:ft); %time array
p=5; % discretization in SHX
m=10; %discretizations in SHX

%% preallocation
%SHX
tci=zeros(ft/dt+1,p); % SHX cold in
dtco=zeros(ft/dt+1,1); % Change in SHX cold out
tco=zeros(ft/dt+1,p); % SHX cold out
thi=zeros(ft/dt+1,p); % SHX hot in
tho=zeros(ft/dt+1,p); % SHX hot out
tw=zeros(ft/dt+1,p); %SHX wall temperature
dGh=zeros(ft/dt+1,p); % Change in SHX hot side flow rate
dGc=zeros(ft/dt+1,p); % Change in SHX cold side flow rate
Gh=zeros(ft/dt+1,p); % SHX hot side flow rate
Gc=zeros(ft/dt+1,p); % SHX cold side flow rate
hh=zeros(ft/dt+1,p); % SHX hot side heat transfer coefficient
hc=zeros(ft/dt+1,p); % SHX cold side heat transfer coefficient
vh=zeros(ft/dt+1,p); % SHX hot side velocity
vc=zeros(ft/dt+1,p); % SHX cold side velocity
tau_h=zeros(ft/dt+1,p); % SHX hot side time delay
tau_c=zeros(ft/dt+1,p); % SHX cold side time delay
mh=zeros(ft/dt+1,p);  % SHX mass of coolant on hot side
mc=zeros(ft/dt+1,p);  % SHX mass of coolant on cold side

%IHX
tci2=zeros(ft/dt+1,m); % IHX cold in
tco2=zeros(ft/dt+1,m); % IHX cold out
thi2=zeros(ft/dt+1,m); % IHX hot in
dtho2=zeros(ft/dt+1,m); % Change in IHX hot out
tho2=zeros(ft/dt+1,m); % IHX hot out
tw2=zeros(ft/dt+1,m);  % IHX wall temperature
dGh2=zeros(ft/dt+1,m); % Change in IHX hot side flow rate
dGc2=zeros(ft/dt+1,m); % Change in IHX cold side flow rate
Gh2=zeros(ft/dt+1,m);  % IHX hot side flow rate
Gc2=zeros(ft/dt+1,m);  % IHX cold side flow rate
```

```matlab
hh2=zeros(ft/dt+1,m);  % IHX hot side heat transfer coefficient
hc2=zeros(ft/dt+1,m);  % IHX cold side heat transfer coefficient
v_tube_FTHX=zeros(ft/dt+1,m); % IHX tube side velocity
v_shell_FTHX=zeros(ft/dt+1,m); % IHX shell side velocity
tau_h2=zeros(ft/dt+1,m); % IHX hot side time delay
tau_c2=zeros(ft/dt+1,m); % IHX cp;d side time delay
mh2=zeros(ft/dt+1,m); % IHX mass of coolant on hot side
mc2=zeros(ft/dt+1,m); % IHX mass of coolant on cold side

%Reactor
dtco3=zeros(ft/dt+1,1); % Change in reactor coolant outlet temp
tci3=zeros(ft/dt+1,1);  % Reactor coolant inlet temp
mdot_core=zeros(ft/dt+1,1); %Coolant flow rate through core
rho_r=zeros(ft/dt+1,1); % Reativity change due to disturbance
rho_r2=zeros(ft/dt+1,1); % reactivity change due to control rod movement
rho=zeros(ft/dt+1,1); % reactivity
Tf=zeros(ft/dt+1,1); % Fuel temperature
tco3=zeros(ft/dt+1,1); % Reactor coolant outlet temp
n=zeros(ft/dt+1,1); % neutron density
cc1=zeros(ft/dt+1,1); % precursor concentration for group 1
cc2=zeros(ft/dt+1,1); % precursor concentration for group 2
cc3=zeros(ft/dt+1,1); % precursor concentration for group 3
P=zeros(ft/dt+1,1); % Reactor power

%Duties
Qc=zeros(ft/dt+1,1); % SHX cold side duty
Q2c=zeros(ft/dt+1,1); % IHX cold side duty
Qh=zeros(ft/dt+1,1); % SHX hot side duty
Q2h=zeros(ft/dt+1,1); % IHX hot side duty
QR=zeros(ft/dt+1,1); % Reactor duty

%controller
ys_prime=zeros(1,ft/dt/2);
ys_prime_2=zeros(1,ft/dt/2);

%% Paramaters and initial values
Gc(1)=12.644 ; % SHX cold flowrate kg/s
Gh(1)=36.606 ; % SHX hot flowrate kg/s
Gc2(1)=36.606 ;      % IHX cold flowrate kg/s
Gh2(1)=40.299 ;     % IHX hot flowrate kg/s

VW=.05524; %Volume of metal in SHX m^3
W_rho=7940; %density of metal in SHX kg/m^3
VW2=.11697;  %Volume of metal in IHX m^3
W_rho2=W_rho; %density of metal in IHX kg/m^3
MW=VW*W_rho; %mass of metal in SHX kg
MW2=VW2*W_rho2; %mass of metal in IHX kg
```

```
Cpc=5.193 ; %Helium heat capacity kJ/(kg*C)
Cph=1.884 ; %FLiNaK heat capacity kJ/(kg*C)
Cpc2=Cph ;  %FLiNaK heat capacity kJ/(kg*C)
Cph2=2.386 ; %FLiBe heat capacty kJ/(kg*C)
Cpw=.460;  %metal heat capacity kJ/(kg*C)
Cpw2=Cpw;  %metal heat capacity kJ/(kg*C)

tci(1)=498.9; %SHX cold inlet temp C
tco(1)=651.2; %SHX cold outlet temp C
thi(1)=690;   %SHX hot inlet temp C
tho(1)=545;   %SHX hot outlet temp C
tci2(1)=tho(1); %IHX cold inlet temp C
tco2(1)=thi(1); %IHX cold outlet temp C
thi2(1)=704;  %IHX hot inlet temp C
tho2(1)=600;  %IHX hot outlet temp C
tci3(1)=600; %Reactor inlet temp C
tco3(1)=704; %Reacto outlet temp C

dTlm1=((thi(1)-tco(1))-(tho(1)-tci(1)))/log((thi(1)-tco(1))/ ...
   (tho(1)-tci(1)));    %LMTD of SHX
dTlm2=((thi2(1)-tco2(1))-(tho2(1)-tci2(1)))/log((thi2(1)-tco2(1))/ ...
   (tho2(1)-tci2(1)));  %LMTD of IHX

%Heat transfer area determination

[hh(1),vh(1),hc(1),vc(1)] = HTCV_OSFSHX((thi(1)+tho(1))/2,...
   (tci(1)+tco(1))/2,Gh(1),Gc(1));

[hh2(1), v_tube_FTHX(1),hc2(1), v_shell_FTHX(1)] = ...
   HTCV_FTHX((thi2(1)+tho2(1))/2,(tci2(1)+tco2(1))/2,Gh2(1),Gc2(1));

L1=.6;  % Length of SHX m
L2=5.7; % Length of IHX m

kc(1)=(1/hc(1)+1/hh(1))^-1;
%cold side overall heat transfer coefficient of SHX kW/(m^2*K)
kh(1)=kc(1);
%hot side overall heat transfer coefficient of SHX kW/(m^2*K)
kc2(1)=(1/hc2(1)+1/hh2(1))^-1;
%cold side overall heat transfer coefficient of IHX kW/(m^2*K)
kh2(1)=kc2(1);
%hot side overall heat transfer coefficient of IHX kW/(m^2*K)

Ac=Q/dTlm1/kc+.2312562;  %Cold side heat transfer area required for SHX m^2
Ah=Q/dTlm1/kh+.2312562;  %Hot side heat transfer area required for SHX m^2
Ac2=Q/dTlm2/kc2+.2908;  %Cold side heat transfer area required for IHX m^2
Ah2=Q/dTlm2/kh2+.2908;  %hot side heat transfer area required for IHX m^2
```

```matlab
%% Reactor data
beta=0.006502;
beta1= 0.001639;
beta2= 0.003842;
beta3= 0.001021;
lambda1 = 0.025598; %1/s
lambda2= 0.192013; %1/s
lambda3= 1.367097; %1/s
Lambda=0.0003; %s
nr0=1;
mdot_core(1)=40.299; %kg/s
[h_core]=hv_core((tco3(1)+tci3(1))/2,mdot_core(1)); %w/(m^2*C)
flibe_miu=0.006717; %Pa*s
flibe_rho=1961.6; %kg/m^3
pebble_rho=2000;
cpf=0.9466;
cpc=2.386; %kJ/(kg*C);

%Core properties
height_core = 152.9*10^-2;              % Height of Reactor, [m]
radius_core = 43.7*10^-2;               % Radius of Reactor, [m]
v_core = pi*radius_core^2*height_core;         % Volume of Reactor, [m^3]

radius_pebble = 1.5*10^-2;              % Pebble radius, [m]
v_pebble = 4/3*pi*radius_pebble^3;
% Volume of one pebble, [m^3]

e_bed = 0.375+0.34*radius_pebble/radius_core;
%Porosity of randomly closed packed bed
f_bed = 1-e_bed;                        % Packing fraction

N_pebble = f_bed*(v_core/v_pebble);   % Number of pebble in the core
V_pebble = N_pebble*(4/3*pi*radius_pebble^3); %m^3
Ar = N_pebble*4*pi*(radius_pebble)^2;
% Total heat transfer area in the core, [m^2]
Omega=h_core*Ar/1000;

Re_core = mdot_core(1)*2*radius_pebble/(pi*radius_core^2*flibe_miu);
% Reynold number in the core
velocity_core = mdot_core(1)/(flibe_rho*pi*radius_core^2);
% Superficial velocity, [m/s]
space_time=height_core/velocity_core;  %s

mcR=V_pebble*pebble_rho; %kg
mf=mdot_core(1)*space_time; %kg
miu_c=mcR*cpc;
miu_f=mf*cpf;
Mc=mdot_core(1)*cpc;
```

```matlab
tci3(1)=600; %C
tco3(1)=704;
Tc0=(tci3(1)+tco3(1))/2;

alpha_f=-3.85*10^-5; % fuel reactivity coeffiicient
alpha_c=-0.34*10^-5; % coolant reactivity coefficient

%% time delays

tau_h(1)=L1/vh(1);  %time delay (s)
tau_c(1)=L1/vc(1);
tau_p=137.3;
tau_h2(1)=L2/v_tube_FTHX(1);
tau_c2(1)=L2/v_shell_FTHX(1);
tau_p2=137.3;
tau_p3=10;


%% initial controller parameters

%IHX1
dtho2_s=0;              % Reference to follow
dGh2(1) = 0;
yold1_2=0;
yp_2 = [];
ys_prime_2(1) = [];
er_2 = dtho2_s;          % Error (Initial error = Reference)
er1_2 = 0;              % First derivative of error
er2_2 = 0;              % Second derivative of error
eold_2 = dtho2_s;
eold2_2 = 0;

%SHX1
dtco_s = 0;            % Reference to follow
dGh(1) = 0;
yold1=0;
yp = [];
ys_prime(1) = [];
er = dtco_s;          % Error (Initial error = Reference)
er1 = 0;              % First derivative of error
er2 = 0;              % Second derivative of error
eold = dtco_s;
eold2 = 0;

%reactor
n_s = 1;              % Reference to follow
rho_r(1) = 0;
```

```matlab
yold1_3=0;
yp_3 = [];
ys_prime_3 = [];
er_3 = n_s;              % Error (Initial error = Reference)
er1_3 = 0;              % First derivative of error
er2_3 = 0;              % Second derivative of error
eold_3 = n_s;
eold2_3 = 0;


%% Discretized initial value calculation for IHX and SHX
tic;
    k=1; % setting for controller
  %SHX
  thi(1,1)=690;
  tco(1,1)=651.2;
  tci(1,p)=498.9;
  tho(1,p)=545;
  dGh(1,1)=0;
  Gh(1,1)=Gh(1)+dGh(1,1);
  [hh(1,1), vh(1,1) ,hc(1,1), vc(1,1)] = ...
     HTCV_OSFSHX(thi(1,1),tco(1,1),Gh(1),Gc(1));

  hh(1,1)= real(hh(1,1));
  vh(1,1)= real(vh(1,1));
  hc(1,1)= real(hc(1,1));
  vc(1,1)= real(vc(1,1));

  %IHX
  thi2(1,1)=704;
  tco2(1,1)=690;
  tci2(1,m)=545;
  tho2(1,m)=600;
  dGh2(1,m)=0;
  [hh2(1,1), v_tube_FTHX(1,1),hc2(1,1), v_shell_FTHX(1,1)] = ...
     HTCV_FTHX(thi2(1,1),tco2(1,1),Gh2(1),Gc2(1));

  hh2(1,1)= real(hh2(1,1));
  v_tube_FTHX(1,1)= real(v_tube_FTHX(1,1));
  hc2(1,1)= real(hc2(1,1));
  v_shell_FTHX(1,1)= real(v_shell_FTHX(1,1));

%Initial values
for i=1:p

  %SHX
  Gh(1,i)=Gh(1);
```

```matlab
A=[-hh(1,i)*Ah/p-Cph*Gh(1,i) 0 hh(1,i)*Ah/p -Cph*Gh(1,i)*thi(1,i); ...
   0 Cpc*Gc(1) hc(1,i)*Ac/p (hc(1,i)*Ac/p+Cpc*Gc(1))*tco(1,i);...
   hh(1,i)*Ah/p 0 -hh(1,i)*Ah/p-hc(1,i)*Ac/p -hc(1,i)*Ac/p*tco(1,i) ];

A13=A(3,1)/A(1,1);

A(3,1)=A(3,1)-A(1,1)*A13;
A(3,3)=A(3,3)-A(1,3)*A13;
A(3,4)=A(3,4)-A(1,4)*A13;

tw(1,i)=A(3,4)/A(3,3);
tci(1,i)=(A(2,4)-A(2,3)*tw(1,i))/A(2,2);
tho(1,i)=(A(1,4)-A(1,3)*tw(1,i))/A(1,1);

[hh(1,i+1), vh(1,i+1),hc(1,i+1), vc(1,i+1)] = ...
   HTCV_OSFSHX(tho(1,i),tci(1,i),Gh(1,i),Gc(1));

hh(1,i+1)= real(hh(1,i+1));
vh(1,i+1)= real(vh(1,i+1));
hc(1,i+1)= real(hc(1,i+1));
vc(1,i+1)= real(vc(1,i+1));

tco(1,i+1)=tci(1,i);
thi(1,i+1)=tho(1,i);

Qc(1)=Gc(1)*Cpc*(tco(1,1)-tci(1,p));
Qh(1)=Gh(1)*Cph*(thi(1,1)-tho(1,p));
end

for i=1:m
  %IHX
  Gh2(1,i)=Gh2(1);

  B=[-hh2(1,i)*Ah2/m-Cph2*Gh2(1,i) 0 hh2(1,i)*Ah2/m -Cph2*Gh2(1,i)...
     *thi2(1,i); 0 Cpc2*Gc2(1) hc2(1,i)*Ac2/m (hc2(1,i)*Ac2/m+Cpc2...
     *Gc2(1))*tco2(1,i);hh2(1,i)*Ah2/m 0 -hh2(1,i)*Ah2/m-hc2(1,i)...
     *Ac2/m -hc2(1,i)*Ac2/m*tco2(1,i) ];

  B13=B(3,1)/B(1,1);

  B(3,1)=B(3,1)-B(1,1)*B13;
  B(3,3)=B(3,3)-B(1,3)*B13;
  B(3,4)=B(3,4)-B(1,4)*B13;

  tw2(1,i)=B(3,4)/B(3,3);
  tci2(1,i)=(B(2,4)-B(2,3)*tw2(1,i))/B(2,2);
  tho2(1,i)=(B(1,4)-B(1,3)*tw2(1,i))/B(1,1);
```

```
   [hh2(1,i+1), v_tube_FTHX(1,i+1),hc2(1,i+1), v_shell_FTHX(1,i+1)] = ...
      HTCV_FTHX(tho2(1,i),tci2(1,i),Gh2(1,i),Gc2(1));

   hh2(1,i+1)= real(hh2(1,i+1));
   v_tube_FTHX(1,i+1)= real(v_tube_FTHX(1,i+1));
   hc2(1,i+1)= real(hc2(1,i+1));
   v_shell_FTHX(1,i+1)= real(v_shell_FTHX(1,i+1));

   tco2(1,i+1)=tci2(1,i);
   thi2(1,i+1)=tho2(1,i);

   Q2c(1)=Gc2(1)*Cpc2*(tco2(1,1)-tci2(1,m));
   Q2h(1)=Gh2(1)*Cph2*(thi2(1,1)-tho2(1,m));
end

for l=1:10
for i=1:p
   [hh(1,i), vh(1,i),hc(1,i), vc(1,i)] = HTCV_OSFSHX(tho(1,i),tco(1,i),...
      Gh(1,i),Gc(1));

   hh(1,i)= real(hh(1,i));
   vh(1,i)= real(vh(1,i));
   hc(1,i)= real(hc(1,i));
   vc(1,i)= real(vc(1,i));

   A=[-hh(1,i)*Ah/p-Cph*Gh(1,i) 0 hh(1,i)*Ah/p -Cph*Gh(1,i)*thi(1,i); ...
      0 Cpc*Gc(1) hc(1,i)*Ac/p (hc(1,i)*Ac/p+Cpc*Gc(1))*tco(1,i);...
      hh(1,i)*Ah/p 0 -hh(1,i)*Ah/p-hc(1,i)*Ac/p -hc(1,i)*Ac/p*tco(1,i) ];

   A13=A(3,1)/A(1,1);

   A(3,1)=A(3,1)-A(1,1)*A13;
   A(3,3)=A(3,3)-A(1,3)*A13;
   A(3,4)=A(3,4)-A(1,4)*A13;

   tw(1,i)=A(3,4)/A(3,3);
   tci(1,i)=(A(2,4)-A(2,3)*tw(1,i))/A(2,2);
   tho(1,i)=(A(1,4)-A(1,3)*tw(1,i))/A(1,1);
   tco(1,i+1)=tci(1,i);
   thi(1,i+1)=tho(1,i);
end
Qc(1)=Gc(1)*Cpc*(tco(1,1)-tci(1,p));
Qh(1)=Gh(1,1)*Cph*(thi(1,1)-tho(1,p));
end

for l=1:10
   for i=1:m
      [hh2(1,i), v_tube_FTHX(1,i),hc2(1,i), v_shell_FTHX(1,i)] = ...
```

```
        HTCV_FTHX(tho2(1,i),tco2(1,i),Gh2(1,i),Gc2(1));

    hh2(1,i)= real(hh2(1,i));
    v_tube_FTHX(1,i)= real(v_tube_FTHX(1,i));
    hc2(1,i)= real(hc2(1,i));
    v_shell_FTHX(1,i)= real(v_shell_FTHX(1,i));

    B=[-hh2(1,i)*Ah2/m-Cph2*Gh2(1,i) 0 hh2(1,i)*Ah2/m -Cph2*Gh2(1,i)...
        *thi2(1,i); 0 Cpc2*Gc2(1) hc2(1,i)*Ac2/m (hc2(1,i)*Ac2/m+Cpc2...
        *Gc2(1))*tco2(1,i);hh2(1,i)*Ah2/m 0 -hh2(1,i)*Ah2/m-hc2(1,i)...
        *Ac2/m -hc2(1,i)*Ac2/m*tco2(1,i) ];

    B13=B(3,1)/B(1,1);

    B(3,1)=B(3,1)-B(1,1)*B13;
    B(3,3)=B(3,3)-B(1,3)*B13;
    B(3,4)=B(3,4)-B(1,4)*B13;

    tw2(1,i)=B(3,4)/B(3,3);
    tci2(1,i)=(B(2,4)-B(2,3)*tw2(1,i))/B(2,2);
    tho2(1,i)=(B(1,4)-B(1,3)*tw2(1,i))/B(1,1);
    tco2(1,i+1)=tci2(1,i);
    thi2(1,i+1)=tho2(1,i);
    end
    Q2c(1)=Gc2(1)*Cpc2*(tco2(1,1)-tci2(1,m));
    Q2h(1)=Gh2(1)*Cph2*(thi2(1,1)-tho2(1,m));
end


%% Initial Reactor values
    Tf(1)=((2*Mc+Omega)/miu_c*tco3(1)-(2*Mc-Omega)/miu_c*tci3(1)) ...
        *miu_c/(2*Omega); %C
    n(1)=(Omega/miu_f*Tf(1)-Omega/(2*miu_f)*tci3(1)-Omega/...
        (2*miu_f)*tco3(1))*miu_f/P0;
    cc1(1)=beta1/(Lambda*lambda1)*n(1);
    cc2(1)=beta2/(Lambda*lambda2)*n(1);
    cc3(1)=beta3/(Lambda*lambda3)*n(1);
    P(1)=P0;
    rho(1)=0;
    rho_r(1)=0;
    dtci3(1)=0;
    dtco3(1)=0;
    mdot_core(1)=mdot_core(1);
    tci3(1)=dtci3(1)+tci3(1);
    tco3(1)=dtco3(1)+tco3(1);

    QR(1)=mdot_core(1)*cpc*(tco3(1)-tci3(1));
```

```matlab
%% Transient code
for j=2:ft/dt+1

    for i=1:p
        dGh(j,i)=dGh(j-1,1);
        %dGh(j,i)=0*Gh(1,1);
        if z<2
            dGc(j,i)=0.1*Gc(1);
        elseif z>1 && z<3
            dGc(j,i)=-0.1*Gc(1);
        else
            dGc(j,i)=0*Gc(1);
        end
        Gh(j,i)=Gh(1)+dGh(j,i);
        Gc(j,i)=Gc(1)+dGc(j,i);
    end
    for i=1:m
        dGh2(j,i)=dGh2(j-1,m);
        %dGh2(j,i)=0*Gh2(1,1);
        dGc2(j,i)=dGh(j,1);
        Gh2(j,i)=Gh2(1,1)+dGh2(j,i);
        Gc2(j,i)=Gc2(1)+dGc2(j,i);
    end
    thi2(j,1)=thi2(j-1,1);
    if z>2 && z<4
        tci(j,p)=tci(1,p)+10;
    elseif z>3 && z<5
        tci(j,p)=tci(1,p)-10;
    else
        tci(j,p)=tci(1,p);
    end
    tci2(j,m)=tci2(j-1,m);
    thi(j,1)=thi(j-1,1);
    %reactor
    tci3(j)=tci3(j-1);
    mdot_core(j)=Gh2(j,1);
    rho_r(j)=rho_r(j-1);
    rho_r2(j)=0*beta;
    %dGhc(j,1)=dGhc(j-1,1);
    %dGh2c(j,m)=dGh2c(j-1,1);


for i=1:p
%SHX transients
[hh(j,i), vh(j,i) ,hc(j,i), vc(j,i)] = HTCV_OSFSHX(tho(j-1,i),...
    tco(j-1,i),Gh(j,i),Gc(j,i));

hh(j,i)= real(hh(j,i));
```

```matlab
vh(j,i)= real(vh(j,i));
hc(j,i)= real(hc(j,i));
vc(j,i)= real(vc(j,i));

tau_h(j,i)=L1/p/vh(j,i);
tau_c(j,i)=L1/p/vc(j,i);

mh(j,i)=tau_h(j,i)*Gh(j,i);
mc(j,i)=tau_c(j,i)*Gc(j,i);


%RK 4th order
a1=(hh(j,i)*Ah/p*(tw(j-1,i)-tho(j-1,i))-Cph*Gh(j,i)...
    *(tho(j-1,i)-thi(j-1,i)))/(Cph*mh(j,i));
a2=(hc(j,i)*Ac/p*(tw(j-1,i)-tco(j-1,i))-Cpc*Gc(j,i)...
    *(tco(j-1,i)-tci(j-1,i)))/(Cpc*mc(j,i));
a3=(hh(j,i)*Ah/p*(tho(j-1,i)-tw(j-1,i))-hc(j,i)*Ac/p*...
    (tw(j-1,i)-tco(j-1,i)))/(MW/p*Cpw);
b1=(hh(j,i)*Ah/p*((tw(j-1,i)+dt/2*a3)-(tho(j-1,i)+dt/2*a1))...
    -Cph*Gh(j,i)*((tho(j-1,i)+dt/2*a1)-thi(j-1,i)))/(Cph*mh(j,i));
b2=(hc(j,i)*Ac/p*((tw(j-1,i)+dt/2*a3)-(tco(j-1,i)+dt/2*a2))...
    -Cpc*Gc(j,i)*((tco(j-1,i)+dt/2*a2)-tci(j-1,i)))/(Cpc*mc(j,i));
b3=(hh(j,i)*Ah/p*((tho(j-1,i)+dt/2*a1)-(tw(j-1,i)+dt/2*a3))...
    -hc(j,i)*Ac/p*((tw(j-1,i)+dt/2*a3)-(tco(j-1,i)+dt/2*a2)))/(MW/p*Cpw);
c1=(hh(j,i)*Ah/p*((tw(j-1,i)+dt/2*b3)-(tho(j-1,i)+dt/2*b1))...
    -Cph*Gh(j,i)*((tho(j-1,i)+dt/2*b1)-thi(j-1,i)))/(Cph*mh(j,i));
c2=(hc(j,i)*Ac/p*((tw(j-1,i)+dt/2*b3)-(tco(j-1,i)+dt/2*b2))...
    -Cpc*Gc(j,i)*((tco(j-1,i)+dt/2*b2)-tci(j-1,i)))/(Cpc*mc(j,i));
c3=(hh(j,i)*Ah/p*((tho(j-1,i)+dt/2*b1)-(tw(j-1,i)+dt/2*b3))...
    -hc(j,i)*Ac/p*((tw(j-1,i)+dt/2*b3)-(tco(j-1,i)+dt/2*b2)))/(MW/p*Cpw);
d1=(hh(j,i)*Ah/p*((tw(j-1,i)+dt*c3)-(tho(j-1,i)+dt*c1))...
    -Cph*Gh(j,i)*((tho(j-1,i)+dt*c1)-thi(j-1,i)))/(Cph*mh(j,i));
d2=(hc(j,i)*Ac/p*((tw(j-1,i)+dt*c3)-(tco(j-1,i)+dt*c2))...
    -Cpc*Gc(j,i)*((tco(j-1,i)+dt*c2)-tci(j-1,i)))/(Cpc*mc(j,i));
d3=(hh(j,i)*Ah/p*((tho(j-1,i)+dt*c1)-(tw(j-1,i)+dt*c3))...
    -hc(j,i)*Ac/p*((tw(j-1,i)+dt*c3)-(tco(j-1,i)+dt*c2)))/(MW/p*Cpw);

tho(j,i)=tho(j-1,i)+dt/6*(a1+2*b1+2*c1+d1);
tco(j,i)=tco(j-1,i)+dt/6*(a2+2*b2+2*c2+d2);
tw(j,i)=tw(j-1,i)+dt/6*(a3+2*b3+2*c3+d3);

%SHX Duty
Qc(j)=Gc(j,i)*Cpc*(tco(j,1)-tci(j,p));
Qh(j)=Gh(j,i)*Cph*(thi(j-1,1)-tho(j,p));

end

for i=1:p-1
```

```
    tci(j,i)=tco(j,i+1);
end

for i=2:p
   thi(j,i)=tho(j,i-1);
end
   dtco(j,1)=tco(j,1)-tco(1,1);

for i=1:m
%IHX transients
[hh2(j,i), v_tube_FTHX(j,i),hc2(j,i), v_shell_FTHX(j,i)] =...
   HTCV_FTHX(tho2(j-1,i),tco2(j-1,i),Gh2(j,i),Gc2(j,i));

hh2(j,i)= real(hh2(j,i));
v_tube_FTHX(j,i)= real(v_tube_FTHX(j,i));
hc2(j,i)= real(hc2(j,i));
v_shell_FTHX(j,i)= real(v_shell_FTHX(j,i));

tau_h2(j,i)=L2/v_tube_FTHX(j,i);
tau_c2(j,i)=L2/v_shell_FTHX(j,i);

mh2(j,i)=tau_h2(j,i)*Gh2(j,i);
mc2(j,i)=tau_c2(j,i)*Gc2(j,i);

%RK 4th order
e1=(hh2(j,i)*Ah2/m*(tw2(j-1,i)-tho2(j-1,i))-Cph2*Gh2(j,i)...
   *(tho2(j-1,i)-thi2(j-1,i)))/(Cph2*mh2(j,i)/m);
e2=(hc2(j,i)*Ac2/m*(tw2(j-1,i)-tco2(j-1,i))-Cpc2*Gc2(j,i)...
   *(tco2(j-1,i)-tci2(j-1,i)))/(Cpc2*mc2(j,i)/m);
e3=(hh2(j,i)*Ah2/m*(tho2(j-1,i)-tw2(j-1,i))-hc2(j,i)...
   *Ac2/m*(tw2(j-1,i)-tco2(j-1,i)))/(MW2/m*Cpw);
f1=(hh2(j,i)*Ah2/m*((tw2(j-1,i)+dt/2*e3)-(tho2(j-1,i)+dt/2*e1))...
   -Cph2*Gh2(j,i)*((tho2(j-1,i)+dt/2*e1)-thi2(j-1,i)))/(Cph2*mh2(j,i)/m);
f2=(hc2(j,i)*Ac2/m*((tw2(j-1,i)+dt/2*e3)-(tco2(j-1,i)+dt/2*e2))...
   -Cpc2*Gc2(j,i)*((tco2(j-1,i)+dt/2*e2)-tci2(j-1,i)))/(Cpc2*mc2(j,i)/m);
f3=(hh2(j,i)*Ah2/m*((tho2(j-1,i)+dt/2*e1)-(tw2(j-1,i)+dt/2*e3))-hc2(j,i)...
   *Ac2/m*((tw2(j-1,i)+dt/2*e3)-(tco2(j-1,i)+dt/2*e2)))/(MW2/m*Cpw);
g1=(hh2(j,i)*Ah2/m*((tw2(j-1,i)+dt/2*f3)-(tho2(j-1,i)+dt/2*f1))...
   -Cph2*Gh2(j,i)*((tho2(j-1,i)+dt/2*f1)-thi2(j-1,i)))/(Cph2*mh2(j,i)/m);
g2=(hc2(j,i)*Ac2/m*((tw2(j-1,i)+dt/2*f3)-(tco2(j-1,i)+dt/2*f2))...
   -Cpc2*Gc2(j,i)*((tco2(j-1,i)+dt/2*f2)-tci2(j-1,i)))/(Cpc2*mc2(j,i)/m);
g3=(hh2(j,i)*Ah2/m*((tho2(j-1,i)+dt/2*f1)-(tw2(j-1,i)+dt/2*f3))-hc2(j,i)...
   *Ac2/m*((tw2(j-1,i)+dt/2*f3)-(tco2(j-1,i)+dt/2*f2)))/(MW2/m*Cpw);
h1=(hh2(j,i)*Ah2/m*((tw2(j-1,i)+dt*g3)-(tho2(j-1,i)+dt*g1))...
   -Cph2*Gh2(j,i)*((tho2(j-1,i)+dt*g1)-thi2(j-1,i)))/(Cph2*mh2(j,i)/m);
h2=(hc2(j,i)*Ac2/m*((tw2(j-1,i)+dt*g3)-(tco2(j-1,i)+dt*g2))...
   -Cpc2*Gc2(j,i)*((tco2(j-1,i)+dt*g2)-tci2(j-1,i)))/(Cpc2*mc2(j,i)/m);
h3=(hh2(j,i)*Ah2/m*((tho2(j-1,i)+dt*g1)-(tw2(j-1,i)+dt*g3))-hc2(j,i)...
```

```matlab
   *Ac2/m*((tw2(j-1,i)+dt*g3)-(tco2(j-1,i)+dt*g2)))/(MW2/m*Cpw);

tho2(j,i)=tho2(j-1,i)+dt/6*(e1+2*f1+2*g1+h1);
tco2(j,i)=tco2(j-1,i)+dt/6*(e2+2*f2+2*g2+h2);
tw2(j,i)=tw2(j-1,i)+dt/6*(e3+2*f3+2*g3+h3);

%IHX Duty
Q2c(j)=Gc2(j,i)*Cpc2*(tco2(j,1)-tci2(j-1,m));
Q2h(j)=Gh2(j,i)*Cph2*(thi2(j,1)-tho2(j,m));

end

for i=1:m-1
   tci2(j,i)=tco2(j,i+1);
end

for i=2:m
   thi2(j,i)=tho2(j,i-1);
end
   dtho2(j,m)=tho2(j,m)-tho2(1,m);

if t(j)<=tau_p
   thi(j,1)=thi(1,1);
else
   thi(j,1)=tco2(j-tau_p/dt,1);
end

if t(j)<=tau_p
   tci2(j,m)=tci2(1,m);
else
   tci2(j,m)=tho(j-tau_p/dt,p);
end

if t(j)<=tau_p3
   tci3(j)=tci3(1);
else
   tci3(j)=tho2(j-tau_p3/dt,m);
end

%Reactor transients
   velocity_core = mdot_core(j)/(flibe_rho*pi*radius_core^2);
   % Superficial velocity, [m/s]
   space_time=height_core/velocity_core;    %s

   mcR=V_pebble*pebble_rho; %kg
   mf=mdot_core(j)*space_time; %kg
   miu_c=mcR*cpc;
   miu_f=mf*cpf;
```

```
    Mc=mdot_core(j)*cpc;

    [h_core]=hv_core((tco3(j-1)+tci3(j))/2,mdot_core(j)); %w/(m^2*C)
    Omega=h_core*Ar/1000;

    %Runge Kutta 4th order
a1= (rho(j-1)-beta)/Lambda*n(j-1)+lambda1*cc1(j-1)+lambda2...
    *cc2(j-1)+lambda3*cc3(j-1);
a2= beta1/Lambda*n(j-1)-lambda1*cc1(j-1);
a3= P(j-1)/miu_f*n(j-1)-Omega/miu_f*Tf(j-1)+Omega/(2*miu_f)...
    *tci3(j-1)+Omega/(2*miu_f)*tco3(j-1);
a4= 2*Omega/miu_c*Tf(j-1)+((2*Mc-Omega)/miu_c)*tci3(j-1)-...
    ((2*Mc+Omega)/miu_c)*tco3(j-1);
a5= beta2/Lambda*n(j-1)-lambda2*cc2(j-1);
a6= beta3/Lambda*n(j-1)-lambda3*cc3(j-1);
b1= (rho(j-1)-beta)/Lambda*(n(j-1)+dt/2*a1)+lambda1*(cc1(j-1)...
    +dt/2*a2)+lambda2*(cc2(j-1)+dt/2*a5)+lambda3*(cc3(j-1)+dt/2*a6);
b2= beta1/Lambda*(n(j-1)+dt/2*a1)-lambda1*(cc1(j-1)+dt/2*a2);
b3= P(j-1)/miu_f*(n(j-1)+dt/2*a1)-Omega/miu_f*(Tf(j-1)+dt/2*a3)...
    +Omega/(2*miu_f)*tci3(j-1)+Omega/(2*miu_f)*(tco3(j-1)+dt/2*a4);
b4= 2*Omega/miu_c*(Tf(j-1)+dt/2*a3)+((2*Mc-Omega)/miu_c)*tci3(j-1)...
    -((2*Mc+Omega)/miu_c)*(tco3(j-1)+dt/2*a4);
b5= beta2/Lambda*(n(j-1)+dt/2*a1)-lambda2*(cc2(j-1)+dt/2*a5);
b6= beta3/Lambda*(n(j-1)+dt/2*a1)-lambda3*(cc3(j-1)+dt/2*a6);
d1= (rho(j-1)-beta)/Lambda*(n(j-1)+dt/2*b1)+lambda1*(cc1(j-1)...
    +dt/2*b2)+lambda2*(cc2(j-1)+dt/2*b5)+lambda3*(cc3(j-1)+dt/2*b6);
d2= beta1/Lambda*(n(j-1)+dt/2*b1)-lambda1*(cc1(j-1)+dt/2*b2);
d3= P(j-1)/miu_f*(n(j-1)+dt/2*b1)-Omega/miu_f*(Tf(j-1)+dt/2*b3)...
    +Omega/(2*miu_f)*tci3(j-1)+Omega/(2*miu_f)*(tco3(j-1)+dt/2*b4);
d4= 2*Omega/miu_c*(Tf(j-1)+dt/2*b3)+((2*Mc-Omega)/miu_c)*tci3(j-1)...
    -((2*Mc+Omega)/miu_c)*(tco3(j-1)+dt/2*b4);
d5= beta2/Lambda*(n(j-1)+dt/2*b1)-lambda2*(cc2(j-1)+dt/2*b5);
d6= beta3/Lambda*(n(j-1)+dt/2*b1)-lambda3*(cc3(j-1)+dt/2*b6);
e1= (rho(j-1)-beta)/Lambda*(n(j-1)+dt*d1)+lambda1*(cc1(j-1)+dt*d2)...
    +lambda2*(cc2(j-1)+dt*d5)+lambda3*(cc3(j-1)+dt*d6);
e2= beta1/Lambda*(n(j-1)+dt*d1)-lambda1*(cc1(j-1)+dt*d2);
e3= P(j-1)/miu_f*(n(j-1)+dt*d1)-Omega/miu_f*(Tf(j-1)+dt*d3)...
    +Omega/(2*miu_f)*tci3(j-1)+Omega/(2*miu_f)*(tco3(j-1)+dt*d4);
e4= 2*Omega/miu_c*(Tf(j-1)+dt*d3)+((2*Mc-Omega)/miu_c)*tci3(j-1)...
    -((2*Mc+Omega)/miu_c)*(tco3(j-1)+dt*d4);
e5= beta2/Lambda*(n(j-1)+dt*d1)-lambda2*(cc2(j-1)+dt*d5);
e6= beta3/Lambda*(n(j-1)+dt*d1)-lambda3*(cc3(j-1)+dt*d6);

n(j)=n(j-1)+dt/6*(a1+2*b1+2*d1+e1);
cc1(j)=cc1(j-1)+dt/6*(a2+2*b2+2*d2+e2);
Tf(j)=Tf(j-1)+dt/6*(a3+2*b3+2*d3+e3);
tco3(j)=tco3(j-1)+dt/6*(a4+2*b4+2*d4+e4);
cc2(j)=cc2(j-1)+dt/6*(a5+2*b5+2*d5+e5);
```

```
        cc3(j)=cc3(j-1)+dt/6*(a6+2*b6+2*d6+e6);


        rho(j)=rho_r(j)+rho_r2(j)+alpha_f*(Tf(j)-Tf(1))...
            +alpha_c/2*(tci3(j)-tci3(1))+alpha_c/2*(tco3(j)-tco3(1));

        P(j)=n(j)/n(1)*P0;

        dtco3(j,1)=tco3(j)-tco3(1);

        if t(j)<=tau_p3
            thi2(j,1)=thi2(1,1);
        else
            thi2(j,1)=tco3(j-tau_p3/dt);
        end

        %Reactor Duty
        QR(j)=mdot_core(j)*cpc*(tco3(j)-tci3(j));

%% Control of temperatures
        tt=t(j);
        dtt=.1;
        rm=rem(tt,dtt);

        er = dtco_s - dtco(j,1); %SHX error C

        er_2 = dtho2_s - dtho2(j,m); %IHX error C

        er_3 = n_s - n(j); % Reactor error


%controller SHX tco
        if rm==0
            dtspan = [t(j) t(j)+100*dt];
            eold2 = eold ;
            eold = er;
            er = dtco_s - dtco(j,1);
            er2 = er + eold2 - 2*eold;
            er1 = er - eold;
            init_con = [dGh(j,1) ; (dGh(j,1)-yold1)];
            % Initial conditions for the diffrential equations
            options = [];
            [t2,y]  = ode45(@pid_ctrl_2,dtspan,init_con,options,er,er1,er2,k);
            yold1 = dGh(j,1);
            ys = y(length(y),1);
            ys_prime = [ys ys_prime];
            dGh = ys_prime(1);
            yq = [yp dGh];
```

```
        dGh(j,1)=yq;
        Gh(j,1)=Gh(1,1)+dGh(j,1);

%controller IHX tho2
        dtspan2 = [t(j) t(j)+100*dt];
        eold2_2 = eold_2 ;
        eold_2 = er_2;
        er_2 = dtho2_s - dtho2(j,m);
        er2_2 = er_2 + eold2_2 - 2*eold_2;
        er1_2 = er_2 - eold_2;
        init_con2 = [dGh2(j,m) ; (dGh2(j,m)-yold1_2)];
        % Initial conditions for the diffirential equations
        options2 = [];
        [t3,y2]  = ode45(@pid_ctrl2_2,dtspan2,init_con2,options2,er_2, ...
           er1_2,er2_2,k);
        yold1_2 = dGh2(j,m);
        ys_2 = y2(length(y2),1);
        ys_prime_2 = [ys_2 ys_prime_2];
        dGh2 = ys_prime_2(1);
        yq_2 = [yp_2 dGh2];

        dGh2(j,m)=yq_2;
        Gh2(j,m)=Gh2(1)+dGh2(j,m);


%{
 %if abs(er_3)/n_s<0.1

    if rm==0

        %controller Reactor

        dtspan3 = [t(j) t(j)+100*dt];
        eold2_3 = eold_3 ;
        eold_3 = er_3;
        er_3 = n_s - n(j);
        er2_3 = er_3 + eold2_3 - 2*eold_3;
        er1_3 = er_3 - eold_3;
        init_con3 = [rho_r(j) ; (rho_r(j)-yold1_3)];
        options3 = [];
        [t4,y3]  = ode45(@pid_ctrlR,dtspan3,init_con3,options3,er_3,...
           er1_3,er2_3,k);
        yold1_3 = rho_r(j);
        ys_3 = y3(length(y3),1);
        ys_prime_3 = [ys_3 ys_prime_3];
        rho_r = ys_prime_3(1);
        yq_3 = [yp_3 rho_r];
```

```matlab
        rho_r(j)=yq_3;
    end
%}
    else
    end

end


elapse=toc; % time to run simulation

%% Figures

    figure(1+(z-1)*9)
    plot(t,Qc,'-k','LineWidth', 2)
    hold on
    plot(t,Qh,':k','LineWidth', 2)
    plot(t,Q2c,'--k','LineWidth', 2)
    plot(t,Q2h,'-.k','LineWidth', 2)
    plot(t,QR,'-r','LineWidth', 2);
    hold off
    grid on
    h=legend('SHX-cold','SHX-hot','IHX-cold','IHX-hot','Reactor');
    set(h,'FontSize',14);
    xlabel('Time (s)', 'fontsize',14)
    set(gca,'fontsize',13)
    ylabel('Duty (kW)', 'fontsize',14)

    figure(2+(z-1)*9);
    plot(t,Gh2,'-k','LineWidth', 2)
    grid on
    h=legend('IHX hot side flow rate');
    set(h,'FontSize',14);
    xlabel('Time (s)', 'fontsize',14)
    set(gca,'fontsize',13)
    ylabel('Flow Rate (kg/s)', 'fontsize',14)

    figure(3+(z-1)*9);
    plot(t,Gh,'-k','LineWidth', 2)
    grid on
    h=legend('SHX hot side flow rate');
    set(h,'FontSize',14);
    xlabel('Time (s)', 'fontsize',14)
    set(gca,'fontsize',13)
    ylabel('Flow Rate (kg/s)', 'fontsize',14)

    figure(4+(z-1)*9);
```

```matlab
plot(t,tho(:,p),'-k','LineWidth', 2)
grid on
h=legend('SHX-Hot Out');
set(h,'FontSize',14);
xlabel('Time (s)', 'fontsize',14)
set(gca,'fontsize',13)
ylabel('Temperature (^oC)', 'fontsize',14)

figure(5+(z-1)*9);
plot(t,tco(:,1),'-k','LineWidth', 2)
grid on
h=legend('SHX-Cold Out');
set(h,'FontSize',14);
xlabel('Time (s)', 'fontsize',14)
set(gca,'fontsize',13)
ylabel('Temperature (^oC)', 'fontsize',14)
line('XData', [0 ft], 'YData', [tco(1,1) tco(1,1)], 'LineStyle', ...
    '--', 'LineWidth', 2)

figure(6+(z-1)*9);
plot(t,tho2(:,m),'-k','LineWidth', 2)
grid on
h=legend('IHX-Hot Out');
set(h,'FontSize',14);
xlabel('Time (s)', 'fontsize',14)
set(gca,'fontsize',13)
ylabel('Temperature (^oC)', 'fontsize',14)
line('XData', [0 ft], 'YData', [tho2(1,m) tho2(1,m)], 'LineStyle', ...
    '--', 'LineWidth', 2)

figure(7+(z-1)*9);
plot(t,tco2(:,1),'-k','LineWidth', 2)
grid on
h=legend('IHX-Cold Out');
set(h,'FontSize',14);
xlabel('Time (s)', 'fontsize',14)
set(gca,'fontsize',13)
ylabel('Temperature (^oC)', 'fontsize',14)

figure(8+(z-1)*9)
plot(t,tco3,'-k','LineWidth', 2);
grid on
h=legend('Reactor-Out');
set(h,'FontSize',14);
xlabel('Time (s)', 'fontsize',14)
set(gca,'fontsize',13)
ylabel('Temperature (^oC)', 'fontsize',14)
```

```matlab
    figure(9+(z-1)*9)
    plot(t,tci3,'-k','LineWidth', 2);
    grid on
    h=legend('Reactor-In');
    set(h,'FontSize',14);
    xlabel('Time (s)', 'fontsize',14)
    set(gca,'fontsize',13)
    ylabel('Temperature (^oC)', 'fontsize',14)

end
```